UNIVERSITY OF OKLAHOMA

GRADUATE COLLEGE

THEORETICAL AND EXPERIMENTAL INVESTIGATIONS OF THE BEHAVIOR OF BOWED STRINGS UTILIZING A MAGNETIC PICKUP SYSTEM

A THESIS

SUBMITTED TO THE GRADUATE FACULTY

in partial fulfillment of the requirements for the

Degree of

MASTER OF SCIENCE

By

FELIX COOPER ADAMO
Norman, Oklahoma
2024

Downloaded from SHAREOK. Persistent Handle URL: https://hdl.handle.net/11244/340339

THEORETICAL AND EXPERIMENTAL INVESTIGATIONS OF THE BEHAVIOR OF BOWED STRINGS UTILIZING A MAGNETIC PICKUP SYSTEM

A THESIS APPROVED FOR THE
SCHOOL OF AEROSPACE AND MECHANICAL ENGINEERING

BY THE COMMITTEE CONSISTING OF

Dr. Prakash Vedula, Chair

Dr. Peter Attar

Dr. Diogo Merguizo Sanchez

© Copyright by FELIX COOPER ADAMO 2024
All Rights Reserved.

Abstract

Pickup systems for musical instruments generally serve the purpose of improving the perceived quality of instrument sound through appropriate amplification of electrical signals. While different pickups like a microphone or piezoelectric pickup are common to many string instruments, magnetic pickups are mostly used for plucked string instruments like the electric guitar or electric bass guitar. For a bowed instrument like a violin, microphones and piezoelectric pickups are commonly used, but magnetic pickups (which convert mechanical oscillations of a magnetized string to oscillatory changes in magnetic flux, manifesting in changes in voltage) are rarely used. The primary objective of this work was to establish foundational insights for new designs of magnetic pickups for bowed instruments like the violin. A secondary objective of this work was to motivate a modified damping factor term or modified external force term associated with dampening of vertical bowed string motion based on experimental evidence. To achieve these objectives, a new experimental setup was considered for exploration of the behavior of a bowed string-magnetic pickup system, specifically examining maximum and average voltage outputs across different frequency distributions, magnetic flux densities and their evolution over time for different rotational positions of the magnetic pickup about a magnetized, monochord string. Validation studies showed that the findings were consistent with expected results from tonal theory and literature, based on analysis of frequency spectra, voltage output (both obtained from magnetic pickup and optical switches) and magnetic flux densities. Based on the new experimental setup, an optimal position of the magnetic pickup was determined according to selected performance criteria. This work showed ample experimental evidence demonstrating the prevalence of significant damping of the vertical string oscillations by the combination of the presence of bow hairs at the point of bow-string interface and the downward bow force applied. Based on the insights and findings of this work, new and advanced designs of magnetic pickups for bowed string instruments could be achieved.

Dedications

"Praise ye the Lord in his holy places: praise ye him in the firmament of his power.... Praise him with timbrel and choir: praise him with strings and organs." **Psalm 150**

To Mike Lyddane (Lolo)

for instilling in me the love of mathematics, even when I did not yet know it.

To Karin Enebo

for teaching me to love the violin.

Acknowledgements

I am greatly indebted to Dr. Prakash Vedula for believing in me and believing in this work. His guidance and enthusiasm throughout the process pushed me forward to learn new ideas and extract new findings. Dr. Tom Boone was always available to help as he always proved to be an excellent foil, offering fresh perspectives when I was attempting to resolve issues during my work. I would also like to express my appreciation for Dr. Thomas Moore and Dr. John Woodhouse. They both helped me gather confidence in the work with their insight and helped provide a fruitful direction for the whole study when it was in its initial stage.

I would also like to thank the University of Oklahoma's Aerospace and Mechanical Engineering (AME) Department and the AME machine shop. My education through the department and the help from Billy Mays and Greg Williams in the shop gave me all the mental and physical tools necessary to complete this thesis.

Finally, I would like to thank my family. My parents, Felix and Teresa Adamo, supported me in so many ways during my education and during this work and I am glad they can see their efforts come to fruition. And I want to thank my brother, Zane Adamo, for having me become a member of his band, the Soda Crackers; I do not think I would have pursued this topic if I had not taken that deeper dive into the world of music.

Contents

Abstract iv

Dedications v

Acknowledgements vi

Contents vii

List of Figures xi

1 Introduction 1

1.1 Amplification of Musical Instrument Sounds 1

1.2 Literature Survey 2

1.3 Purpose of Thesis 4

1.4 Hypothesis 6

1.5 Potential Advantages of a Magnetic Pickup 6

1.6 Overview of Study 9

2 Theory Overview and Exploration 11

2.1 Development of Bowed String Equations 12

2.2 Faraday's Law of Induction 16

2.3 Rotating the Components of a Magnetic Field 24

2.4 Proposal to Account for Vertical String Oscillation Damping in Governing Bowed String Equations . . . 30

3 Parameters and Dimensions of Experiment 32

3.1 Bow and String Parameters . . . 32
3.2 Measurement Position Piece Design . . . 33
3.3 Monochord Design . . . 34
3.4 Magnetic Pickup Design . . . 37
3.5 Optical Switches and Fixtures . . . 40
3.6 Bow Stroke Mechanism Design . . . 40
3.7 Interference Reduction . . . 43

4 Data Collection 44

4.1 Magnetic Pickup Voltage Signal . . . 44
4.2 Horizontal and Vertical String Displacement . . . 45
4.3 Magnetic Flux Density . . . 46
4.4 Use of Digital Oscilloscope . . . 46
4.5 Procedure for an Experiment Repetition of Data Collection . . . 46

5 Post-Processing of Data 48

5.1 Maximum Voltage . . . 49
5.2 Average Voltage . . . 49
5.3 Fast Fourier Transform Analysis . . . 50
5.4 Short-Time Fourier Transform: Spectrograms . . . 52
5.5 Magnetic Flux Density over Time . . . 52

6 Comparison with Previous Studies 55

6.1 Construction of Monochord . . . 56
6.2 Magnetic Flux Density as Function of Distances . . . 58

6.3 Capturing an Accurate Frequency Spectrum 59
6.4 Capturing Bowed String Motion Displacement 62
6.5 Wave Polarization Types 65
6.5.1 0.05 Seconds Period 66
6.5.2 0.5 Seconds Period 67
6.5.3 0.05 Seconds Period: Subjectively Plucked String 68
6.5.4 0.05 Seconds Period: Subjectively Bowed String 69
6.6 Expected Results of Voltages, Magnetic Flux Density, and Frequency Distributions 72

7 Results and Discussion **73**
7.1 Maximum Voltage and Average Voltage 73
7.2 Frequency Spectra and Timbre: comparing spectra between magnetic pickup positions 81
7.3 Frequency Spectra: pickup position-string polarization comparisons 92
7.4 Spectrograms Between Positions: Frequency Over Time 96
7.5 Spectrograms of Transverse String Displacements: Frequency Over Time . . 103
7.6 Magnetic Flux Density Over Time 106
7.7 Subjectively Bowed String 116
7.7.1 Waveforms And Voltage Outputs 117
7.7.2 Frequency Spectra 118
7.7.3 Spectrograms 120
7.7.4 Magnetic Flux Density Over Time 122
7.8 Subjectively Plucked String 123
7.8.1 Waveforms and Voltage Outputs 123
7.8.2 Frequency Spectra 125
7.8.3 Spectrograms 127
7.8.4 Magnetic Flux Density Over Time 128

8 Conclusion **131**

8.1 Summary 131

8.2 Suggestions for Improvement 141

8.3 Future Work 142

Bibliography **146**

List of Figures

3.1 Pickup Coil Diagram 39

6.1 All experiment components. 57

6.2 Monochord and bow stroke mechanism. 57

6.3 Monochord 57

6.4 Bow stroke mechanism. 58

6.5 Magnetic flux density as a function of probe height above the top magnetic pole face. 60

6.6 Magnetic flux density as a function of probe distance from the center of the magnet, fixed at a height of 7.1 mm above the top magnetic pole face. 60

6.7 Example of an accurate frequency spectrum for a bowed string when the string is tuned to 196 Hz, a G_3. This spectrum comes from a 0.05 second long signal obtained by a magnetic pickup. 62

6.8 Example of an accurate frequency spectrum for a bowed string when the string is tuned to 196 Hz, a G_3. This spectrum comes from a 0.05 second long signal obtained by an horizontally placed optical switch. 62

6.9 Voltage signal, 0.05 seconds long, of the horizontal optical switch. The signal was generated by a bowed string of the same downward bow force and bow velocity used for the main experiment repetitions. 63

6.10 Voltage signal, 0.05 seconds long, of the horizontal optical switch. The signal was generated by a bowed string of subjective bow force. 64
6.11 Simulation of horizontal transverse string displacement for a bowed string tensioned such that it has a fundamental frequency of 196 Hz. The simulation code used comes from Bilbao [2]. 64
6.12 Unfiltered wave polarization for a bowed string for a period of 0.05 seconds. . 66
6.13 Filtered wave polarization for a bowed string for a period of 0.05 seconds. . . 67
6.14 Unfiltered wave polarization for a bowed string for a period of 0.5 seconds. . 68
6.15 Filtered wave polarization for a bowed string for a period of 0.5 seconds. . . 68
6.16 Unfiltered wave polarization for a subjectively plucked string for a period of 0.05 seconds. 69
6.17 Filtered wave polarization for a plucked string of subjective force for a period of 0.05 seconds. 70
6.18 Unfiltered wave polarization for a bowed string of subjective force for a period of 0.05 seconds. 71
6.19 Filtered wave polarization for a bowed string of subjective force for a period of 0.05 seconds. 71

7.1 Maximum and average voltage outputs of all 8 magnetic pickup signals for the first iteration of the experiment. 74
7.2 Maximum and average voltage outputs of all 8 magnetic pickup signals for the second iteration of the experiment. 74
7.3 Maximum and average voltage outputs of all 8 magnetic pickup signals for the third iteration of the experiment. 75
7.4 Maximum and average voltage outputs of each horizontal optical switch measurement taken during the measurement of the magnetic pickup signal for a specific position for the first iteration of the experiment. 75

7.5 Maximum and average voltage outputs of each horizontal optical switch measurement taken during the measurement of the magnetic pickup signal for a specific position for the second iteration of the experiment. 76
7.6 Maximum and average voltage outputs of each horizontal optical switch measurement taken during the measurement of the magnetic pickup signal for a specific position for the third iteration of the experiment. 76
7.7 Maximum and average voltage outputs of each vertical optical switch measurement taken during the measurement of the magnetic pickup signal for a specific position for the first iteration of the experiment. 77
7.8 Maximum and average voltage outputs of each vertical optical switch measurement taken during the measurement of the magnetic pickup signal for a specific position for the second iteration of the experiment. 77
7.9 Maximum and average voltage outputs of each vertical optical switch measurement taken during the measurement of the magnetic pickup signal for a specific position for the third iteration of the experiment. 78
7.10 Normalized amplitude frequency spectrum of the signal from the magnetic pickup at the first position for a total time period of 0.05 seconds. 84
7.11 Normalized amplitude frequency spectrum of the signal from the magnetic pickup at the first position for a total time period of 0.5 seconds. 85
7.12 Normalized amplitude frequency spectrum of the signal from the magnetic pickup at the second position for a total time period of 0.5 seconds. 85
7.13 Normalized amplitude frequency spectrum of the signal from the magnetic pickup at the third position for a total time period of 0.5 seconds. 86
7.14 Normalized amplitude frequency spectrum of the signal from the magnetic pickup at the fourth position for a total time period of 0.5 seconds. 86
7.15 Normalized amplitude frequency spectrum of the signal from the magnetic pickup at the fifth position for a total time period of 0.5 seconds. 87

7.16 Normalized amplitude frequency spectrum of the signal from the magnetic pickup at the sixth position for a total time period of 0.5 seconds. 87
7.17 Normalized amplitude frequency spectrum of the signal from the magnetic pickup at the seventh position for a total time period of 0.5 seconds. 88
7.18 Normalized amplitude frequency spectrum of the signal from the magnetic pickup at the eighth position for a total time period of 0.5 seconds. 88
7.19 Linear amplitude frequency spectrum of the signal from the magnetic pickup at the eighth position for a total time period of 0.5 seconds. 89
7.20 Linear amplitude frequency spectrum of the signal from the magnetic pickup at the eighth position for a total time period of 0.5 seconds. 89
7.21 Linear amplitude frequency spectrum of the signal from the magnetic pickup at the eighth position for a total time period of 0.5 seconds. 90
7.22 Normalized amplitude frequency spectrum of a horizontal optical switch signal for a total time period of 0.5 seconds. 93
7.23 Normalized amplitude frequency spectrum of a vertical optical switch signal for a total time period of 0.5 seconds. 94
7.24 Normalized amplitude frequency spectrum of a horizontal optical switch signal for a total time period of 0.05 seconds. 94
7.25 Normalized amplitude frequency spectrum of a vertical optical switch signal for a total time period of 0.05 seconds. 95
7.26 Normalized amplitude spectrogram of the signal from the magnetic pickup at the first position for a total time period of 0.05 seconds. 97
7.27 Normalized amplitude spectrogram of the signal from the magnetic pickup at the first position for a total time period of 0.5 seconds. 97
7.28 Normalized amplitude spectrogram of the signal from the magnetic pickup at the second position for a total time period of 0.5 seconds. 98

7.29 Normalized amplitude spectrogram of the signal from the magnetic pickup at the third position for a total time period of 0.5 seconds. 98
7.30 Normalized amplitude spectrogram of the signal from the magnetic pickup at the fourth position for a total time period of 0.5 seconds. 99
7.31 Normalized amplitude spectrogram of the signal from the magnetic pickup at the fifth position for a total time period of 0.5 seconds. 99
7.32 Normalized amplitude spectrogram of the signal from the magnetic pickup at the sixth position for a total time period of 0.5 seconds. 100
7.33 Normalized amplitude spectrogram of the signal from the magnetic pickup at the seventh position for a total time period of 0.5 seconds. 100
7.34 Normalized amplitude spectrogram of the signal from the magnetic pickup at the eighth position for a total time period of 0.5 seconds. 101
7.35 Normalized amplitude spectrogram of a horizontal optical switch signal for a total time period of 0.05 seconds. 103
7.36 Normalized amplitude spectrogram of a vertical optical switch signal for a total time period of 0.05 seconds. 104
7.37 Normalized amplitude spectrogram of a horizontal optical switch signal for a total time period of 0.5 seconds. 104
7.38 Normalized amplitude spectrogram of a vertical optical switch signal for a total time period of 0.5 seconds. 105
7.39 Magnetic flux density over time for the signal from the magnetic pickup at the first position for a total time period of 0.05 seconds. 107
7.40 Magnetic flux density over time for the signal from the magnetic pickup at the eighth position for a total time period of 0.05 seconds. This was from the third iteration of the experiment. 107

7.41 Magnetic flux density over time for the signal from the magnetic pickup at the eighth position for a total time period of 0.05 seconds. This was from the second iteration of the experiment. 107
7.42 Magnetic flux density over time for the signal from the magnetic pickup at the fifth position for a total time period of 0.05 seconds. This was from the second iteration of the experiment. 108
7.43 Magnetic flux density over time for the signal from the magnetic pickup at the seventh position for a total time period of 0.05 seconds. 108
7.44 Magnetic flux density over time for the signal from the magnetic pickup at the first position for a total time period of 0.5 seconds. 108
7.45 Magnetic flux density over time for the signal from the magnetic pickup at the second position for a total time period of 0.5 seconds. 109
7.46 Magnetic flux density over time for the signal from the magnetic pickup at the third position for a total time period of 0.5 seconds. 109
7.47 Magnetic flux density over time for the signal from the magnetic pickup at the fourth position for a total time period of 0.5 seconds. 109
7.48 Magnetic flux density over time for the signal from the magnetic pickup at the fifth position for a total time period of 0.5 seconds. 110
7.49 Magnetic flux density over time for the signal from the magnetic pickup at the sixth position for a total time period of 0.5 seconds. 110
7.50 Magnetic flux density over time for the signal from the magnetic pickup at the seventh position for a total time period of 0.5 seconds. 110
7.51 Magnetic flux density over time for the signal from the magnetic pickup at the eighth position for a total time period of 0.5 seconds. 111
7.52 Magnetic pickup signal waveform of a bowed string of subjective force at the specified pickup position. 117

7.53 Magnetic pickup signal waveform of a bowed string of subjective force at the specified pickup position. 118
7.54 Magnetic pickup signal waveform of a bowed string of subjective force at the specified pickup position. 118
7.55 The frequency spectrum of the magnetic pickup signal of a bowed string of subjective force at the specified pickup position. 119
7.56 The frequency spectrum of the magnetic pickup signal of a bowed string of subjective force at the specified pickup position. 119
7.57 The frequency spectrum of the magnetic pickup signal of a bowed string of subjective force at the specified pickup position. 120
7.58 The spectrogram of the magnetic pickup signal of a bowed string of subjective force at the specified pickup position. 121
7.59 The spectrogram of the magnetic pickup signal of a bowed string of subjective force at the specified pickup position. 121
7.60 The spectrogram of the magnetic pickup signal of a bowed string of subjective force at the specified pickup position. 122
7.61 The magnetic flux density over time for the magnetic pickup signal of a bowed string of subjective force at the specified pickup position. 122
7.62 The magnetic flux density over time for the magnetic pickup signal of a bowed string of subjective force at the specified pickup position. 123
7.63 The magnetic flux density over time for the magnetic pickup signal of a bowed string of subjective force at the specified pickup position. 123
7.64 Magnetic pickup signal waveform of a plucked string of subjective force at the specified pickup position. 124
7.65 Magnetic pickup signal waveform of a plucked string of subjective force at the specified pickup position. 124

7.66 Magnetic pickup signal waveform of a plucked string of subjective force at the specified pickup position. 124
7.67 The frequency spectrum of the magnetic pickup signal of a plucked string of subjective force at the specified pickup position. 125
7.68 The frequency spectrum of the magnetic pickup signal of a plucked string of subjective force at the specified pickup position. 126
7.69 The frequency spectrum of the magnetic pickup signal of a plucked string of subjective force at the specified pickup position. 126
7.70 The spectrogram of the magnetic pickup signal of a plucked string of subjective force at the specified pickup position. 127
7.71 The spectrogram of the magnetic pickup signal of a plucked string of subjective force at the specified pickup position. 127
7.72 The spectrogram of the magnetic pickup signal of a plucked string of subjective force at the specified pickup position. 128
7.73 The magnetic flux density over time for the magnetic pickup signal of a plucked string of subjective force at the specified pickup position. 128
7.74 The magnetic flux density over time for the magnetic pickup signal of a plucked string of subjective force at the specified pickup position. 129
7.75 The magnetic flux density over time for the magnetic pickup signal of a plucked string of subjective force at the specified pickup position. 129

Chapter 1

Introduction

1.1 Amplification of Musical Instrument Sounds

Amplification of the sounds produced by musical instruments has always been a pertinent issue among musicians since the inception of instruments. Before the advent of electricity, achieving more amplification came from a heuristic development of instrument bodies, instrument material choices, and musical venue design. With electricity commonplace in the modern day, musicians experienced a great improvement in amplification of music, whether they found themselves in a music hall or a club setting.

There are various modern electrical methods for instrument amplification. Of these are the use of microphones, piezoelectric pickups, and magnetic pickups. Each use different methods of generating a voltage signal that is related to the amplitudes and frequencies of sounds produced by an instrument. The magnetic pickup began as a pursuit to amplify the acoustic guitar in swing bands featuring large brass sections that overpowered string instruments. The guitar was one of the lead instruments of a swing band and struggled to overcome the volume of brass instruments. In short, the magnetic pickup for musical instruments acts as a musical application of Faraday's Law of Induction, where string oscillation information is preserved in a proportional voltage wave signal or the mechanical vibrations

of the string are transformed into a voltage waveform. And it is this voltage waveform that can be amplified, what many refer to as amplifying an instrument.

As previously noted, magnetic pickups are not the only type of pickups for musical instruments. There also exist specifically designed microphones and piezoelectric pickups. Microphones are usually reserved for acoustic instruments and the complete sound of the instrument, as a whole system, is expressed. Piezoelectric pickups are more common for acoustic instruments as well. These optimize a piezoelectric effect on a crystal, which in turn produces a voltage. The stress experienced by the crystal is transformed into a voltage waveform, preserving the wave information in the pressures felt.

For bowed instruments like a violin, microphones and piezoelectric pickups are most common. But, there are very few magnetic pickups available commercially. And the ones that are, are not usually sought out. This thesis began with the question "why are magnetic pickups not common for bowed instruments?" With this in mind, analysis of a magnetic pickup and bowed string is pursued in this work.

1.2 Literature Survey

The recognized start of the sub-area of acoustics, bowed string dynamics, can be traced back to Helmholtz's work on the subject in 1863 [12]. It is through this work that the sawtooth-like displacement of a bowed string was first observed, which was subsequently named "Helmholtz motion." Raman advanced the area further with the introduction of an early theoretical model of a bowed string in the early twentieth century [26]. Further developments towards better theoretical models came from both Friedlander and Keller in the mid-twentieth century [8, 15]. Another key development of bowed string dynamics was by Schelleng, providing the "Schelleng Diagram" which describes general minimum and maximum bowing force bounds along the string to describe different types of sounds, be they pleasant or unlikable [31]. Schelleng contributed a plethora of contributions to the

area. Woodhouse is another key contributor to the area of bowed string dynamics [36]. Woodhouse and Galluzzo provide a cursory overview of the developments of this area from Helmholtz to the time of publication [36]. In the early 1980s, Cremer provided a commanding work, covering many physics topics of the violin, including very detailed work regarding the bowed string of a violin [4]. In the early 1990s, Ricca made contributions to bowed string dynamics through studying impedance to a bowed string by a bow [28]. Ricca's work also serves as one of few works that addresses damping of vertical string oscillations by the bow.

When discussing bowed string dynamics, certain nonlinear characteristics can be found. For a general elastic string, there is nonlinear coupling between the two transverse oscillations in the overall string displacement. This investigation started initially with Kirchhoff in 1883 but was later expounded upon by Carrier, resulting in the "Kirchhoff-Carrier Equations" [3]. These equations serve as a good modeling of average nonlinear string tension in a physical, elastic string. As it is a popular area of study, other authors who have made contributions to this area for either bowed string motion or general string motion are Bilbao, Tan, and Cremer (non-extensive) [2, 35, 4]. Another area concerning nonlinear effects in a physical string is the study of pitch glide. Near the initial instance of excitation of a string, a string can experience small changes in frequency. Kartofelev et al. and Lee et al. have made helpful contributions to this area [14, 19].

More recently, the areas of sound synthesis and more advanced modeling of bowed instruments are increasingly popular. A staple work for sound synthesis comes from Smith, detailing many concepts of audio signal processing [34]. Russo et al. have recently contributed to better modeling bowed string motion with nonlinear effects from the friction between the bow and string [30]. Akar and Willner recently took a finite element approach to modeling Helmholtz motion of a bowed string [1]. Mansour has provided a very detailed work towards developing even more accurate violin models [21]. Desvages has put forward a rich contribution for both modeling of a violin and work towards sound synthesis of the instrument [6]. For cost-effective experimental measurement of string oscillations, Le Carrou

et al. provide a concise and comprehensive work [18].

Alongside bowed string dynamics, nonlinear string behavior, and bowed instrument modeling and sound synthesis, there is also research being conducted for magnetic pickups which are common to guitar. Modeling of magnetic pickups is a popular and fruitful area, which Norton and Moore, Lemarquand and Lemarquand, Guadagnin et al., and Ray et al. have all contributed to [23, 20, 11, 27]. Perov et al. took an experimental route and developed experimental results in frequency analysis for a guitar and magnetic pickup setup [25]. In addition to modeling and frequency analysis with experiment, other authors have taken interest in the nonlinear effects generated by magnetic pickups in guitar signals. Novak et al. take an experimental and modeling approach to the topic [24]. Mustonen et al. contribute to the area of study by providing experimental results demonstrating nonlinear behavior in a string-magnetic pickup system [22].

There are many other notable contributors to the area of bowed string dynamics, nonlinearity in strings, electromagnetism for magnetic pickups, and modeling, simulation, and sound synthesis of bowed instruments that were not mentioned. But, of the authors and works mentioned, all provide excellent insight into these topics.

1.3 Purpose of Thesis

Suppose there is a monochord whose string is fixed along the x-axis such that when looking at the $y-z$ plane, the bridge is viewed in front of the nut and the string passes through the origin. The magnetic pickup's center is fixed at a specific x-position along the string. The cylindrical axis through the pickup can be rotated in the $y-z$ plane such that the axis is coincident with the origin and the pickup's exposed pole face looks inward on the string at a fixed distance from the string. Rotating this pickup cylindrical axis about the origin from 0 radians to any angle up to 2π radians rotates the pickup around the string the same amount. For this experiment specifically, eight magnetic pickup positions are considered,

equally spaced $\frac{1\pi}{4}$ radians or 45° from each other. So the positions are $\frac{0\pi}{4}$ to $\frac{7\pi}{4}$ every $\frac{1\pi}{4}$ radians. These positions of the pickup (note, not the direction in which they point) can be thought of as the cardinal and inter-cardinal directions: *east*, *northeast*, *north*, *northwest*, *west*, *southwest*, *south*, and *southeast*. An alternative naming convention of these positions, which is commonly used in this work, is: right horizontal, top right diagonal, top vertical, top left diagonal, left horizontal, bottom left diagonal, bottom vertical, and bottom right diagonal. An experiment repetition is conducted by exciting the string with a bow via the bow stroke mechanism at a constant string location, constant bow forces, and constant bow velocity, such that signals from appropriately placed optical switches (which will generate signals related to string displacement) and from the magnetic pickup at a position for that specific experiment repetition are recorded by an oscilloscope. These repetitions also all begin at the same time and with the same bow location. For the specific experiment repetition, the data is then post-processed and the specific results are obtained. This process is then repeated but for the next sequential position, such that the magnetic pickup is placed in that next position. With this in mind, the purposes of the work can be better understood.

The purpose of this thesis is multifaceted. A crucial component to this thesis, serving as part of its purpose, is to provide novel findings, through experimentation, for the behaviors of signal amplitude, frequency distributions, spectrograms, and magnetic flux density for a bowed string-magnetic pickup system. These results can help to inform the current theory of bowed string motion, particularly that of the vertical transverse bowed string equation, Eq. 2.1.14. In addition, the results of the experimentation can help to inform what sort of assumptions can be made regarding the use of Faraday's Law of Induction to simplify the problem for magnetic pickup modeling. Another key purpose of the thesis is to lay down the groundwork for designing a magnetic pickup for bowed instruments, particularly based on angling the magnetic pickup. Only a few patents for bridge motion actuated magnetic pickups of violins can be found for the past ninety years. There are a few luthiers who have made violins with magnetic pickups applied to the strings, but a quick overview of

market available electric violins would direct players almost exclusively to ones amplified through microphones or piezoelectric pickups. Better understanding bowed string motion and how electromagnetism figures in a magnetic pickup are essential to the design of a bowed instrument magnetic pickup. And the experimentation and its results involving a bowed string-magnetic pickup system can realize these theoretical descriptions and provide a foundation for a future design.

1.4 Hypothesis

Consider a bowed string-magnetic pickup system where the magnetic pickup can be rotated as described in Sec. 1.3. A few result types are considered. This work considers the effects in voltage, frequency distribution, frequencies over time, and magnetic flux density, as functions of magnetic pickup position around the monochord. This work posits that when considering the subset of 8 pickup positions, when a magnetic pickup is placed horizontally to a bowed string, it will produce the best outcomes in voltage output, frequency distribution, frequencies over time, and magnetic flux density. In addition, a vertically placed pickup will show that vertical transverse string displacement is significantly smaller than horizontal transverse string displacement for a bowed string, lending to useful assumptions for bowed string dynamics. The results of the experiment inform the governing equations for this work and will test the veracity of these hypotheses. Regardless of the outcome concerning the hypotheses, the results will in turn advance the development and design of a magnetic pickup for bowed instruments, which ares uncommon in musical circles.

1.5 Potential Advantages of a Magnetic Pickup

There are certain advantages that magnetic pickups enjoy and avoid certain disadvantages of other pickup designs. For this, magnetic pickups are considered in general and microphone and piezoelectric pickups specifically for violins. A fault of microphones is the potential

presence of background noise or any unwanted sound. Particularly for violin microphones (sometimes called gooseneck microphones), the microphone is pointed near and at the f-hole, which acoustically projects the violin's acoustic sound. One disadvantage to the microphone is that sounds made by the player like a sneeze or talking can also be picked up. Stage noise from other instruments or even the ambient sound of the room has the potential to interfere with the signal produced solely by the instrument. If a stationary microphone is being used, certain positional and ergonomic problems arise. The violinist's bodily movement and movement and direction of the violin's f-holes (the openings of the violin body that project a majority of the instrument's sound) invite many more variables when it comes to how the violin's sound is received. It should be noted that a gooseneck microphone avoids this issue, given its position is fixed always to the direction of sound projection coming from the violin f-hole. So the player is free to move without compromising amplification. The magnetic pickup on the other hand does not respond to sound waves. One could yell into a magnetic pickup and the yelling would not be picked up by the pickup or interfere with the signal from the instrument's strings' mechanical vibrations Sounds from the player or background noise does not affect the magnetic pickup. This can be demonstrated easily.

The piezoelectric pickup is a reliable pickup method, but still has downsides. For the violin, the use of a piezoelectric pickup typically necessitates the use of a "pre-amplifier" which is a device that allows the player to "soften" the signal, when the signal's higher frequencies are very amplified. Settings like "gain," "treble" "middle" and "bass" are typically seen. Gain nominally refers to the amplitude level of the input signal, while the latter three terms refer to frequency ranges where "treble" is usually the $1000 - 7000$ Hz range, "bass" the $20 - 250$ Hz range, and "middle," the $250 - 1000$ Hz range. For the piezoelectric pickup for violin, treble or higher frequencies are usually favored. This produces a sharp, nasally sound. Many professional violinists strongly suggest using a pre-amplifier to process the violin signal into a sound that is more usable and pleasant.

Another disadvantage of the piezoelectric pickup is that it has a higher risk of acoustic

feedback. The piezoelectric pickup functions on pressure more generally. Pressure waves can come from all vibrating parts of the violin, which will feed into the pickup's signal. There is a certain threshold to be cognizant of when amplifying a signal from a piezoelectric pickup or one runs the risk of having the signal being subject to a positive feedback loop. If a magnetic pickup were being used on an acoustic instrument, this problem is still there, but the difference is that the problem is scaled down because the magnetic pickup will only pickup the velocity of the vibrating ferromagnetic string. Vibrations of the whole acoustic body will have to first feed into the mechanical vibrations of the string before the magnetic pickup.

A magnetic pickup thrives best in a non-hollow instrument, where acoustic feedback is virtually eliminated. Acoustic amplification is not a problem to be solved as it was before the advent of electric amplification. A piezoelectric pickup would also thrive in a non-hollow instrument, but for many models, the extra cost of a pre-amplifier is a necessity.

To the best of the author's knowledge and literature survey, there is currently no research being conducted in the research area of magnetic pickup behavior for a bowed string-magnetic pickup system. The only works that could be found are early 1970s works on bowed string behavior that used a magnet of dense magnetic field as merely a measurement tool [32, 17]. Experimental frequency analysis, amplitude observations, and deriving magnetic flux density over time for a magnetic pickup whose signal comes from a bowed string has not yet been explored. Many works also focus on the horizontal transverse string displacement of a bowed string, but fewer look into vertical transverse string displacement of a bowed string. Ricca and Desvages are two authors that address this specific string displacement [28, 6]. Intuitively, these oscillations can be expected to be dampened by the bow, but aside from their contributions, considering an additional damping factor in relation to bow hair motion or an external force term to the bowed string equation for vertical transverse motion has not been investigated as much as other topics in bowed string dynamics. Given the effectiveness of a magnetic pickup is a function of directional dependence through the angle between the

area vector of the measurement coil and an arbitrary magnetic field line, having equations that capture key behaviors of bowed string motion is important. For future works, modeling of a bowed string-magnetic pickup system would benefit greatly from this acknowledgement of significant vertical oscillation dampening and directional dependence of a magnetic pickup.

1.6 Overview of Study

This thesis is structured as follows. Chapter 2 consists of an overview of bowed string theory overview and development, connecting certain governing equations of bowed string dynamics to Faraday's Law of Induction. It provides a rotational and translational transformation of coordinates for an analytic model for components of a magnetic pickup's magnetic field. It also briefly describes the need for a modified dampening factor term or external force term to account for the dampening of vertical string oscillations of a bowed string.

Chapter 3 includes a discussion of key parameters and dimensions of the experiment. It also includes a discussion on the design and construction of the experiment's different components.

Chapter 4 covers the collection of data from the measurement tools of the experiment. This covers how the measurement tools operate and how they are used. And it also provides a procedure for how a full experiment iteration of experiment repetitions is conducted.

Chapter 5 goes into detail on the post-processing of the collected data. There are a group of results that will be considered, concerning voltage outputs, frequency distributions, frequency distributions over time, and magnetic flux density over time. These results inform the investigation and will provide better insight into what magnetic pickup position is the most optimal given such results and will also provide insight into the governing bowed string equations and the modified Faraday's Law of Induction equation. The results also provide a foundation for the design of a magnetic pickup for a bowed instrument.

Chapter 6 provides a discussion of results that resemble and correlate with results from

previous authors in the field of acoustics, string dynamics, and electromagnetism (focusing on magnetic pickups). In addition, this work also makes note of certain common quantities or general results (particularly voltage output, magnetic flux density, and tonal theory) of electric guitar magnetic pickups which are very common and reliable as products. Certain results from the experiment can be compared to these expected results, lending to the viability of a magnetic pickup design for bowed instruments.

Chapter 7 details the results of the experiment and provides discussion and analysis of them. The specific results of the experiment repetition signals are the maximum and average voltage outputs, frequency spectra, spectrograms, and magnetic flux density over time.

Finally, Chapter 8 concludes the investigation and summarizes the work overall. In addition, suggestions for improvement to the experiment were given and future areas of potential research are proposed.

Chapter 2

Theory Overview and Exploration

The main purpose of this chapter is to provide a theoretical underpinning to the bowed string motion of the experiment, the behavior of the magnetic field, the generation of voltage from a magnetic pickup, and the rotation of the magnetic field of the magnetic pickup in relation to transverse string displacements which remain directionally constant throughout the experiment. In these, a thread is connected between all of them, showing how the governing equations of bowed string motion are present in Faraday's Law of Induction applied to a magnetic pickup and how the magnetic field of said pickup can be rotated to correlate with the main experiment variable in consideration, rotation of the magnetic pickup's position. With these equations to be developed, a foundation is laid for the discussion of adding an extra damping factor or external force term to account for significant damping from the bow to the vertical string oscillations. With this in mind, a brief qualitative consideration of the interactions between the string and bow as the string vertically oscillates is given. There are various results of specific result types in Chapter 6 and Chapter 7 that will indicate significant damping of the vertical string oscillations. And with respect to the magnetic pickup, a theoretical foundation and understanding of Faraday's Law of Induction is needed for deriving an approximate solution for magnetic flux density over time using the voltage signals derived from the experiment.

2.1 Development of Bowed String Equations

The motions of a bowed string come in the form of waves and can partially be described using the wave equation as the foundation. One may first consider the unsteady, second-order partial differential equation, the 1-D wave equation,

$$\frac{\partial^2}{\partial t^2}u(x,t) = c^2\frac{\partial^2}{\partial x^2}u(x,t), \tag{2.1.1}$$

where $u(x,t)$ is the displacement of the wave and c is the wave speed.

Building off of Eq. 2.1.1, a system of transverse wave equations can be constructed. A wave is called a transverse wave if the propagation of the wave is perpendicular to the direction of its oscillations. For example, a transverse wave that oscillates up and down will have its wave travel from left to right. Therefore, it is useful to consider transverse waves with the use of 1-D wave equations like Eq. 2.1.1. Consider a 3-dimensional space with the z-axis as the vertical axis. A system of transverse wave equations is then,

$$\frac{\partial^2}{\partial t^2}\eta(x,t) = c_t^2\frac{\partial^2}{\partial x^2}\eta(x,t), \tag{2.1.2}$$

$$\frac{\partial^2}{\partial t^2}\zeta(x,t) = c_t^2\frac{\partial^2}{\partial x^2}\zeta(x,t), \tag{2.1.3}$$

where $\eta(x,t)$ is the transverse displacement of a wave in the y-direction, $\zeta(x,t)$ is the transverse displacement in the z-direction, and c_t is the transverse wave speed. The system, Eq. 2.1.2 and Eq. 2.1.3 can be extended to a physical string, once string mass and string tension is considered. It should be noted, too, that $\eta(x,t)$ is the horizontal transverse displacement of the string and $\zeta(x,t)$ is the vertical transverse displacement of the string. Recall the coordinates in relation to the monochord detailed in Sec. 1.3. Following Cremer's definition and extending it to the present system of wave equations, if the transverse wave speed were defined as,

$$c_t = \sqrt{\frac{F_s}{m'_s}}, \tag{2.1.4}$$

then Eq. 2.1.2 and Eq. 2.1.3 become,

$$m' \frac{\partial^2 \eta_s}{\partial t^2} - F_s \frac{\partial^2 \eta_s}{\partial x^2} = 0, \tag{2.1.5}$$

$$m'_s \frac{\partial^2 \zeta_s}{\partial t^2} - F_s \frac{\partial^2 \zeta_s}{\partial x^2} = 0, \tag{2.1.6}$$

where F_s is the constant string tension, and m'_s is the string mass per unit length [4]. And because this study concerns itself with a physical string, stiffness is also present in the governing equations. This introduces a fourth-order term to each equation of system, Eq. 2.1.5 and Eq. 2.1.6, so that the following is defined as such,

$$m'_s \frac{\partial^2 \eta_s}{\partial t^2} - F_s \frac{\partial^2 \eta_s}{\partial x^2} + B \frac{\partial^4 \eta_s}{\partial x^4} \eta_s = 0, \tag{2.1.7}$$

$$m'_s \frac{\partial^2 \zeta_s}{\partial t^2} - F_s \frac{\partial^2 \zeta_s}{\partial x^2} + B_s \frac{\partial^4 \zeta_s}{\partial x^4} = 0, \tag{2.1.8}$$

where $B_s = E_s \frac{a^2 \pi}{4}$ such that E_s is the string's Young Modulus and a is the radius of the string.

Again, following Cremer, dampening is also considered for the string equations [4]. A physical string is not a lossless system. There is dampening of the string oscillations due to friction with air. With the damping factor, viscous impedance per unit length for a string, r'_s, the system, Eq. 2.1.7 and Eq. 2.1.8, becomes,

$$m_s' \frac{\partial^2 \eta_s}{\partial t^2} + r_s' \frac{\partial \eta_s}{\partial t} + B_s \frac{\partial^4 \eta_s}{\partial x^4} - F_s \frac{\partial^2 \eta_s}{\partial x^2} = 0, \tag{2.1.9}$$

$$m_s' \frac{\partial^2 \zeta_s}{\partial t^2} + r_s' \frac{\partial \zeta_s}{\partial t} + B_s \frac{\partial^4}{\partial x^4} - F_s \frac{\partial^2 \zeta_s}{\partial x^2} = 0 [4]. \tag{2.1.10}$$

With the system, Eq. 2.1.9 and Eq. 2.1.10, a good foundation is laid to then extending the use of the wave equation to the topics aimed in this investigation. The wave equation theory will extend to a continuous excitation force from a bow, nonlinearity, and a coupled system.

It is simple enough to incorporated bowing into the system of string equations. With the same axes convention, suppose that a violin bow makes continuous contact with the string at a specific x value and thus applies a continuous excitation force to the string for a specific amount of time. With this in mind, a force term can be introduced to both transverse equations for string motion. A force is applied downward and tangentially across the string (which for this study is assumed to be applied directly to the center of the string instead) So, the system, Eq. 2.1.9 and Eq. 2.1.10 become,

$$m_s' \frac{\partial^2 \eta_s}{\partial t^2} + r_s' \frac{\partial \eta_s}{\partial t} + B_s \frac{\partial^4 \eta_s}{\partial x^4} - F_s \frac{\partial^2 \eta_s}{\partial x^2} = F_{y,s}'(x,t), \tag{2.1.11}$$

$$m_s' \frac{\partial^2 \zeta_s}{\partial t^2} + r_s' \frac{\partial \zeta_s}{\partial t} + B_s \frac{\partial^4}{\partial x^4} - F_s \frac{\partial^2 \zeta_s}{\partial x^2} = F_{z,s}'(x,t). \tag{2.1.12}$$

The two transverse oscillations of the bowed string can exhibit coupled and nonlinear behavior due to nonlinear string tension. Kirchhoff and Carrier introduced a nonlinear coupling factor for string tension, because there is a tendency of physical strings to have oscillations of different planes to transfer energy to one another and have string tension change with respect to different components of position. This means that the initial constant tension term, F_s, will be replaced. The new factor is an average of the sum of the squared

spatial change of either displacement. Converting the system, Eq. 2.1.11 and Eq. 2.1.12, to a Kirchhoff-Carrier form renders,

$$m_s' \frac{\partial^2 \eta_s}{\partial t^2} + r_s' \frac{\partial \eta_s}{\partial t} + B_s \frac{\partial^4 \eta_s}{\partial x^4} - (T_{s,0} + N_s) \frac{\partial^2 \eta_s}{\partial x^2} = F_{y,s}'(x,t), \tag{2.1.13}$$

$$m_s' \frac{\partial^2 \zeta_s}{\partial t^2} + r_s' \frac{\partial \zeta_s}{\partial t} + B_s \frac{\partial^4 \zeta_s}{\partial x^4} - (T_{s,0} + N_s) \frac{\partial^2 \zeta_s}{\partial x^2} = F_{z,s}'(x,t) \tag{2.1.14}$$

such that $T_{s,0}$ is the initial string tension and

$$N_s = \frac{E_s A_s}{2L} \int_0^L \left[\left(\frac{\partial \eta_s}{\partial x} \right)^2 + \left(\frac{\partial \zeta_s}{\partial x} \right)^2 \right] dx, \tag{2.1.15}$$

where E_s is, again, the string's Young Modulus, $A_s = \frac{a^2 \pi}{4}$ is the cross-sectional area of the string, and L is the length of the string [16, 3, 35].

When discussing bowed string motion, Helmholtz motion should be addressed, which is the horizontal string oscillations. Friction between the bow and string is the root of Helmholtz motion. When static friction is high between the bow and string, for a rosined bow particularly, the string "sticks" to the bow causing a kink (as seen from the $x-y$ plane, the "bird's-eye-view") in the string to travel from the bow-string interface. This is the stick regime and the string segments on either side of the interface moves in the same direction as the bowing direction. Once the kink travels down the string and reflects back from either end point, when it returns to the interface, the string "slips", enabling slipping friction with the bow. This is the slip regime and the string segments on either side of the interface move in the opposite direction of the bowing direction. Once the string approaches the speed of the bow and moves in the same direction, the stick regime begins. This is a periodic cycle which lasts for as long as the string is continuously excited by the bow. The aforementioned kink travels along the path of an envelope comprised of two parabolic segments, which both intersect at both string end points, mirrored about the x-axis. For a bowed string excited

near an end point, more harmonic frequencies will be present, generating a richer sound. A plucked string's higher frequencies will dissipate quickly after the moment of excitation. In contrast, a bowed string will sustain its higher frequencies as long as the bow continues to excite it.

Associated with Helmholtz motion is the displacement of the string segment, η_s, at time, t. Akar and Willner provided an example of what Helmholtz motion displacement should ideally look like [1]. It resembles a sawtooth waveform. Using Schelleng's Diagram, they provide additional figures to show the displacement over time for bowed strings experiencing different amounts of bow forces [32]. Along with Helmholtz motion displacement, there can be multiple slip motion and no periodic motion, which indicates excessive sticking. In relation to Schelleng's diagram, this makes sense. More slips would occur if there were not enough downward and horizontal bow force applying enough static friction at the bow-string interface and this would cause an empty, high-frequency-oriented sound. Similarly, too much sticking would occur if there is excessive downward and horizontal bow force, not allowing enough slipping friction to occur at the bow-string interface. This would result in a raucous sound. Though, there are other ways through which sticking or slipping can occur, such as the amount of rosin applied to the bow. These considerations will be important for Sec. 7.6.

2.2 Faraday's Law of Induction

One of the crucial aspects of this investigation is the application of electromagnetism, specifically Faraday's Law of Induction. It is thus beneficial to review how Faraday's Law works with respect to a magnetic pickup. Consider a magnetic field produced by a cylindrical magnet with a copper coil wrapped around it such that the entire coil's surface area, S_c, changes with respect to space, radially, in the $x-y$ plane. This surface area is also parallel to the poles of the magnet. Above this magnet is a ferromagnetic string, which is in turn magnetized by the magnet. The magnetic field, $\overrightarrow{B}$, of the magnet and magnetized string

has field lines which represent the direction of magnetic force from the magnet. Faraday's Law of Induction essentially states that an electromotive force or a voltage induced by a source (not to be conflated or confused with a voltage resulting from a potential difference) is generated by the change of the number of field lines of a magnetic field passing through the areas of the whole coil, such that there are certain angles, θ_B, between the area vector (which is perpendicular to the coil areas) and field lines of the magnetic field.

One of the goals of a magnetic pickup using Faraday's Law of Induction is to affect greater magnetic flux, the number of field lines passing through the entire coil surface. This does not induce greater voltage output, but if magnetic flux were to go from a large amount to a small amount, then a greater voltage would be induced. There are three key ways to increase magnetic flux. One could change the maximum size of the coil areas and increase the number of coils, decrease the angle between the area vector and the field lines, or change the magnetic field with a ferromagnetic string such that the field lines concentrate in the coil areas. This list is not exhaustive. For example, a diamagnetic string, such as a string with silver content, could be used to change the magnetic field, though it is not ferromagnetic. For a magnetic pickup, enough voltage signal is desired, such that there is enough of a signal to be amplified without loss of tonal quality.

Consider the entire coil of the previously mentioned magnetic pickup. Its surface area is in effect a large annulus. Within the annulus are coil areas of varying sizes. Increasing magnetic flux can come from increasing the size of this large annulus. This would be such that there would be more larger coils and more coils as well.

The angle between the area vector and field lines, which is defined in the associated dot product between the area vector and the magnetic field, can be reduced by decreasing the distance between the magnet and the ferromagnetic string. Again, large magnetic flux alone does not induce voltage. Large change in magnetic flux over time, however, does induce a larger voltage output.

Changing the magnetic field can both increase and decrease magnetic flux. This can be

done with the oscillations of a ferromagnetic string. In short, certain oscillations of the string can contract the field into the coil surface areas and detract it out of them. This produces an oscillatory voltage, related to the mechanical vibrations of string velocity. As a reiteration, consider the following. Consider a magnetic pickup that has a coil surface area parallel to the poles of the magnet. These coil surface areas are also situated near the bottom pole face along the z-axis. There is also a ferromagnetic string above the top pole face.

Suppose that the displacement over time of a segment of the string is taken to be a 2-D vector whose components are the horizontal and vertical transverse string displacements. An almost necessary condition, or, at least, a more practical requirement, to increasing magnetic flux for a magnetic pickup and ferromagnetic string is to angle the pickup such that at least one of the component vectors of displacement has a small angle between it and the area vector. Note that transverse string displacements for a 3-D string are ideally perpendicular, so usually only one form of displacement will share a small angle with the area vector. This small angle, ideally 0 radians, between the specific transverse displacement component vector and the area vector ensures that the pickup is positioned in a direction where string oscillations can contract more of the magnetic field into the coil surface areas and detract more of the magnetic field out of the surface areas. Less field lines are available for contraction and detraction through the surface the further they are from being perpendicular to the surface. During contraction, the string is closer to the pole face and there is greater magnetic flux. During detraction, the string is further from the pole face and there is less magnetic flux.

Consider the other component vector that has a large angle between it and the area vector, ideally $\frac{\pi}{2}$ radians. The oscillations in this direction will not contract and detract the magnetic field through the surface areas. With these oscillations, the magnetic field would seem to "rock" from side to side or experience a side-to-side deformation similar to strain on an elementary volume. This instead would produce little change in magnetic flux. So, greater change in magnetic flux with respect to time occurs where the string oscillates to

and fro the pole face. But if it oscillates across the pole at a fixed height, there will be much lower change in magnetic flux over time or virtually none.

There are some simple scenarios to further contextualize this behavior. Consider again a magnetic pickup with a magnetized ferromagnetic string above its top pole face. Vertical string oscillations will effect greater magnetic flux over time for a vertical area vector. Horizontal string oscillations will effect greater magnetic flux over time for a horizontal area vector. Vertical and horizontal string oscillations will effect greater magnetic flux over time for a diagonal area vector, given it is composed of vertical and horizontal component vectors. In these three scenarios, contraction and detraction of the magnetic field through the coil surface areas occur. This in turn will generate large voltage outputs.

This introduction serves as a good foundation for extending Faraday's Law of Induction for the purposes of this thesis. A few things are to be accomplished in this section. Faraday's Law of Induction will be extended to include the dimensions of a copper coil. Under certain simple assumptions, the equation can be used to process voltage signal data to achieve results in magnetic flux density over time. This in turn makes it possible to show how Faraday's Law of Induction is mathematically connected to the solutions of the system of wave equations defining the transverse displacements of a bowed string, Eq. 2.1.13 and Eq. 2.1.14 through provided analytical definitions of magnetic field components for a magnetic pickup. Following this specific section, it will also be shown how the magnetic field components for the magnetic pickup can be mathematically transformed such that the definitions of the components correspond to the physical rotation of the experiment's magnetic pickup and its magnetic field in the $y-z$ plane.

Faraday's Law of Induction can be expressed as,

$$U(t) = -\frac{\partial}{\partial t}\left(\int\int_{S_c}\left(\overrightarrow{B}(t)\cdot\hat{n}\right)dS_c\right), \tag{2.2.1}$$

where $U(t)$ is the voltage (electromotive force in volts) over time, dS_c is the elemental surface

area of the coil, $\overrightarrow{B}(t)$ is the magnetic field as it is perturbed over time, and $\hat{n}$ is the unit vector normal to the coil surface area, the area vector as previously mentioned. Eq. 2.2.1 can be extended to include the number of revolutions of present in a coil. This results in,

$$U(t) = -N_c \frac{\partial}{\partial t} \left(\int \int_{S_c} \left(\overrightarrow{B}(t) \cdot \hat{n} \right) dS_c \right), \tag{2.2.2}$$

such that N_c is the number of revolutions in the coil of the magnetic pickup. This scaling of the effects of one coil is done to substitute the solving of Faraday's Law of Induction for all coils of the same area. But, as Eq. 2.2.2 stands, it fails to capture a physical aspect of the coil. As it will be shown in Sec. 3.4, the coil of the magnetic pickup changes with respect to x and y or radially. This should not be conflated with the proposition that the magnetic field changes with respect to x and y inside the coil. This spatial change in the coil is evident by the fact that an innermost coil is smaller than an outermost coil. Thus, the number of revolutions in the entire coil is also dependent on x and y. This ought to be reconciled in this section and especially for Sec. 6.2 where magnetic flux density over time is to be derived from the experiment's magnetic pickup signals. Accounting for the variation in coil area allows for the introduction of some simple assumptions for Eq. 2.2.2. In this reduction is also an opportunity to introduce a basic modeling for a non-uniform magnetic field.

Looking to the derivative term in Eq. 2.2.2, the integral term, which is definitionally, magnetic flux, Φ_B, can be approximated as,

$$\sum_{i=1}^{n} N_{ci} S_{ci} \times \frac{1}{n} (\overrightarrow{B}(t) \cdot \hat{n})_i, \tag{2.2.3}$$

such that $\frac{1}{n}$ is a scaling factor for the iterative dot product term. In Eq. 2.2.3, S_{ci}, is an annular area which can not exceed the inner and outer radii of the magnetic pickup's entire coil, r_1 and r_2 as defined later in Sec. 3.4. With each S_{ci} is an associated number of coil revolutions, N_{ci}, which is dependent on the annular area's specific inner and outer radii. In

the same way that the total number of coil revolutions in the entire magnetic pickup coil was deduced in Sec. 3.4, the number of coil revolutions can be approximated for these discretized annuli elements. $n \in \mathbb{N}$ is the number of discretized annuli for the coil, bounded by the entire coil's inner and outer radii. For the dot product term, $(\overrightarrow{B}(t) \cdot \hat{n})_i = \overrightarrow{B}_i(t)\cos(\theta_i)$. This is such that $\overrightarrow{B}_i(t)$ is locally uniform for its corresponding annulus of same index, the same annulus. This field is considered only when it passes through that annulus. Another step in approximating or modeling the non-uniform magnetic field, $\overrightarrow{B}(t)$, is to artificially apply an angle (which is ordinarily obtained passively due to the non-uniformity of the vector field when applied in a dot product), θ_i, between the locally uniform magnetic field segment, $\overrightarrow{B}_i(t)$ and the area vector, $\hat{n}$. Note that the use of the index, i and the angle, θ_i, has no relation to the uses of i and θ in Sec. 2.3 which is concerned with transforming coordinates to rotate and translate a magnetic field in space. With the related previous assumption of local uniformity, the composition of locally uniform magnetic field segments serves to supplant the surface integral in the same way that a globally uniform magnetic field would allow for. With this in mind, from Eq. 2.2.3, follows

$$\sum_{i=1}^{n} N_{ci}S_{ci} \times \frac{1}{n}B_i(t)\cos\left(\alpha\frac{i}{n}\right) \tag{2.2.4}$$

under the assumption that the angles between $\overrightarrow{B}_i$ and $\hat{n}$ are equal, resulting in $\theta_i = \alpha\frac{i}{n}$ for some α, the maximum angle of segmented field orientation, which must be declared regardless of angular spacing being equal or not. To progress, the summation of products in Eq. 2.2.4 becomes the multiplication of sums,

$$\left(\sum_{i=1}^{n} N_{ci}S_{ci}\cos\left(\alpha\frac{i}{n}\right)\right) \times \left(\frac{1}{n}\sum_{i=1}^{n} B_i(t)\right), \tag{2.2.5}$$

such that for $a_i = N_{ci}S_{ci}\cos\left(\alpha\frac{i}{n}\right)$ and $b_j = B_j(t)$, $a_ib_j = 0$ if and only if $i \neq j$, which also implies index of b_j thus becomes i. With this assumption, suppose that,

$$\frac{1}{n}\sum_{i=1}^{n} B_i(t) \approx B(t), \tag{2.2.6}$$

where $B(t)$ is the magnetic flux density over time. The purpose of this approximation or model of the non-uniform magnetic field is to have the composition of locally uniform vector fields, $\overrightarrow{B_i}(t)$, behave similarly to the actual non-uniform vector field near the magnet's bottom pole face where the coil areas are to be found (recall the bottom of the entire coil is approximately 2.73 mm above the lower magnet pole face). It should be noted that the effects of the coils along the length of the magnet in the z direction are assumed to be captured in the multiplication of the areas of an arbitrary annulus they subside in respectively, S_{ci}, by the number of revolutions, corresponding to the said arbitrary annulus, N_{ci}. With Eq. 2.2.5 and Eq. 2.2.6, Faraday's Law of Induction applied to a magnetic pickup, Eq. 2.2.2, can be approximated as

$$U(t) \approx -\frac{1}{n}\frac{\partial}{\partial t}\left(\left(\sum_{i=1}^{n} N_{ci}S_{ci}\cos\left(\alpha\frac{i}{n}\right)\right) \times B(t)\right). \tag{2.2.7}$$

Only magnetic flux density changes with respect to time in Eq. 2.2.7, so it becomes,

$$U(t) \approx -\frac{1}{n}\left(\sum_{i=1}^{n} N_{ci}S_{ci}\cos\left(\alpha\frac{i}{n}\right)\right)\frac{\partial}{\partial t}B(t). \tag{2.2.8}$$

For the purposes of sufficiently defining the governing equations for this work and specifically for the bowed string-magnetic pickup system, analytical expressions for the magnetic field components from Guadagnin et al. are defined. These magnetic field components are for a non-uniform magnetic field, which is fitting for establishing a theoretical connection between the bowed string equations to Faraday's Law of Induction. For $\overrightarrow{B}(t)$, components, B_y and B_z, can be defined as,

$$B_y(y,z,t) = 2B_0\xi\frac{(y-y_s)(z-z_s)}{((y-y_s)^2+(z-z_s)^2)^2}, \tag{2.2.9}$$

$$B_z(y,z,t) = B_0\left(1+\xi\frac{(z-z_s)^2-(y-y_s)^2}{((y-y_s)^2+(z-z_s)^2)^2}\right), \tag{2.2.10}$$

where $y_s = y_s(t)$, $z_s = z_s(t)$, and $\xi = a^2\frac{\mu_r-1}{\mu_r+1}$ such that a is the string's radius, as mentioned when defining Eq. 2.1.8, and such that the linear relative permeability, μ_r, is equal to $\frac{\mu}{\mu_0}$, the ratio of material permeability and vacuum permeability [11]. In these equations, y_s is the horizontal transverse string displacement in the $x-y$ plane and z_s is the vertical transverse string displacement in the $x-z$ plane.

With these components definitions, Eq. 2.2.9 and Eq. 2.2.10, in mind, Eq. 2.2.8 can be expressed as,

$$\frac{\partial}{\partial t}\left(\sqrt{B_y^2+B_z^2}\right) \approx \frac{-n}{\left(\sum_{i=1}^{n} N_{ci}S_{ci}\cos\left(\alpha\frac{i}{n}\right)\right)} \times U(t). \tag{2.2.11}$$

Eq. 2.2.11 is a fittingly developed equation towards the goals of this thesis because there is now an expression which relates the reduction of Faraday's Law of Induction to the signal of the magnetic pickup, which only relays voltage over time.

With Eq. 2.2.11, it is also true that,

$$U = U(t) = U(y,z,t) = U(y,z,y_s(t),z_s(t)), \tag{2.2.12}$$

$$B_y = B_y(y,z,t) = B_y(y,z,y_s(t),z_s(t)), \tag{2.2.13}$$

$$B_z = B_z(y,z,t) = B_z(y,z,y_s(t),z_s(t)). \tag{2.2.14}$$

Eq. 2.2.12, Eq. 2.2.13, and Eq. 2.2.14 simply state that voltage over time and the magnetic field are functions of both transverse string displacements over time. So that it may be formally stated, this revelation results in the following,

$$y_s(t) = \eta(x,t), \tag{2.2.15}$$

$$z_s(t) = \zeta(x,t). \tag{2.2.16}$$

In this section, an approximation of Faraday's Law of Induction was defined in Eq. 2.2.8, which includes a rudimentary discretizing model of a non-uniform magnetic field. This equation can be used for post-processing of the experiment data with respect to solving for magnetic flux density over time. In addition, with Eq. 2.2.15 and Eq. 2.2.16, the connection between the bowed string equations and Faraday's Law of Induction has been demonstrated. This is fitting for this work, which intends to learn more of the behavior of the bowed string-magnetic pickup system. But, the rotation of the magnetic pickup in relation to the transverse string displacements must also be accounted for in the theory for this type of system. If the pickup is rotated in the $y-z$ plane about the string's center, its magnetic field and coils, which are spatially fixed relatively to one another, are rotated as well. But the string displacements remain the same spatially. Sec. 2.3 develops a matrix transform for an arbitrary 2-D vector field, which can be applied to the y and z arguments of the magnetic field components.

2.3 Rotating the Components of a Magnetic Field

Consider again the components of the magnetic field, Eq. 2.2.13 and 2.2.14, of a magnetic pickup with a single cylindrical magnet centrally located, surrounded by a coil, such that the bottom of the whole coil is coincident with the $x-y$ plane, meaning 2.73 mm of the magnet along its own axis protrudes below the $x-y$ plane. With this placement, the pickup would be at the $\frac{3\pi}{2}$ position if it were being rotated about the string's center, which is taken to be centered through the $y-z$ plane at its origin.

With the transverse string displacement terms present in the magnetic field component

equations, it is possible to define the magnetic field components in terms of the string equation solutions, but only in one position, the aforementioned $\frac{3\pi}{2}$ position, with the bottom of the coil coincident with the origin, perpendicular to the original z-axis, such that the magnet's cylindrical axis is collinear with the z-axis. Note that the magnetic field component equations are also functions of y and z as well. This thesis is primarily concerned with the effects of rotating the magnetic pickup while string displacement in both transverse planes remain sufficiently constant (depending mostly on the consistency of the bow stroke mechanism). While the string displacements remain the same spatially, the y and z arguments of Eq. 2.2.13 and Eq. 2.2.14 can be transformed to match the rotation of the magnetic pickup around the string. This transformation of the y and z arguments is comprised of two rotation matrices and a translation matrix. This leads to the rotation definition,

Definition 1. *First let the $y-z$ plane be such that the pickup coil's bottom is coincident with the horizontal y-axis (this assumption is only made for the rotation of the magnetic field, while considering the monochord in practice takes the origin of the $y-z$ plane to be intersected by the string along the x-axis). Let y and z be coordinates of the $y-z$ plane which make up and is equivalent to the vector, $[y \;\; z]^T$. Let θ be some angle of rotation about the point, $(0, (d_s + d_c))$, denoting the position of a magnetic pickup around a monochord string, such that, d_s is the distance of the magnetic pickup's inward facing pole to the string, h_m is the length of the magnet, and c_b is the depth of the bobbin cavity that holds the magnet in place in the pickup bobbin, and $d_c = (h_m - c_b)$ is distance from the bottom of the pickup coil to the string-facing magnet pole face. Let ϕ be the angle between $[y \;\; z]^T$ and the positive y-axis.*

Then,

$$R_{mag}\left((y,z) \equiv \begin{bmatrix} y \\ z \end{bmatrix}, \theta\right) \equiv (y_{i,j}, z_{i,j}) \equiv \begin{bmatrix} y_i \\ z_i \end{bmatrix}_j,$$

such that,

$$R_{mag}\left((y,z) \equiv \begin{bmatrix} y \\ z \end{bmatrix}, \theta\right)$$

$$= \begin{bmatrix} \cos\psi_{i,j} & -\sin\psi_{i,j} \\ \sin\psi_{i,j} & \cos\psi_{i,j} \end{bmatrix} \cdot \begin{bmatrix} \cos(-\phi_i) & -\sin(-\phi_i) \\ \sin(-\phi_i) & \cos(-\phi_i) \end{bmatrix} \cdot \begin{bmatrix} y \\ z \end{bmatrix} + \begin{bmatrix} (d_s + d_c)\cos\theta_j \\ (d_s + d_c)\sin\theta_j + (d_s + d_c) \end{bmatrix},$$

where

$$j = \begin{cases} 1 & \theta \in [0, \frac{\pi}{2}) \\ 2 & \theta \in [\frac{\pi}{2}, \pi) \\ 3 & \theta \in [\pi, \frac{3\pi}{2}) \\ 4 & \theta \in [\frac{3\pi}{2}, 2\pi) \end{cases}, \quad \theta = \theta_j \ , \ (sgn(y) = 1) \Rightarrow i = \begin{cases} 1 & sgn(y) = sgn(z) = 1 \\ 2 & sgn(y) = -1 \ \wedge \ sgn(z) = 1 \\ 3 & sgn(y) = sgn(z) = -1 \\ 4 & sgn(y) = 1 \ \wedge \ sgn(z) = -1 \end{cases},$$

$$(sgn(y) = -1) \Rightarrow i = \begin{cases} 1 & sgn(-y) = sgn(z) = 1 \\ 2 & sgn(-y) = -1 \ \wedge \ sgn(z) = 1 \\ 3 & sgn(-y) = sgn(z) = -1 \\ 4 & sgn(-y) = 1 \ \wedge \ sgn(z) = -1 \end{cases},$$

$$\phi_i = \frac{i\pi}{2} - \tan^{-1}\left(\frac{y_i^{imod2} \cdot z_i^{(i+1)mod2}}{y_i^{(i+1)mod2} \cdot z_i^{(i)mod2}}\right) \quad , \quad and \ \ \psi_{i,j} = \theta_j + \phi_i + \frac{\pi}{2}.$$

A proof is not provided for this definition but rather a demonstration. The index, j, refers to what quadrant the magnetic pickup is rotated to about the new origin point, the center of a cross-section of the string. This is why $\theta = \theta_j$ for computational and definitional purposes. The z-axis remains the same, though the new y-axis, the y_1-axis, has moved up

$(d_s + d_c)$. Thus, j indexes through the new quadrants of these axes.

The index, i, refers to what the original quadrant $[y \;\; z]^T$ lies in with respect to the original axes, the z-axis and y_0-axis, and original origin. Assigning an original quadrant index, i, for a pair of coordinates or $[y \;\; z]^T$ in question depends on the sign of each coordinate. The $sgn(x)$ function for y and z was used to define the index i for $[y \;\; z]^T$. Though if y were negative, $sgn(-y)$ was used instead.

ϕ_i defines the angle between $[y \;\; z]^T$ and the positive y_0-axis. It was defined in such a way that it is general to a vector of any quadrant with the use of basic trigonometry, the modulo function, and the quadrant index, i, derived from the vector's respective coordinate signs. The first rotation matrix of R_{mag} rotates $[y \;\; z]^T$ clockwise back such that the vector is collinear with the positive y_0-axis. It can be said that $[y \;\; z]^T$ "collapses" into said axis. This allows one to think of the rotation of the axes instead of the rotation of y and z coordinates. The rotation of these axes will depend on θ_j.

To correctly rotate $[y \;\; z]^T$ back to its original position relative to the θ_j-dependent rotated axes, called z_θ and y_θ, requires an expression that incorporates both θ_j and ϕ_i. Here it is beneficial to visualize the rotated axes, z_θ and y_θ, *and* a rotated $[y \;\; z]^T$ such that a translation has already taken place such that the origin of the z_θ and y_θ axes lies along a circle which is centered at $(0, (d_s + d_c))$, of radius, $(d_s + d_c)$, where the positive z_θ-axis faces inward of said circle, passing through its center. Of course, this image prematurely describes the translation matrix's function, but this is only part of better demonstrating how R_{mag} can be derived. With this visualization in mind, also visualize that the original axes, z_0 and y_0, have been translated such that its origin is coincident with the origin of the rotated axes. The z_θ-axis runs through two parallel axes, the y_1-axis that passes through $(0, (d_s + d_c))$ and the superimposed original positive y_0-axis. Thus, there is a corresponding angle between the y_1-axis and the superimposed y_0-axis, θ_j. The positive y_1-axis is considered because it is from that axis that θ_j is defined. The magnetic pickup rotates θ_j around the string at $(0, (d_s + d_c))$ in the $y - z$ plane.

Suppose there is an arbitrary θ_j, θ_a, and arbitrary ϕ_i, ϕ_a, corresponding to an arbitrary vector to be rotated, $[y \quad z]_a^T$. As the original axes were translated and rotated to y_θ and z_θ, the collapsed vector, $[y \quad z]^T$, is also rotated by θ_a. Here, it will be shown how to "uncollapse" $[y \quad z]_a^T$ for rotated axes, y_θ and z_θ. The first observation is that from the superimposed positive y_0-axis, the rotated collapsed vector, $[y \quad z]_a^T$, can rotate θ_a radians counter-clockwise, making it co-linear with the negative z_θ-axis. The second observation is that this arbitrary vector can rotate $\frac{\pi}{2}$ radians counter-clockwise from the negative z_θ-axis to the positive y_θ-axis. $[y \quad z]_a^T$ is now in the same position as the original collapsed $[y \quad z]^T$ vector by analogy, given either vector collapses to the y_θ-axis and y_0-axis respectively. The third and final observation is that $[y \quad z]_a^T$ can rotate an extra ϕ_a radians counter-clockwise, successfully rotating the vector to its final rotational position before translation (notwithstanding the use of translation for purely visualization purposes).

Thus, after rotating the original axes by θ_j counter-clockwise, centered at $(0, (d_s+d_c))$, the original $[y \quad z]_i^T$, after being collapsed into the positive y_0-axis, can be rotated $\psi_{i,j} = \theta_j+\phi_i+\frac{\pi}{2}$ radians, such that it returns to its intended position, which is by analogy, the same as it was in relation to the original axes. After this, a simple translation matrix based on the rectangular-to-polar coordinate formula can be applied to the rotated coordinates or vector such that the new origin is $(0, (d_s + d_c))$, where the string passes through, but the origin of the newly rotated and translated (y, z) vector is always located at the polar coordinates, $((d_s + d_c), \theta_j)$, all of which lie along the circumference of a circle.

These two rotations and translation are in effect a radially symmetric transformation. Consider an arbitrary vector field, $[y \quad z]^T$, with its axes being the z_0-axis and the y_0-axis. The transformation rotates and translates the field in such a way that if one were to rotate their view of the original field about the center, $(0, (d_s + d_c))$, the transformed field would be indistinguishable from the field in the original position in the original view.

Since it is now possible to rotate the (y, z) coordinates, the y and z arguments of the magnetic field components, equations 2.2.13 and 2.2.14, can be rotated. This in turn means

rotation of the magnetic pickup for the experiment can be analytically described. Thus, the rotatable magnetic field component equations are defined as,

$$B_{y_j}(y_{i,j}, z_{i,j}, t) = 2B_0\xi\frac{(y_{i,j} - y_s)(z_{i,j} - z_s)}{((y_{i,j} - y_s)^2 + (z_{i,j} - z_s)^2)^2}, \tag{2.3.1}$$

and

$$B_{z_j}(y_{i,j}, z_{i,j}, t) = B_0\left(1 + \xi\frac{(z_{i,j} - z_s)^2 - (y_{i,j} - y_s)^2}{((y_{i,j} - y_s)^2 + (z_{i,j} - z_s)^2)^2}\right). \tag{2.3.2}$$

With the transformation matrix defined in Def. 1, the components of the magnetic field of the pickup, Eq. 2.2.13 and Eq. 2.2.14, can be rotated in accordance with the possible rotations of the magnetic pickup for this work's experiment. Those components being rotated about the string result in Eq. 2.3.1 and Eq. 2.3.2. These equations can thus be substituted into Eq. 2.2.11. This in turn provides governing bowed string equations whose solutions are independent variables of Faraday's Law of Induction, such that the associated magnetic field components of Faraday's Law and of the magnetic pickup can be rotated in conjunction with the possible rotations of the magnetic pickup about a bowed string.

So far in this section, a system of partial differential equations has been derived to adequately describe the transverse string displacements of the monochord as it is continuously excited by a bow. An extension of Faraday's Law of Induction has been derived such that one can observe the voltage over time and derive magnetic flux density over time with a reduction of Faraday's Law based on some simple assumptions. The solutions of the bowed string equations were also shown to be independent variables of Faraday's Law of Induction as well. And, a vector or coordinate transform for rotating the components of the magnetic pickup's magnetic field has been derived in order to correctly represent the magnetic field of the pickup as it is rotated around the monochord. With all these derivations, there is now a set of equations that can adequately describe the bowed string-magnetic pickup system dynamics and behaviors.

2.4 Proposal to Account for Vertical String Oscillation Damping in Governing Bowed String Equations

Concerning accounting for extra damping of the vertical transverse string displacement by the bow, Eq. 2.1.14 would be the equation affected. Under the assumption that a string can vibrate in two transverse planes, horizontal and vertical, it is evident that with the presence of a bow as a continuous excitation force through the friction of the stick-slip regime at the bow-string interface, the bow's hairs would pose a spatial interference to the string as it oscillates vertically. Note that the main driver of sounds to be produced in a bowed string will be from the horizontal transverse string oscillations. Suppose for a bow stroke, sound is produced. This would imply that there is a constant or arbitrarily quasi-continuous bow-string interface such that the stick-slip regime occurs as long as the bow stroke is sustained. This in turn would imply that as the string oscillates vertically, the bow hair must stay in contact. This would mean, assuming the vertical oscillations are ideally periodic, for any whole period, the downward bow force dampens the wave as it travels vertically up and it either strengthens or makes negligible contributions to wave amplitude as the wave travels vertically down. Because the vertical string displacement is a waveform, one can think the bow hair dampens specifically the amplitude of the wave and specifically the amplitudes of the present modes. Overall, this heavy damping can imply increased energy loss in the vertical string oscillations, reducing overall amplitude. For a bowed string excited by a violin bow, all governing equations would incorporate both transverse string motions, longitudinal string motion, torsional string motion, both transverse bow hair motions, and longitudinal bow hair motion [28]. Many of these can be treated as uncoupled as was done for Eq. 2.1.13 and Eq. 2.1.14 from the other motions, though those two are treated as coupled. But, for vertical transverse bow hair motion and vertical transverse string motion, coupling would also occur, potentially, through the dampening of the string motion by the bow hair motion. This would introduce a third governing equation. For this work, it is uncertain if

this reduction in energy and wave amplitude should be derived from a damping factor as a function of bow hair motion or be derived from an external force as a function of bow hair motion which contributes to the vertical bowed string equation's sum of forces. It is possible that with the presence of the downward bow force term of Eq. 2.1.14, this damping effect is accounted for such that as the string displaces in the positive z-direction, the force term in the negative z-direction deamplifies the displacement. One may consider the bow hair's deflection due to this downward bow force and positive vertical string displacement as well, but this is outside the scope of this work. It should also be noted that through coupling of both transverse string displacements for a bowed string, energy from horizontal oscillations can be transferred to vertical oscillations. The expected presence of low amplitude vertical string oscillations for a bowed string would receive energy in this way, but the main source of these oscillations comes from the transverse displacement of the string by the bow. So, it is more likely that vertical string oscillations are not small because of low energy transfer from horizontal string oscillations, but because of some dampening effect by bow interference.

As the results of the experiment are given throughout Sec. 6 and Sec. 7, various different results will be shown that indicate significant dampening of vertical string oscillations. These results can be taken as evidence for the need of an update of governing bowed string equations for vertical string oscillations. This is particularly important to the development of a magnetic pickup for a bowed string, given that a magnetic pickup is directionally dependent with respect to voltage generation. This specifically will be demonstrated in the results section. As for further research, modeling of bowed string motion with vertical string oscillation dampening is a potential future area of study. It can contribute to more accuracy in sound synthesis, modeling, and modeling for a bowed string-magnetic pickup system as well.

Chapter 3

Parameters and Dimensions of Experiment

This chapter defines and discusses the various experiment components used in the experiment. The discussion of each can vary from elaborating on parameters, dimensions, construction, and determining certain parameters.

3.1 Bow and String Parameters

An Ernie Ball guitar *D* string was used for the monochord. The string core is tin plated high carbon steel, wounded by a tin plated nickel winding. Considering nickel is ferromagnetic and this brand of guitar string is marketed for electric guitar use, the string can be used with the magnetic pickup for the experiment. The string is rated at 26 gauge, where "gauge" in guitar parlance refers to "part per thousandth inch." So, a 26 gauge string should have a string diameter of 0.026 in. or 0.6604 mm. Upon measuring the diameter at multiple string locations it is instead approximately 24 gauge. So, the string diameter is,

$$D_s = 0.6096\ mm. \tag{3.1.1}$$

For the experiment, the string was tuned to 196 Hz, G_3 ,which is the fundamental frequency for the G string of a violin.

The bow has the following dimensions. The bow hair has an average width of 8 mm and the length of the bow hair is 650 mm. The bow's axis is positioned at approximately 64 mm from the bridge end point of the monochord. This places the bow contact in a range of 60 mm to 72 mm from the bridge end point. This position for a violin bow can be called *sul tasto*, meaning "on the touch [of the fingerboard]." For the purposes of designing a magnetic pickup for a violin, both the bow and the magnetic pickup have to share the distance between the violin bridge and end of the fingerboard, which is approximately 55 mm. For the purpose of this work, allowing the magnetic pickup to be in the most probable x position along the string was deemed more important, allowing for some deviation in typical bowing location along the string.

Temperature can affect the tension of the bow hair of the bow and the tension of the monochord, but this was not taken into consideration given the data was collected in one session. The experiment displayed high efficiency in repeatability. Based on how the monochord was initially tuned with a tuner, results showed no significant effects from temperature when comparing results from each magnetic pickup position. The influence of how much rosin was present on the string and on the bow hair was not taken into consideration because the ability to do so was outside the capabilities and scope of this work. It is true that the amount of rosin on the bow and on the string will be inconsistent between experiment repetitions. Though, many expected results were observed despite the potential varying effects from temperature and rosin.

3.2 Measurement Position Piece Design

The root of the experiment concerns measurements from ideal radially symmetric, string-centric pickup positions. These measurements will be made in conjunction with the mea-

surements of string displacement in two transverse directions. For both measurement types to be made, a 3D printed PLA (Polylactic Acid) measurement tool holder was designed such that the magnetic pickup could take 8 radially symmetric positions around the string, where its inward facing pole would always be 2 mm away from said string. The same design was used for mounting the horizontal and vertical optical switches for string displacement measurements. The measurement tool holder can be called a position piece for brevity. The position piece for the pickup was placed along the string axis (x-axis), near the bridge (string end point) so that the pickup might be at a more realistic string position, reminiscent of traditional electric guitar pickup positions: between the end of the fretboard (fingerboard) and the tailpiece (bridge). This is out of spatial necessity to better approximate possible locations of a magnetic pickup for a violin. The magnetic pickup would need to be sufficiently close to the strings to work efficiently. A majority of the fingerboard of a violin must be available to the player for playing. Therefore, the only place that a magnetic pickup could potentially be situated at is between the bridge and fingerboard. Another position piece for the optical switches (which capture a voltage related to string displacement) was placed near the nut side (string end point) of the monochord. This was done to allow the switches to read significantly smaller string displacements.

3.3 Monochord Design

The monochord was designed in such a way to provide a controlled environment to test a magnetic pickup at various rotational positions along with measurements from optical switches to capture string displacement. With a traditional violin, the autonomy of the experiment would be more limited due to spatial restrictions and complexities of the system that otherwise fall outside the scope of this thesis. With ample room around the string, measurement tools can be placed in more complex positions. One of the main purposes of this thesis is to set the groundwork for the development of a magnetic pickup for a violin,

but only at that latter stage of development should physical limitations of the violin be accounted for.

For the materials, the monochord was made up of aluminum for the bridge and nut, the two rigid end points, and particle wood boards of two thicknesses, 12.7 mm and 19.05 mm, where the particle board of the first thickness was only used to allow for more exposure and clearance of tuners pegs.

Like for most full size violins, the distance between the two endpoints is $L = 330$ mm. The height of the string relative to the monochord frame is circumstantial to the parts necessary for measurement. The angles at which the string is tensioned at the guitar tuners, beyond both endpoints, is approximately 73° which is within the angular range that violin luthiers tension the string behind the bridge to the tailpiece.

In order to preserve radial symmetry for the magnetic pickup's coil and pole distance from the string, the relative difference in height of the bridge and nut were of an order of magnitude, 0.01 mm. This is important for when the magnetic pickup is in any diagonal or vertical rotational position, given those positions have a vertical position component relative to the string. But, it should also be noted that because of the position of the measurement position piece for the magnetic pickup is so close to the bridge boundary condition, vertical and diagonal displacement between each position should already be negligible when the string is at rest with no load. But, this precaution was still taken. Horizontal symmetry was also an issue. Measurements from diagonal and horizontal pickup positions could be artificially influenced by bias initial string position. Certain monochord dimensions were calibrated with a "G" (196 Hz) violin string (though the experiment used a guitar string with high ferromagnetic content, but at the same fundamental frequency).

To account for minimal relative displacement of string segments in the y-direction, the probe of a Haas CNC (Computer Numerical Control) mill was used to check the y-component of the positions of string segments relative to the mill's own origin. Imagine facing the monochord with the bridge in front and the string extending away. With this orientation in

mind, one can say that for either the bridge or nut, relative displacement to the left of the endpoint would be visually to the left and the same reasoning applies to relative displacement to the right. The relative displacement between the bridge and nut was approximately 0.63 mm with the nut being slightly left-favoring. From the middle of the string to the bridge and nut respectively, the displacements were approximately 0.42 mm and 1.05 mm, where the middle of the string was displaced to the left relative to both endpoints. But due to string tension, particularly for a string with a lower fundamental frequency when excited, larger relative displacement between the middle of the string and at its endpoints is expected. The relative displacement between the bridge and the pickup was approximately 0.23 mm to the left of the bridge, where the distance of the pickup's magnet axis away from the bridge being approximately 43.45 mm. So there was negligible displacement in the y-directions. For the pickup, radial symmetry of position relative to the string is preserved within a small error margin for displacement. Calibration for the optical switches in relation to the nut was also taken, but their positions will remain static for all iterations.

Holes in the base of the monochord were drilled to help accurately place the position pieces near both endpoints. The idea is to position the measurement tools, the magnetic pickup and both optical switches perpendicular to the string. Mentioned before was the method of string tensioning. Two guitar tuners were used, with the bridge side tuner holding the string in place by the string ball and the nut side tuner acting as the tensioner.

All the designs and key dimensions were initially designed using CAD (Computer Aided Design), specifically in SolidWorks. And finally, the monochord is fastened to a lab jack lift, which allows it to be moved vertically to meet the bow height. This allows for ease of calibration when finding a suitable downward bow force onto the string. Instead of a violinist pressing down on the bow onto the string with more force, a weight on the bow tip along with an appropriate string height achieves a similar result. A 0.071 kg weight was attached to the tip of the bow. Due to this form of applying downward bow force, there is potential for vertical oscillations of the bow to influence the forces, acting as a

cantilever beam. This calibration seeks to find the most amplified signal for each experiment iteration and a typical frequency distribution of a bowed instrument. Calibration of the monochord height in relation to the bow's vertical height can be attained through use of the oscilloscope. Voltage output over time and frequency distribution can be readily viewed on the oscilloscope to make quick, incremental changes in monochord height. Once a favorable or expected voltage output and frequency spectrum is arrived at, the height will remain constant for all iterations. Note that "favorable" and "expected" do not affect the results of each experiment iteration when compared relatively. Bow stroke parameters and monochord height will remain constant throughout.

3.4 Magnetic Pickup Design

The magnetic pickup design was inspired by the classic single-coil magnetic pickup design seen in many electric guitars. It features a 3-D printed PLA (Polylactic Acid) bobbin with an extruded key for placing the pickup in specific rotational, string-centric positions. The magnetic used is an AlNiCo-V magnet with a diameter of 5 mm and length of 18 mm. For the construction of the coil, 42 AWG copper wire was used. Assembling the magnet and bobbin together, the pickup could then be wound.

Using a simple winding method with a power drill, pickup wounding can be achieved quickly, but at a cost. The number of revolutions in the coil is initially unknown when using this method. But, an approximation can be made. Suppose there is a general magnetic pickup whose dimensions are all in millimeters. It has a cylindrical magnet of radius, r_1, and the outer annular radius at the outside of the entire coil is r_2, such that the magnet and coil are concentric. The actual coil is essentially an annular cylinder with r_1 as the inner radius and r_2 as the outer radius, where the copper wire is located in between both radii and vertically within the height to be defined. The entire coil varies radially as well, as mentioned in Sec. 2.2. The height of the coil is h_c. For a copper wire of arbitrary size, the diameter is

D_w. Two observations can be made. To determine the number of revolutions in the coil, it has to be related to the dimensions defined. The first observation for one side of a maximum cross-section of the pickup, is that a single layer of copper wire must be bounded by radii, r_1 and r_2, and that within these bounds, a single revolution of wire occupies a distance, D_w. With this, there is a relation between radii and revolutions for a single layer of copper wire in the coil. This relation is defined as,

$$D_w \cdot \frac{rev}{lyr} = (r_2 - r_1). \tag{3.4.1}$$

Thus the equation for revolutions per layer is,

$$\frac{rev}{lyr} = \frac{(r_2 - r_1)}{D_w}. \tag{3.4.2}$$

Similarly, another observation about the coil dimensions can be made. Copper wire is bounded by the height of the coil. The available vertical space for copper wire decreases by D_w every time an entire layer is laid. With this, there is a relation between height and layers of copper wire in the coil. This relation is defined as,

$$D_w \cdot lyr = h_c. \tag{3.4.3}$$

Therefore, the equation for number of layers of copper wire is,

$$lyr = \frac{h_c}{D_w}. \tag{3.4.4}$$

Using relations 3.4.3 and 3.4.4, we have an equation for the approximate number of revolu-

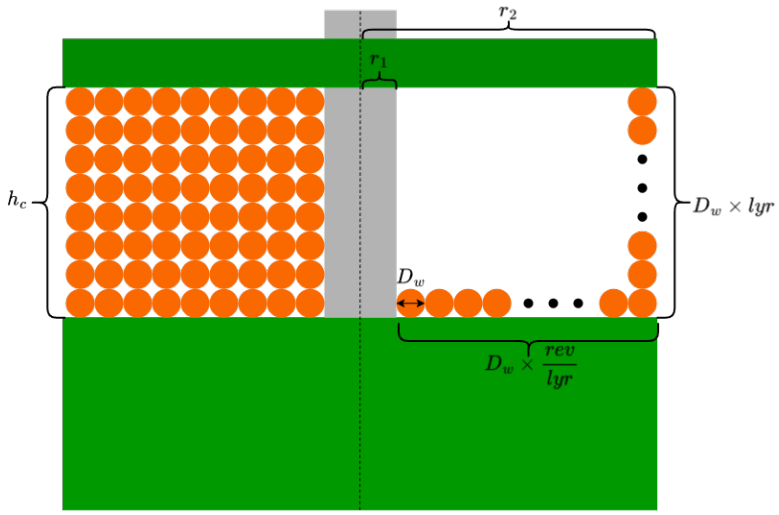


Figure 3.1: Pickup Coil Diagram

tions in a coil,

$$\begin{aligned} rev &= \frac{rev}{lyr} \cdot lyr \\ &\Leftrightarrow \\ rev &= \frac{h_c(r_2 - r_1)}{D_w^2}. \end{aligned} \tag{3.4.5}$$

Figure 3.1 shows a diagram of the magnetic pickup and how equations 3.4.2 and 3.4.1 are represented physically. For this thesis, the magnetic pickup dimensions are defined as, $r_1 = 2.5$ mm, $r_2 = 5.74$ mm, $h_c = 11$ mm, and $D_w = 0.0633$ mm for 42 AWG copper wire. This gives an approximate number of revolutions in the magnetic pickup's coil,

$$N_c = 8,894. \tag{3.4.6}$$

Typical commercially magnetic pickups feature coils with upwards of 8,000 revolutions, which will provide a higher voltage output. In this thesis and experiment, it is beneficial to have more revolutions due to the smaller coil surface area of a single pole pickup in comparison to the much larger coil surface area in a standard 6-pole pickup for a guitar. It should be noted that it is important to this thesis to attempt to get signals from all positions,

given some will inherently output weaker ones.

3.5 Optical Switches and Fixtures

To secure the optical switches in both the horizontal and vertical positions, 3D printed frames were designed. These frames were based off the dimensions of Optek's OPB380T11Z optical switches. Both frames were held in place by a position piece. This piece holds the optical switches instead of the pickup, where only the $\frac{\pi}{2}$ and π positions of the position piece were used. Both switches were situated near the nut, the other boundary condition. The horizontally positioned optical switch was 281 mm ($\frac{0.852}{L}$) from the bridge. The vertically positioned optical switch was 286.4 mm ($\frac{0.868}{L}$) from the bridge.

Each optical switch is rated for 5 volts of power. Both switches were powered by the same 11.1 V Zeee 2200 mAh lithium polymer battery which was used in conjunction with a Drok Step Down Voltage Regulator Module to convert the 11.1 V down to 5 V. The battery was then wired to a breadboard in which both optical switches can receive 5 V. Following the wiring diagram (Le Carrou et al.'s Fig. 1) provided by Le Carrou et al., resistors were required [18]. The 5 volts powered a breadboard such that each row received 5 volts in parallel. Then, the following was done for each optical switch. Two 220 Ω resistors were wired in series from power to the switch's diode anode and the diode cathode was grounded. From power, two 1000 Ω resistors were wired in parallel to the phototransistor's collector and the phototransistor's emitter was also grounded. From the collector and emitter, positive and negative leads were wired to them respectively, such that oscilloscope probes could be properly attached. This was done for both optical switches.

3.6 Bow Stroke Mechanism Design

Repeatability of consistent bow strokes is crucial to the experiment. Maintaining no change in bow velocity, horizontal and vertical bow forces, bow contact width, and bow position

on the string for each experiment iteration with distinct magnetic pickup position is very important for ensuring no bias is felt by any iteration with respect to bowing consistency. In this thesis, voltage output, frequency distributions, frequency distributions over time, and magnetic flux density over time will be considered. Variability in the bow action can lead to biases in voltage output. With Schelleng's diagram in mind, frequency distributions can reflect raucous, normal, or higher-mode oriented tone [32]. And magnetic flux density over time can be artificially weighted by such inconsistencies in downward bow force and bow velocity.

To better avoid these biases due to bow stroke, an electric motor-powered linear motion slider was used to drive the bow. The slider comes from what is traditionally used for constructing a 3-D printer. A sliding plate used to mount the bow and a t-rail made up the main section of the slider. The bow stroke mechanism has a maximum stroke length of 320 mm, which will allow for sufficient bow velocity and recording time for the oscilloscope. The motor is a $12-24$ V DC motor. Fixed to the motor is an aluminum spool with a nylon string fixed to it. The other end of this string is tied to the plate. The bow stroke mechanism acts as a winch. The same model of battery used for the optical switches was used to power the bow stroke mechanism motor.

The bow was secured to the moving plate using zip ties. The whole linear actuator was elevated to an arbitrary height with a particle wood pedestal and remained constant for all experiment repetitions. The monochord, being on a lab jack lift, could be raised or lowered to the bow stroke mechanism's bow height accordingly.

The speed of the bow can be measure and approximated, but because it must be constant for all repetitions, this was not recorded. It must be noted that this quantity can be easily recorded, though. The weight attached to the end of the bow for increased downward force was determined heuristically and again, was chosen to be 0.071 kg. It is sufficient to qualitatively calibrate both bow speed and bow pressure (downward force on the bow onto the string) using a trained ear. The purpose of this calibration is to provide a realistic

bow stroke, one that gives an expected frequency distribution of an excited bowed string, not withstanding the variety of such a distribution. The author is an experienced violinist of over 20 years and can calibrate the experiment's general sound quality. This is fitting because with this type of experience, a realistic sound can be achieved, as opposed to say a calibration that produces only "wolf notes" which do not accurately represent the sound of a bowed instrument. For this work specifically, there is no aim to investigate musical errors or anomalies like that. The calibration was done in conjunction with an oscilloscope, observing the voltage output and frequency distribution for each stroke, as previously mentioned in Sec. 3.3. With these considerations in mind, the experiment errs on the side of higher downward bow force with the use of the aforementioned weight and position of said weight. On the topic of bow forces, the Schelleng diagram, produced by Schelleng, relates bow force to bow position relative to the bridge with respect to what combinations of the two produce what type of horizontal bowed string motion, associated horizontal string displacement, and subjective musical concepts regarding the sound produced like "raucous," "empty," and "brilliant" [32, 1]. The diagram specifies minimum and maximum limits of bow force that delineate types of bowed string motion, string displacement, and sound type. The diagram in general is defined for the distance along the string between the bridge and the bowing position, which, for a violin, does not exceed too far beyond the end of the fingerboard. For this experiment specifically, the bowing position is within the *sul tasto* range, mentioned in Sec. 3.1. At this position, the range of bow force that generates Helmholtz motion, its associated string displacement, and a "brilliant" sound, is much wider. In short, it is easier to produce a good sound from a violin when drawing the bow near the fingerboard than near the bridge. The Schelleng diagram will be important when discussing the results for voltage outputs in Sec. 7.1 and magnetic flux density over time in Sec. 7.6 for the signals of the magnetic pickup at each rotational position.

Note that the results of the magnetic pickup signals will be compared relatively to one another and to the results of the optical switch signals. Though for some results like voltage

output, the bow forces used will be addressed alongside considering common, expected results detailed in Sec. 6.6.

3.7 Interference Reduction

Certain precautions were taken to ensure there was no EMF wave interference or general ground noise interference with the magnetic pickup and the measurements from it. The magnetic pickup was properly grounded to a small piece of steel, reducing ground noise emanating from the pickup. The experiment was conducted in a room during the daytime because the lights in the room emitted interfering EMF waves. In addition, cellphones were kept sufficiently far away from the experiment and not utilized during it. The oscilloscope is a digital type, which required plugging it into a laptop. The laptop could not be charged at the same time during signal recording, or there would have been EMF interference. There was some noise present in the magnetic pickup signals, but through visual inspection with no excitation of the string for the measurement tools, comparing the real-time pickup signal to the real-time optical switch signals without any known EMF influences, noise in either signal channel seemed to be indistinguishable from one another. This led to the plausible conclusion that the noise or sensitivity of the channels were inherent to the specific oscilloscope used.

Chapter 4

Data Collection

This chapter is concerned with briefly describing how data is collected for all three measurement tools, describing how an oscilloscope captures the voltage signals from these measurement tools, and giving a short procedure description for how an experiment repetition is done such that the data is collected and can be processed after collection.

4.1 Magnetic Pickup Voltage Signal

The magnet pickup acts as a data collector itself, given that its design is essentially the musician's application of Faraday's Law. The voltage signal generated by change in magnetic flux is a type of measurement of string velocity. As it was previously discussed in Sec. 2.2, the magnetic pickup produces an electromotive force in volts that preserves key components of the string's mechanical vibrations, most notably, the frequency distribution of string velocity. Using the oscilloscope to read a voltage signal over time, the signal of the magnetic pickup can be captured.

4.2 Horizontal and Vertical String Displacement

For measuring the string displacement in both transverse planes, horizontal and vertical, two optical switches were used. An optical switch was chosen such that the apertures of the switch's LED diode and its phototransistor were smaller than the diameter of the string. The aperture of both components were 0.254 mm and the string diameter was 0.6096 mm. As it was mentioned in Sec. 3.5, the specific model of optical switch used was Optek's OPB380T11Z. Both switches have a defined optical center line where the infrared laser beam is centered at as it travels from the diode to the phototransistor. The optical switch works by the act of the laser hitting the phototransistor such that the phototransistor then allows a current and voltage to pass through the circuit. As the string passes in an oscillatory fashion, this beam is uninterrupted, interrupted, or partially interrupted in a proportional oscillatory fashion, maintaining the frequency distribution information of the string's mechanical vibrations. These voltage outputs can be recorded by the oscilloscope and can describe a voltage function of string displacement in either transverse plane.

It is possible to solve for transverse string displacement over time using the equation from La Carrou et al.,

$$V = (V_{max} - V_{min}) \left(1 + \frac{\gamma}{2} + \frac{\gamma}{\pi} arcsin(\frac{\chi}{r}) + \frac{\gamma\chi}{\pi r}\sqrt{1 - (\frac{\chi}{r})^2}\right) + V_{LE}, \tag{4.2.1}$$

where γ is the string's opacity, r is the radius of the phototransistor, V_p is the switch's voltage output in a dark room with no obstructions to diode beam, V_{LE} is the voltage output of the switch in the lighted environment in which the switch is used, and χ is the displacement of the string in one of two transverse directions [18].

4.3 Magnetic Flux Density

In an effort to achieve similar results to those of other authors on magnetic flux density as a function of vertical distance and horizontal distance across the magnet pole face at a fixed vertical distance, a GLTL Gaussmeter was used at incremental distances, one millimeter at a time for 30 mm. The Gaussmeter was also used to determine suitable initial conditions for magnetic flux density over time when solving Faraday's Law of Induction for all the magnetic pickup signals.

4.4 Use of Digital Oscilloscope

A digital oscilloscope is used for the collection of voltage signals from the magnetic pickup and from both optical switches. The specific model is a Hantek $1008C$ oscilloscope. It features a frequency range of $0 - 250$ kHz and sample rate of 2.4 MSa/s. It also provides internal Fourier analysis and other signal processing methods.

4.5 Procedure for an Experiment Repetition of Data Collection

The collection of data follows a clear procedure for each repetition of rotating the pickup around the string. First, the digital oscilloscope is set to its trigger mode, where it will record the three signals simultaneously once a respective minimum voltage "triggers" the start of the data collection for an experiment repetition. One only needs a single channel with a trigger function. The channel used is the one for the horizontal optical switch. The voltage signals to record are from the magnetic pickup in a certain position, the horizontal optical switch, and the vertical optical switch. All signals will be recorded on separate channels of the oscilloscope. Assuming a satisfactory bow velocity and downward bow force, both of which will remain constant for all pickup positions, are decided, the bow can be drawn. The

bow stroke mechanism is set at its initial position and a battery supply is applied to the linear actuator of the mechanism, initiating a bow stroke. Assuming the voltage signal of the horizontal optical switch surpasses the minimum voltage necessary for the trigger, the data will be recorded. Once an iteration is complete, the data can be saved as a comma-separated values file or ".csv" file, which will later be used for post-processing and analysis via Python.

Chapter 5

Post-Processing of Data

All the collected data was converted to ".csv" files which can be processed in Python. The data collected from the pickup and both optical switches can be better understood with post-processing, which produces the intended result types. Each repetition of the experiment refers to the position of the magnetic pickup around the string. An experiment repetition corresponds to the position of the pickup as it is rotated around the string. For this experiment, an arbitrary position is $(k-1)\frac{\pi}{4}$ for some experiment repetition, $k \in [1,8] \mid k \in \mathbb{N}$. With the repetition number in mind, one can speak clearly of the results of each experiment repetition.

Each of these result types are for an experiment repetition, k. The maximum absolute voltage over time for $v_k(t)$ is v_k^{max}. The average voltage of absolute local extrema voltage over time for $v_k(t)$ is v_k^{avg}. Both frequency spectrum results and spectrogram results will be treated differently, while this section clearly defines what results match which repetitions. And finally, magnetic flux density over time is denoted as $B_k(t)$. These quantities are defined in order to provide formal distinctions between result types and results. Though, most results are represented in figures.

5.1 Maximum Voltage

One of the key goals of this thesis is to show the advantages and disadvantages of a magnetic pickup's rotational position. With respect to signal strength, this work considers the maximum voltage output of the magnetic pickup. For a viable pickup design, it must be able to convert and relate mechanical vibrations of a string into a large enough voltage signal for the purpose of amplification. A weak signal is not beneficial to the musician. A weak signal can also imply a loss in amplitude of otherwise amplified modes. In Sec. 6.6, details on typical voltage outputs will be discussed.

Consider an experiment repetition, k. The pickup sends an alternating current which means voltage over time, $v_k(t)$, can oscillate from positive to negative and vice versa. To consider the maximum voltage output, an absolute value is applied. This results in an expression for maximum voltage for $v_k(t)$,

$$\texttt{max}(\ |v_k(t)|\ ) = v_k^{max}. \tag{5.1.1}$$

Using Python and the Python package, NumPy, maximum voltage can be calculated using the NumPy functions for absolute value and maximum value respectively, `numpy.abs()` and `numpy.max()`.

5.2 Average Voltage

Much like maximum voltage, this work aims to see how a magnetic pickup in a specific position performs with respect to average voltage of a signal. An effective way of determining average voltage is to first apply an absolute value to $v_k(t)$ for some experiment repetition, k. With $|v_k(t)|$, the local maxima, over a specified range, of the absolute voltage over time can be determined using a signal processing function provided by SciPy, `scipy.signal.argrelextrema()`. Aside from the data provided, this function can take

other arguments into consideration. There are comparator and order arguments which allow first, the function to compare two data points and second, how many points on each side are to be compared before resulting in a maximum. The comparator used was `numpy.greater()` and the order was the length of $v_k(t)$, v_k, floor divided by 100. The signals of the main experiment repetitions were 0.5 seconds long, discretized around 1000 samples. This, of course, would alter the coming average value, but determining a reasonable choice for an order argument is possible. Once the values of the local maxima are determined, this particular average can be taken. Since this work uses Python for the post-processing, the `numpy.average()` works for this. With these considerations, the average voltage of local maxima of absolute voltage over time can be defined as,

$$v_k^{avg}. \tag{5.2.1}$$

5.3 Fast Fourier Transform Analysis

For the purposes of this work and particular processing of specific data's tonal quality, or "timbre", is considered. Timbre is the subjective interpretation or experience of sound by a person. This is an sub-area of study under "psychoacoustics" which relates mechanical vibrations felt by the human ear and the perception of these sounds by the brain. Timbre is an expression of why an "A_4" played by a violin, guitar, or trumpet may be in tune with what is traditional considered "A" but still have a certain unique character to each instrument as the note is played. In short any two instruments can play the same note but still sound distinct from one another. Mathematically, a considerable portion of timbre of an instrument is determined by the frequency distribution of the vibrations produced.

For results from frequency analysis, the reader should be cognizant of this. Many instruments today are the results of meticulous research and heuristics for their designs. Instruments were not only designed to acoustically amplify but to also produce favorable tonal character to said instruments. For this thesis, the "instrument" in consideration is the mono-

chord, materially comprised of particle fiber wood, aluminum, and a ferromagnetic nickel and steel string. It is designed to be simple enough to conduct measurements for a simple bowed string as opposed to a complex instrument like a violin. The results from the experiment will inform the more complex string systems that fundamentally stem from a simple one like the monochord. With that said, the monochord is not designed to optimize tonal quality, for it is not a musical instrument. For a high quality violin designed to produce beautiful sounds, a typical frequency spectrum for a single sustained note would feature the fundamental frequency having the largest amplitude among the following harmonics. The presence of the harmonics may vary in amplitude, but a more brilliant sound would feature high amplitudes for higher harmonics. This is an example of the sort of accessible subjective descriptions of sound that have an objective source in the physics of the sound.

For the monochord's frequency analysis results, there is the potential for "unideal" frequency spectra simply due to the simple, nonmusical construction of the monochord. Though, the string used is designed specifically for playing music. A common instrument, say a violin, has a body, material, and geometry that allows for the expression and amplification of certain modes. Supposing a magnetic pickup were fixed to said violin, these modes would feedback into the modes present in the string vibration, which would then be captured in the corresponding frequency spectrum of good tonal quality. Or if the monochord of this experiment were to have an exceptional well crafted string, one would see a frequency spectrum of good tonal quality. Note that in Sec. 7.2, tonal theory will be addressed more in depth.

As it has been mentioned before, bow force is also a contributing factor to frequency distribution in a signal. This of course opens the door to future investigation into applying magnetic pickups to an actual bowed instrument and seeing if frequency spectra are captured by the pickup are similar to those of a piezoelectric pickup or microphone.

For the experiment results and comparing certain results to previous studies, certain signal processing functions were used and different parameters for signal processing were

derived. The sample rate for a signal was determined by dividing the size of the signal array by the length of time elapsed. Thus, the sampling interval was the inverse of the sample rate. The specific fast Fourier transform function used was `numpy.fft.fft()` and the frequency discretization was determined with `numpy.fft.fftfreq()`. From there, the frequency spectra of the experiment's collected data could be retrieved.

5.4 Short-Time Fourier Transform: Spectrograms

For deriving spectrograms for all the experiment signal data, the short-time Fourier transform (STFT) was applied. To apply the STFT transform specifically for the data collected, SciPy's function `scipy.signal.spectrogram()` was used. The number of samples per time segment to apply the Fourier transform was the length of the signal array floor divided by 5. And the amount of overlap between segments was defined to be the length of the signal array floor divided by 10.

5.5 Magnetic Flux Density over Time

Per Sec. 2.2, Faraday's Law of Induction can be extended such that the magnitude of magnetic field over time can be solved for. For some experiment repetition, k, using the derived Faraday's Law equation, Eq. 2.2.8, for a voltage, $v_k(t)$, magnetic flux density over time can be approximated with,

$$B_k(t) \approx \frac{-n}{\left(\sum_{i=1}^{n} N_{ci} S_{ci} cos(\alpha \frac{i}{n})\right)_k} \int_0^{t_f} v_k(t) dt, \tag{5.5.1}$$

such that t_f is the length of time the signal spans. This is much more difficult to solve analytically due to the complexity of the signal produced. If one also considers the presence of nonlinearities in the signal due to the nature of a magnetic pickup, an analytical approach may either be impossible or would require more effort to solve analyti-

cally. A solver will be used instead to approximate a solution. SciPy's solver function, `scipy.integrate.solve_ivp()` was used. To calculate Eq. 5.5.1 using the solver, $(B_i(t))_k$ is solved for with,

$$\frac{-1}{\left(N_{ci}S_{ci}cos\left(\alpha\frac{i}{n}\right)\right)_k}\int_0^{t_f} v_k(t)dt, \tag{5.5.2}$$

for $\alpha = \frac{\pi}{3}$. The total angle to discretize over was decided by evaluating the periodicity of sample signals. As it will be shown in Sec. 6.4, experiment repetitions exhibit periodicity in their horizontal optical switch signals. If magnetic flux density over time depends on the displacement of the string, particularly its horizontal transverse displacement, it is possible to expect periodicity in magnetic flux density over time. This was observed as different total angles were checked. $\alpha = \frac{\pi}{3}$ was chosen given it returned a waveform for magnetic flux density that was most periodic.

But, to approximate $B_k(t)$, Eq. 5.5.1 must be iterated n times, where all iterations are summed and scaled by $\frac{1}{n}$. The number of annuli of equal area, n, was determined by not only the presence of periodicity in magnetic flux over time but also the range of the outputs. Based on the expected range of magnetic flux density for the specific magnet used, as detailed in Sec. 6.6, n was chosen to be 100 because it gave realistic magnetic flux density values while maintaining a sense of periodicity.

With an α and n chosen, Eq. 5.5.1 can be iterated with the solver such that,

$$B_k(t) \approx \frac{1}{n}\sum_{i=1}^{n}(B_i(t))_k \tag{5.5.3}$$

for $\alpha = \frac{\pi}{3}$ and $n = 100$ in conjunction with Eq. 5.5.2. Once the solver was executed n times, Eq. 5.5.3 can be calculated. But, when solving a differential equation, an initial condition is required. Consider the initial instance of time for an experiment iteration, k, $t = 0$. Then an initial condition for $B_k(t)$ at $t = 0$, t_k, is recorded before the k^{th} repetition begins. The approximation of Faraday's Law and modeling of the magnetic field does not

incorporate unique initial conditions based on the annulus position. This is something that could be improved in the future. As discussed previously, a Gaussmeter can be used to capture the initial condition for magnetic flux density over time. Sec. 7.6 discusses how the initial conditions for experiment repetitions were recorded. As it will be addressed later in Sec. 7.1, the initial conditions for magnetic flux density are not equal, given the influence of the downward bow force on the equilibrium of the string at rest.

Chapter 6

Comparison with Previous Studies

The purpose of this chapter is to demonstrate that various measurement and post-processing methods used in this work's experiment can generate results that are fundamentally similar to results in the literature, demonstrating that they are of the same family. Material or physical differences of the experimental set-up prevent exact replication of these results. By doing this, confidence can be given to the experiment, including its construction and methods. This section will aid in demonstrating the reliability of the measurement tools used and various post-processing techniques. There are various results from previous studies on magnetic flux density and frequency distributions which can be replicated within the limits of available materials like types of magnets, strings of various gauges and tunings, and optical switch capabilities.

Specifically, this section covers construction of the monochord briefly, magnetic flux density as a function of vertical distance over the pickup and of horizontal distance along the centerline of the pickup at a fixed height, capturing accurate frequency spectra of a bowed string, wave polarization types for a bowed and plucked string, and some of the commonly expected results for voltage output, magnetic flux density, and frequency distributions.

6.1 Construction of Monochord

The monochord design takes inspiration from Schelleng and Ricca [32, 28]. From Schelleng's construction, the use of a tuning peg and rigid end points for the bridge and nut were used in the construction of this monochord. Instead of using a traditional violin tailpiece or a new fixture, another tuning peg was used to hold the string in place. All of these features can be seen in Fig. 6.3. Schelleng used a magnet to generate an electrical current in the string to then measure string displacement and string velocity. This magnet could be moved axially along the string to place the magnet at different string nodes. The experiment of this work moves the magnetic pickup rotationally around the string in a fixed x-position to simulate the physical restraints imposed by a violin. It cannot be reliably placed under or through the fingerboard without sacrificing playability at those fingerboard sections. But this monochord uses the magnetic pickup to measure string velocity and optical switches to measure string displacement. These measurement tools can be seen in Fig. 6.1, which shows the experiment apparatus in its entirety.

The monochord construction is also similar to the one Ricca's work, particularly Fig. 2.7, [28]. The terminating bridges are the bridge and nut. Ricca uses diagonally placed photodectors, or optical switches, (forming an "X" pattern with the bottom of the pattern directed at the bottom of the monochord) for string displacement measurement. For this monochord, optical switches are positioned horizontally and vertically near the nut boundary condition. Calibration of the switches followed the procedure detailed by La Carrou, which was compared to how Jiolat calibrated an optical switch for a string instrument, using the same calibration technique [18, 13].

The whole experiment without the electronics is shown in Fig. 6.2. The bow stroke mechanism was designed independently, but with the goal of creating a repeatably consistent bow stroke for one whole experiment iteration. This is shown by itself in Fig. 6.4. An old design for a programmable bowing machine, MUMS, can be found in Cronhjort, where bow velocity and downward bow force can be inputted [5]. Future research into the behaviors of

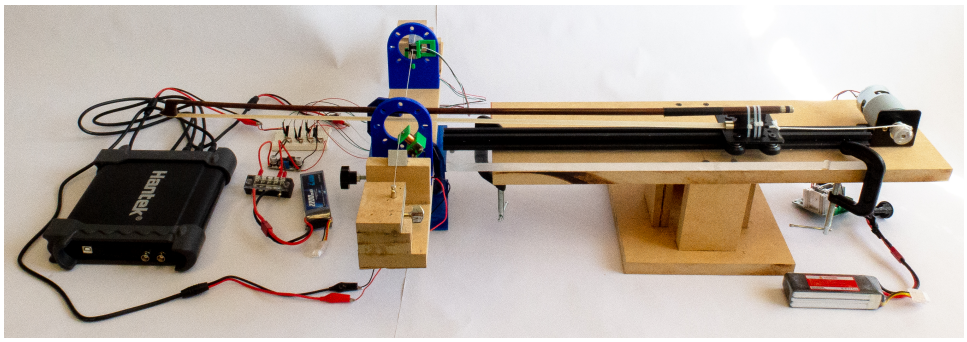


Figure 6.1: All experiment components.

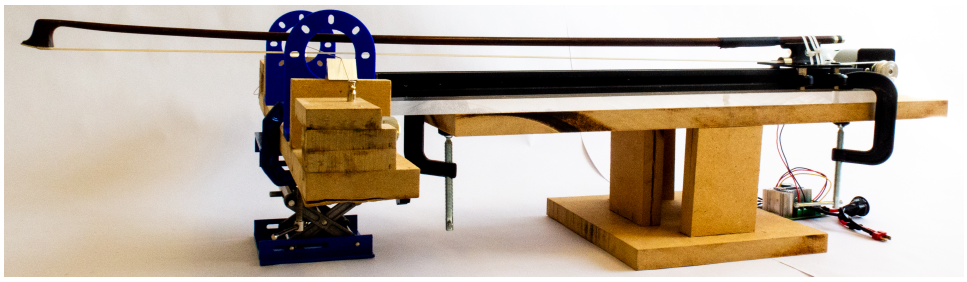


Figure 6.2: Monochord and bow stroke mechanism.

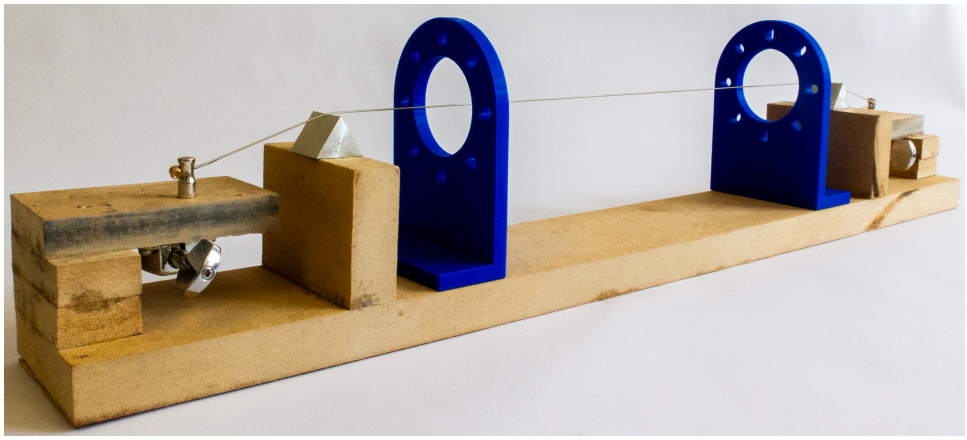


Figure 6.3: Monochord

a bowed string-magnetic pickup system can be done by varying bow velocity and downward bow force. A potential modern bow stroke machine of this sort would be to modify a belt-driven linear actuator used for a 3-D printer extruder. Bowing velocity in either bowing direction, "up bow" or "down bow", can be programmed in Arduino. Downward bow force would require a wider carrier plate which can mount a motor to actuate a cantilever beam upward and against the bottom of the bow's frog (the end where the player holds the bow.



Figure 6.4: Bow stroke mechanism.

It is a few centimeters behind the usual point of downward load application to the bow), following the design of the MUMS. This too can be programmed through Arduino. It is possible to apply a variable velocity and a variable force which is natural of much violin playing.

6.2 Magnetic Flux Density as Function of Distances

It is the magnetic pickup that gave rise to the electric guitar. Its construction will partially dictate its outputs in voltage, magnetic flux density, and frequency distribution. A critical component is the magnet itself, which magnetizes the string such that its mechanical vibrations in turn oscillate the magnetic field to generate a voltage output. The basic fabrication of a magnetic pickup is a straight forward process. Its different components and materials contribute to the solving of Faraday's Law of Induction for the purpose of deriving magnetic flux density over time. Most notable of these components are: magnetic pole face and coil surface areas, wire gauge, magnet length, and number of coil revolutions. Specifically, for the magnet material and dimensions, magnetic flux density in either Gauss or Tesla can be measured as a function of vertical or horizontal distance in relation to a magnet pole. Achieving results for these sorts of magnetic flux density functions, similar to those of other authors, proves to be beneficial in justifying the magnetic pickup as a reliable translator of a bowed string's wave information.

Looking to Norton's and Moore's results, Fig. 6 and Fig. 7, similar results have been

developed [23]. Fig. 6.5 shows magnetic flux density as a function of vertical distance of a Gaussmeter probe from the magnet pole face, where the Gaussmeter probe is centered on the pole face. Given the difference in magnet materials, magnet dimensions, and points of measurement, the results of Fig. 6.5 are different from Norton's and Moore's Fig. 6, but both figures reveal that the experimental data are of the same family, resembling $\frac{1}{x}$ for $x \in (0, L]$ for some distance, L cm [23]. Note that does not imply this is the actual family of curves they exist in. Both results demonstrate asymptotic behavior at both axes. In both results from Norton and Moore and this work, magnetic flux density decreases as the measurement probe's height increases. Guadagnin et al. also have a similar plot in Fig. 5 [11].

Fig. 6.6 shows magnetic flux density as a function of lateral distance across the magnet pole face where the Gaussmeter probe is at a fixed height above the magnet pole face, approximately 7.1 mm above it. As the probe moves laterally, it moves along the centerline of the magnet pole face. Like previously, the exact values are not the same as the results found by Norton and Moore, specifically for Fig. 7, given the difference in magnet material and dimensions [23]. But the values from the experiment and the curves they respectively fit resemble a family of curves indicative of Gaussian distribution. Note that this is not a formal statement about these function's families of curves, but that they both display a bell curve-like shape. For the specific magnet of this work's experiment, its magnetic flux density respectively over vertical and horizontal distance matches well with results from previous studies.

6.3 Capturing an Accurate Frequency Spectrum

Frequency distributions are a critical result type to obtain for this work since it provides valuable information for a musical device design, namely a magnetic pickup for a bowed instrument. Frequency analysis in relation to tonal theory informs us more on the design of a bowed instrument magnetic pickup. Being able to compare the frequency spectra from

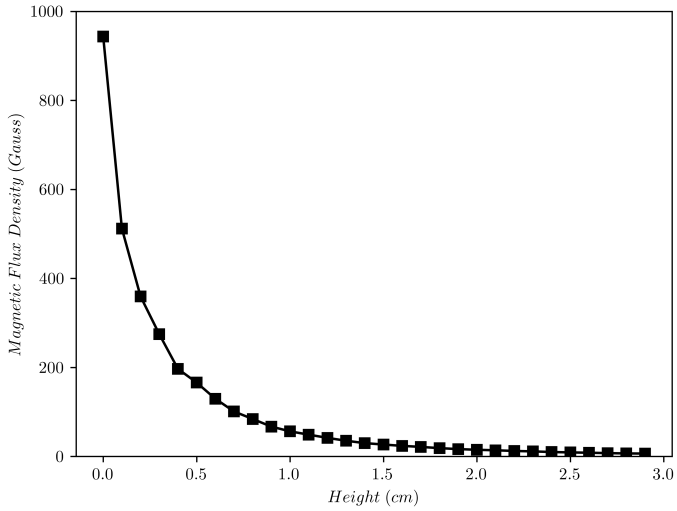


Figure 6.5: Magnetic flux density as a function of probe height above the top magnetic pole face.

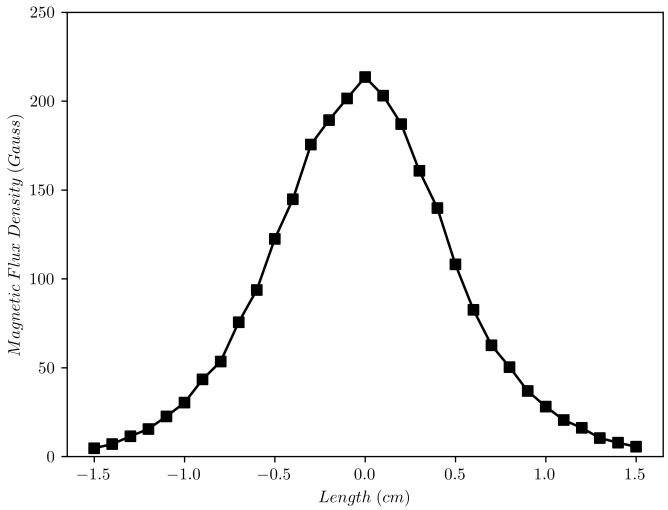


Figure 6.6: Magnetic flux density as a function of probe distance from the center of the magnet, fixed at a height of 7.1 mm above the top magnetic pole face.

magnetic pickup signals to the spectra of the optical switch signals which are related to the transverse string displacements is also important. In Ricca's work, a string has bow hair placed on top of it and a driver plays a sound with only a frequency of 440 Hz, A_4. This in effect simulated a bowed string without moving the bow (it also allows for isolating bow hair

interactions). This in turn produces a frequency distribution shown in Ricca's Fig. 3.2 which represents the frequency spectrum of a signal related to both transverse string displacements, such that Ricca used two pohtotransistors for only one spectrum [28]. There are two peaks near 440 Hz both of which emanate from the signal produced by either photodetector. But for this experiment, frequency analysis is reserved for whatever is generated by the bowed string-magnetic pickup system and the non-intrusive optical switches. Ricca's Fig. 3.3 shows the frequency spectrum for the photodectors signals, once differentiated [28]. This spectrum also had two peaks, but one being decisively greater than the other in amplitude. Because the signal was once differentiated with respect to time, the spectrum represents the frequencies related to a bowed string's velocity over time. Given the physical limitations of the optical switches' LED beam and phototransistor apertures and the string thickness and tension necessary to tune to a fundamental frequency of 440 Hz, this work shows, instead, accurate, expected frequency distributions for a string tuned to 196 Hz, G_3. Fig. 6.7 and Fig. 6.8 show the frequency spectra for the signals of a magnetic pickup placed horizontally around the bowed string at position $\frac{0\pi}{4}$ and of a horizontal optical switch capturing a voltage signal related to the string's horizontal transverse displacement. Note that the magnetic pickup signal is related to string velocity and the optical switch signals are related to string displacement. Both spectra for the magnetic pickup and the horizontal optical switch show that the fundamental frequency of 196 Hz is being derived from the bowed string oscillations for both the pickup and optical switch, which operates fundamentally the same as Ricca's photodetectors. When comparing Fig. 6.7 to Ricca's string velocity frequency spectrum in his Fig. 3.3 and Fig. 6.8 to Ricca's string displacement frequency spectrum in his Fig. 3.2, qualitative similarities are achieved [28]. In addition, despite potential nonlinearities arising from the magnet or optical components respectively, only harmonics are showing considerably amplified peaks. With this, this work's method of capturing and computing frequency distributions is sufficient for frequency analysis.

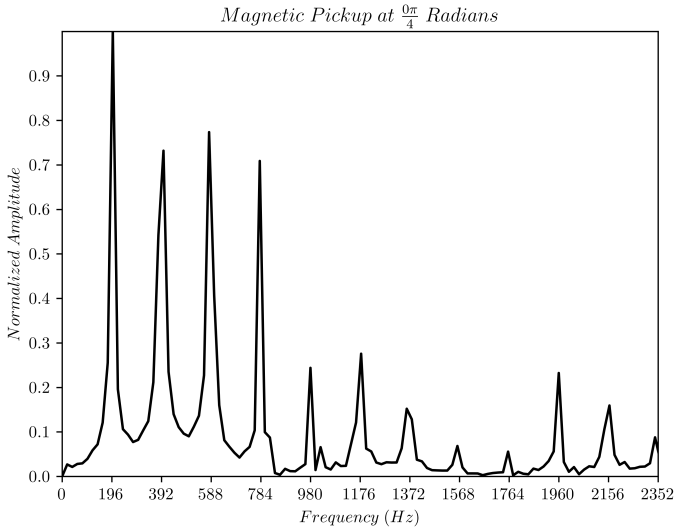


Figure 6.7: Example of an accurate frequency spectrum for a bowed string when the string is tuned to 196 Hz, a G_3. This spectrum comes from a 0.05 second long signal obtained by a magnetic pickup.

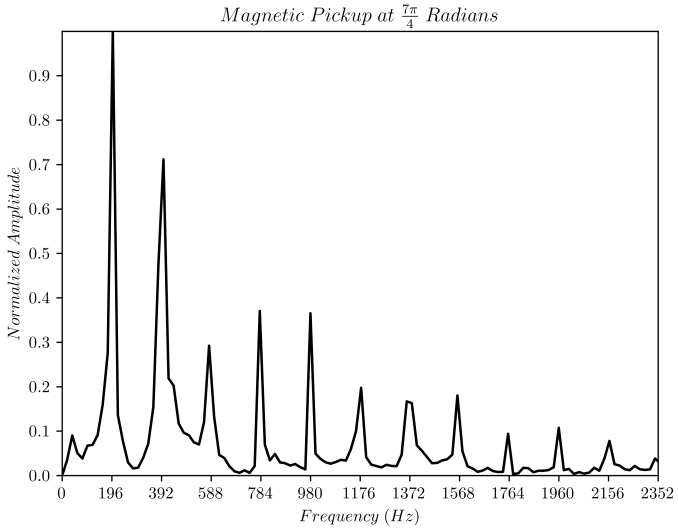


Figure 6.8: Example of an accurate frequency spectrum for a bowed string when the string is tuned to 196 Hz, a G_3. This spectrum comes from a 0.05 second long signal obtained by an horizontally placed optical switch.

6.4 Capturing Bowed String Motion Displacement

Recall from Sec. 2.1, that for bowed strings, displacement of the string in the horizontal transverse direction exhibits a sawtooth waveform. Considering one wavelength of Helmholtz

motion displacement, the sloped section corresponds to the stick phase, when there is static friction at the bow-string interface. The string travels with the bow at the speed of the bow in the same direction as it. The vertical section of the wavelength corresponds to the slip phase, when there is slipping friction initiated at the bow-string interface. The string travels in the opposite direction of the bow movement. The sawtooth waveform emerges from how static friction and slipping friction change over time. It is possible for bowed string motion displacement to exhibit a triangular waveform based on the stick-slip regime.

With that being said, consider again that the horizontal optical switch being used produces a voltage signal related to horizontal transverse string displacement, shown by Eq. 4.2.1 in Sec. 4.2 and is subject to inherent noise, assumed to be due to the oscilloscope used. Cremer demonstrates a triangular wave displacement for bowed string motion in his own Fig. 3.4, which was sourced from another author's unpublished work [4]. It shows the result of passing an oscilloscope signal through an integrator, such that the oscilloscope signal was derived from electrodynamic sensing about a bowed string. That specific experiment used a magnet to move current through the oscillating, magnetized string as it was bowed. The oscilloscope was connected to the string, receiving a signal related to string velocity. For this experiment, the horizontal optical switch also displays a triangular waveform for a signal that is proportional to horizontal transverse string displacement for a bowed string.

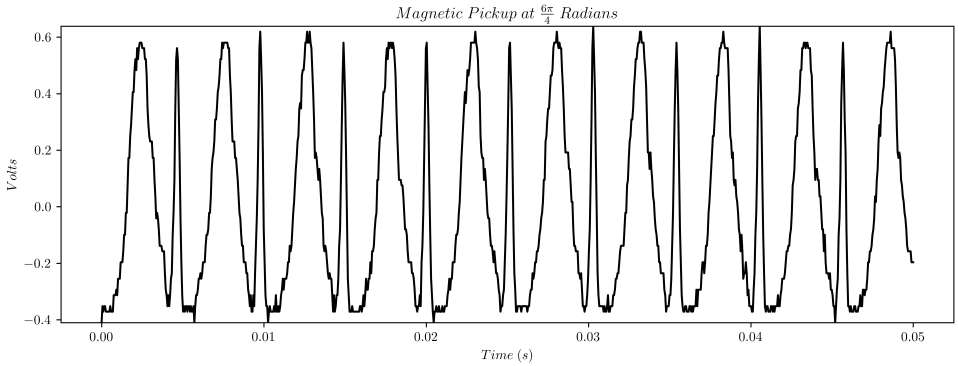


Figure 6.9: Voltage signal, 0.05 seconds long, of the horizontal optical switch. The signal was generated by a bowed string of the same downward bow force and bow velocity used for the main experiment repetitions.

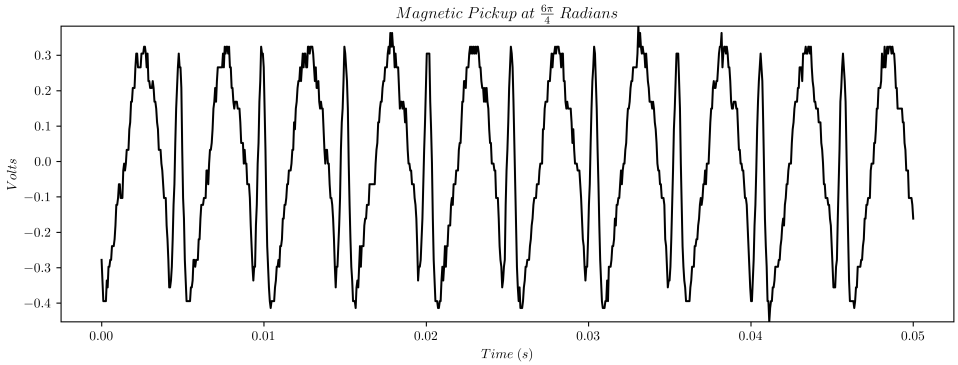


Figure 6.10: Voltage signal, 0.05 seconds long, of the horizontal optical switch. The signal was generated by a bowed string of subjective bow force.

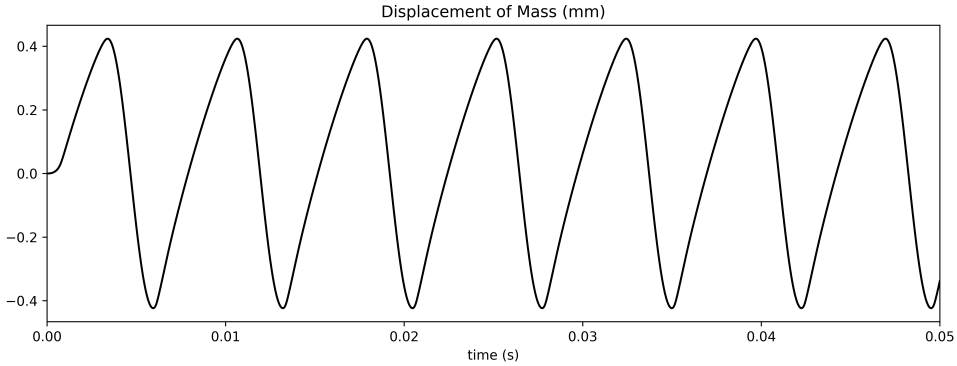


Figure 6.11: Simulation of horizontal transverse string displacement for a bowed string tensioned such that it has a fundamental frequency of 196 Hz. The simulation code used comes from Bilbao [2].

Looking at Fig. 6.9, there is an anomaly where there are very tall spikes of short time lengths near the lower crests. The noise inherent to the oscilloscope can explain the jagged nature of the plot mostly. But, using the fact that the signal is discretized, it can be visually confirmed these thin peaks do not occupy more than a few data points. An argument can be made that they are artifacts that do not stem from the horizontal bowed string motion. Supposing it is ignored, the resulting signal demonstrates a thin triangular waveform. Though, the qualitative elements of a sawtooth waveform can be potentially inferred. The same type of artifact is seen in Fig. 6.10 and the signal also demonstrates a triangular waveform. The corners of these waves appear to be somewhat more rounded, which is possible, but recall that these figures are zoomed in on a smaller time domain. Though, this would not entirely

exclude the presence of some rounding. This rounding can be partially attributed to the issues of a lower discretization of the signal and of noise from the oscilloscope. On the entire time domain of the signal, from 0 seconds to 0.05 seconds, the wave demonstrates sharper corners. Secondly, the kink in Helmholtz motion and the corners in the associated displacement tend to be rounded due to energy loss of the wave at higher frequencies [36, 4]. A sufficient cause of this is the lack of horizontal bow force applied to the string. This could occur through a lower static friction coefficient of the bow. Musicians increase static friction between the bow and string through the use of rosin, a resin-like material, and increased downward bow force. Aside from scaling differences, qualitatively comparing the figures of this section to the results from Cremer, it is seen that the horizontal optical switch of this experiment is capturing a signal proportional to that of horizontal transverse string displacement of a bowed string [4]. In addition, the resulting displacements shown in Fig. 6.9 and Fig. 6.10 correlate with a standard simulation of horizontal bowed string displacement. Fig. 6.11 shows a similar sawtooth or triangular waveform expected of a bowed string. The simulation is provided by Bilbao [2], which approximately solves for a simpler version of Eq. 2.1.13, a more basic horizontal bowed string displacement equation. With expected theoretical results, the results from a previous study and horizontal bowed string displacement simulation, it can be strongly argued that the horizontal optical switch produces accurate results. This same type of sawtooth waveform can also be derived from certain magnetic pickup signals indicating the measurement tool's capability, assuming certain assumption about Faraday's Law of Induction, of accurately representing expected results and results of other authors. This will be discussed further in Sec. 7.6.

6.5 Wave Polarization Types

Given the voltage signals from the horizontal and vertical optical switches and the fact that they are functions of either transverse string displacement over time, each signal can be

treated as parametric equations. Suppose the horizontal optical switch signal is $V_y(t)$ and the vertical optical switch signal is $V_z(t)$. It is possible to look at a parametric plot in the $y-z$ plane which describes a function of string motion polarization. For a plucked string with two boundary conditions at the end of the string, the polarization is typically elliptical [35, 9, 22]. This occurs because the string is free to vibrate in both transverse planes, $x-y$ and $x-z$. If a string is bowed, it should approach a linear polarization with a bias towards displacement in the y-direction, horizontally. Ideal polarization of a bowed string would be exactly linear. For a physical string, it may exhibit a polarization that appears to be a thin ellipse due to the small presence of vertical string oscillations.

In addition to the voltage signal polarization plots, there are corresponding plots where the signals have been filtered. A high-pass filter was applied with a threshold of 0.5 normalized linear amplitude for the frequencies in the signals. After the filter was applied in the frequency domain, the inverse Fourier transform was applied to return filtered signals for filtered voltage signal polarization plots.

6.5.1 0.05 Seconds Period

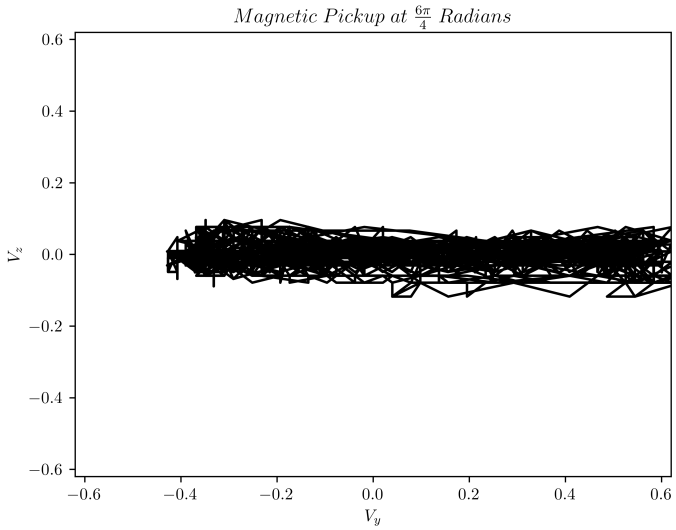


Figure 6.12: Unfiltered wave polarization for a bowed string for a period of 0.05 seconds.

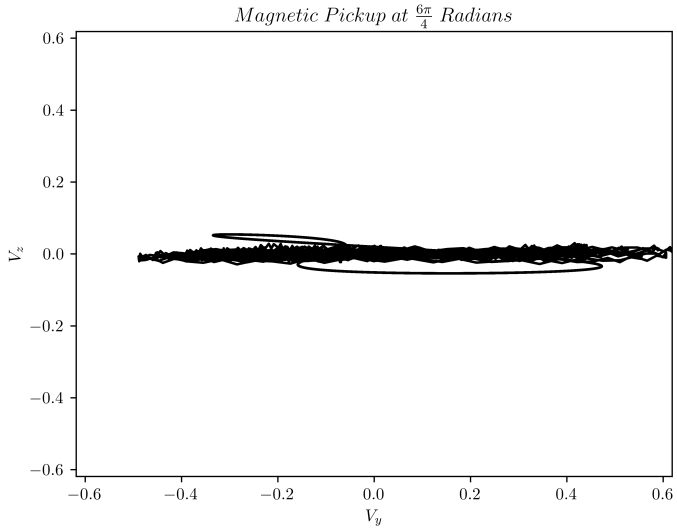


Figure 6.13: Filtered wave polarization for a bowed string for a period of 0.05 seconds.

Consider the wave polarization for a signal of 0.05 seconds of a bowed string shown in Fig. 6.12. There is an inherent noise to the oscilloscope used, but with both signals unfiltered, there is clear linear polarization of the bowed string displacement. Looking to Fig. 6.13 with the signals cleaned up by the high-pass filter, one can see the linear nature of the string displacement polarization. This is evidence for the proposal for updating the bowed string equations in Sec. 2.4, given how small vertical oscillations in the voltage signal are.

6.5.2 0.5 Seconds Period

For a longer signal of 0.5 seconds, the ratio of amplitudes per frequency appear to not result in an integer. With that in mind and a longer signal, the periodicity of the polarization can greatly increase. Such would be the case even for heavily filtered signals. Despite this, the displacement from the origin horizontally is approximately 3× greater than that of displacement vertically for the unfiltered plot and approximately 2.6× greater for the filtered plot. These are shown in figures, Fig. 6.14 and Fig. 6.15. Just as for 0.05 second signals, these results argue in favor in updating Eq. 2.1.14 in order to account for vertical string oscillation dampening, as discussed previously in Sec. 2.4.

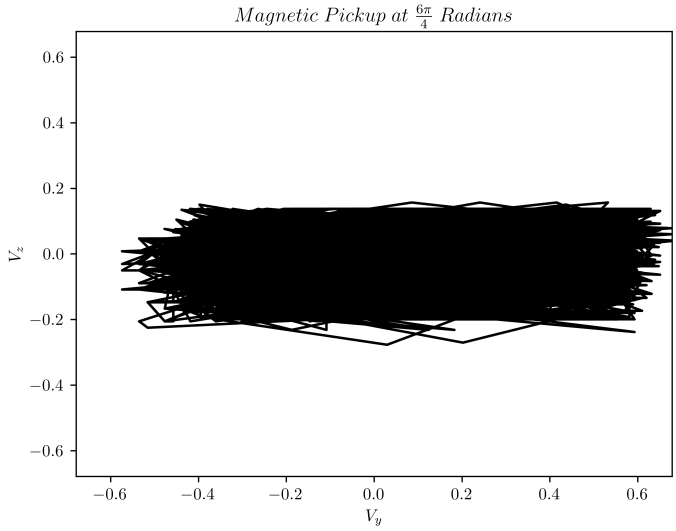


Figure 6.14: Unfiltered wave polarization for a bowed string for a period of 0.5 seconds.

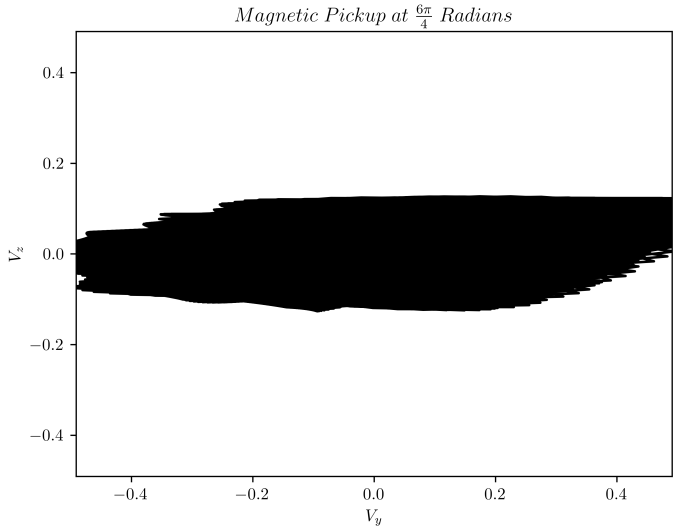


Figure 6.15: Filtered wave polarization for a bowed string for a period of 0.5 seconds.

6.5.3 0.05 Seconds Period: Subjectively Plucked String

For a subjectively plucked string such that the excitation force was not measured, it was expected that the string displacement polarization would be elliptical. For both horizontal and vertical voltage signals, captured for 0.05 seconds, both the unfiltered and filtered polarization plots exhibited a hyperbolic polarization. They are shown in figures, Fig. 6.16 and Fig.

6.17. Many attempts with different plucking styles and strengths were attempted, but an elliptical polarization could not be reproduced. When comparing the filtered and unfiltered polarizations, the hyperbolic projection seems to mirror its orientation about the vertical axis, such that the bottom of the saddle first points to the left then to the right. Though, the main concern of this section is to demonstrate linear polarization of a bowed string's oscillations, so this result does not need to be explored further. Though it does warrant consideration in the future. Future research on this topic may be started in investigating the materials used to create a monochord and establishing a well-defined and repeatable excitation method.

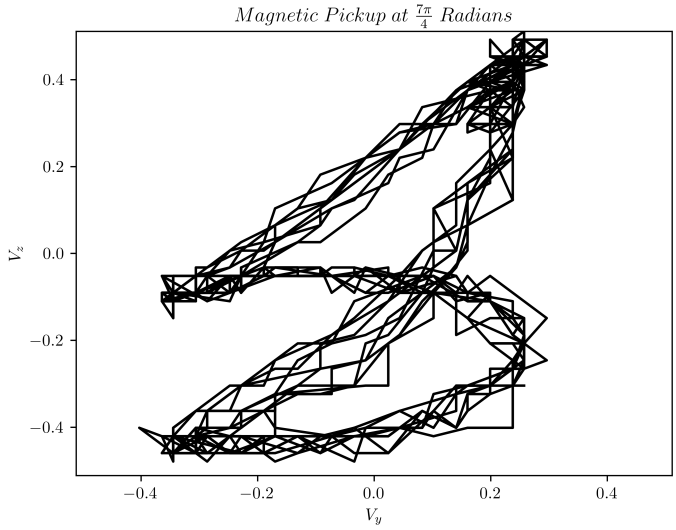


Figure 6.16: Unfiltered wave polarization for a subjectively plucked string for a period of 0.05 seconds.

6.5.4 0.05 Seconds Period: Subjectively Bowed String

Looking to a bowed string with subjective bow forces and bow velocity applied, there are figures, Fig. 6.18 and Fig. 6.19, showing the unfiltered and filtered string displacement polarization plots. At first glance of the unfiltered plot, it appears that there may be two prongs pointing in the negative y-direction, indicating a potentially hyperbolic polarization.

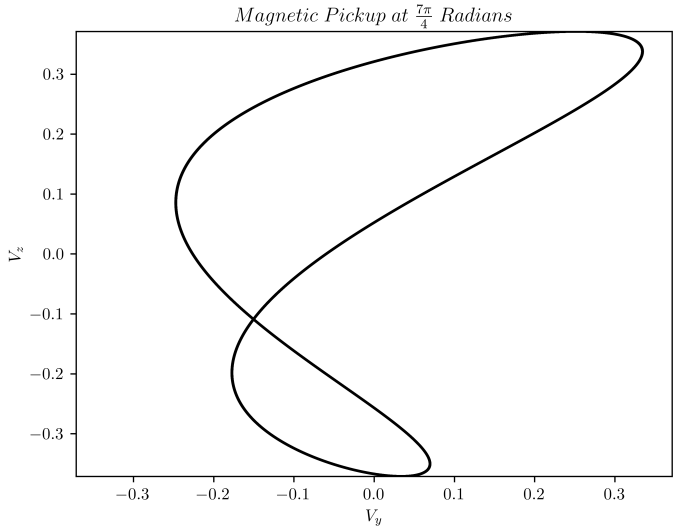


Figure 6.17: Filtered wave polarization for a plucked string of subjective force for a period of 0.05 seconds.

Given the same monochord used for the plucking is used here, it is possible that this may be the polarization type. But there is a considerable amount of noise which may hide the true general path. Looking to the filtered polarization plot, however, the horizontal and vertical optical switch signals decidedly form a thin ellipse. The horizontal displacement from the origin is approximately 3× greater than that of the vertical displacement. This supports the conclusion that the plot shown in Fig. 6.18 probably approaches a linear polarization. Even for the subjectively excited bowed string, this linear polarization behavior holds. Just as for the 0.05 and 0.5 second signals derived from a bowed string, these polarization plots and results strengthen the proposal in Sec. 2.4 to update the bowed string equations with a new term for the bow hairs' dampening effects.

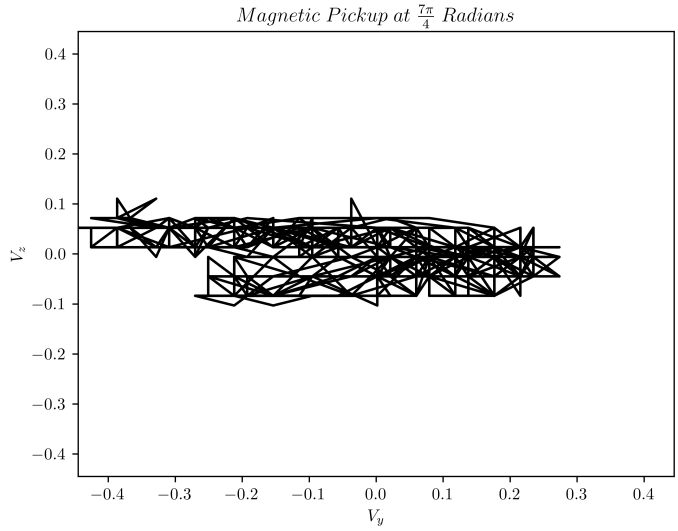


Figure 6.18: Unfiltered wave polarization for a bowed string of subjective force for a period of 0.05 seconds.

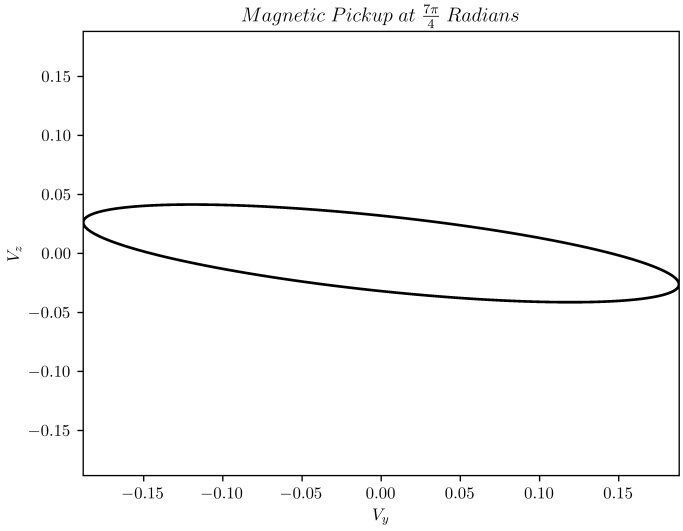


Figure 6.19: Filtered wave polarization for a bowed string of subjective force for a period of 0.05 seconds.

6.6 Expected Results of Voltages, Magnetic Flux Density, and Frequency Distributions

A general rule of thumb for voltage output of an electric guitar's magnetic pickup is that it should be at least 0.1 volts and typically can reach up to 1 volt. Given the subjectivities of how much force is applied to a string by the player and in what direction with respect to the magnet pole, what type of magnetic is used, or how many windings of the copper coil there are in the pickup, this voltage range can change. The magnet type and number of coil revolutions are what mostly drive the voltage range for an electric instrument in a passive fashion. In an active fashion, it is the player who can apply a greater force to the string to increase the voltage output. For this experiment, a stronger magnet and a high number of coil revolutions were used to better amplify the signal produced by string oscillations in the service of analysis. For a commercial application, these different materials and quantities would be tested and compared among each other. Recall that the magnetic used for the magnetic pickup is an AlNiCo-V magnet. According to Gough, the expected magnetic flux density of the magnet when measured at the pole face is typically within the range, 0.09 Tesla to 0.11 Tesla [29, 10]. For frequency distributions, the main expectation is that the fundamental frequency and following harmonics are what are amplified. Given inherent nonlinearities of the magnetic pickup and optical switches, there is potential for non-harmonic frequencies to emerge. Noise due to various sources may also inform the frequency distributions, but care was taken to properly ground the magnetic pickup and reduce EMF waves that may come from expected sources.

Chapter 7

Results and Discussion

7.1 Maximum Voltage and Average Voltage

One of the main concerns for the design and analysis of a magnetic pickup is its signal strength. For the purposes of amplification of a bowed instrument, sufficient amplitude is needed. In Sec. 7.1, maximum and average voltage outputs of the magnetic pickup in eight positions and of the two optical switches, horizontal and vertical, corresponding to each position, are recorded and shown.

There are many observations that can be made by looking at these voltage outputs. The first result to notice with the magnetic pickup voltages in Fig. 7.1, Fig. 7.2, and Fig. 7.3, is that for both the maximum and average voltages, they are not constant across the eight pickup positions. Across all three iterations of the whole experiment, the higher maximum voltages were found at positions, $\frac{0\pi}{4}$, $\frac{4\pi}{4}$, $\frac{5\pi}{4}$, and $\frac{7\pi}{4}$. The range of maximum voltages for these positions for all three iterations is from approximately 1.5 volts to 3 volts. Recall the calibration of the bow force and bow velocity. The forces and velocities are constant between all iterations. A decision was made to err on the side of greater downward bow force and bow velocity to ensure a more consistent and expected frequency output. A result of this will be a larger voltage output than expected. As mentioned in Sec. 6.6, the typical range expected

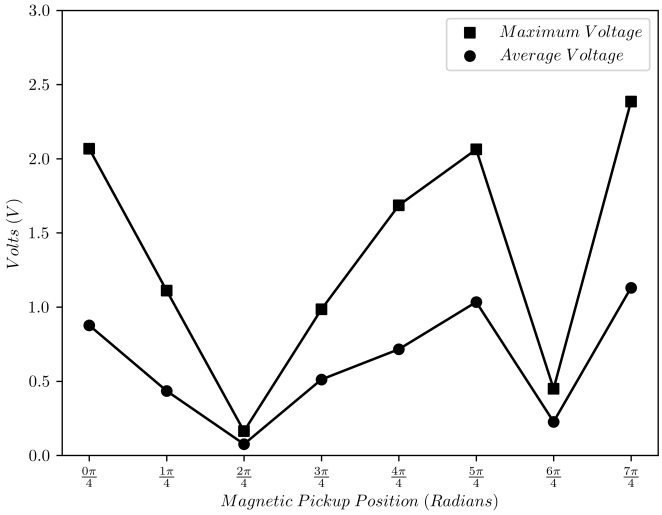


Figure 7.1: Maximum and average voltage outputs of all 8 magnetic pickup signals for the first iteration of the experiment.

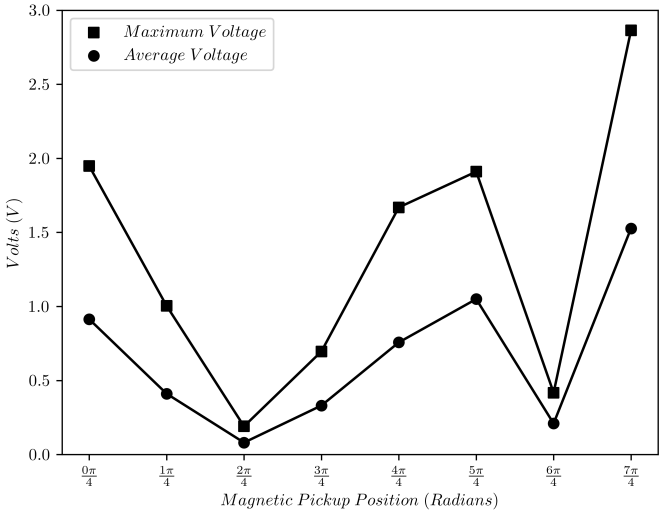


Figure 7.2: Maximum and average voltage outputs of all 8 magnetic pickup signals for the second iteration of the experiment.

of an electric guitar pickup is approximately $0.1 - 1.0$ volts, but this varies so much with the strength with which the player strikes the strings and with the design and materials of the pickup. The experiment, which maintains constant downward and horizontal bow forces between repetitions for each position, exhibits stronger bowing, hence a higher-than-expected

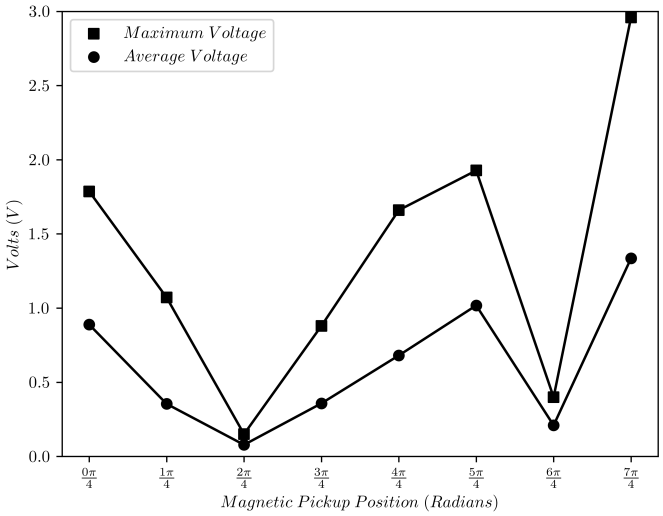


Figure 7.3: Maximum and average voltage outputs of all 8 magnetic pickup signals for the third iteration of the experiment.

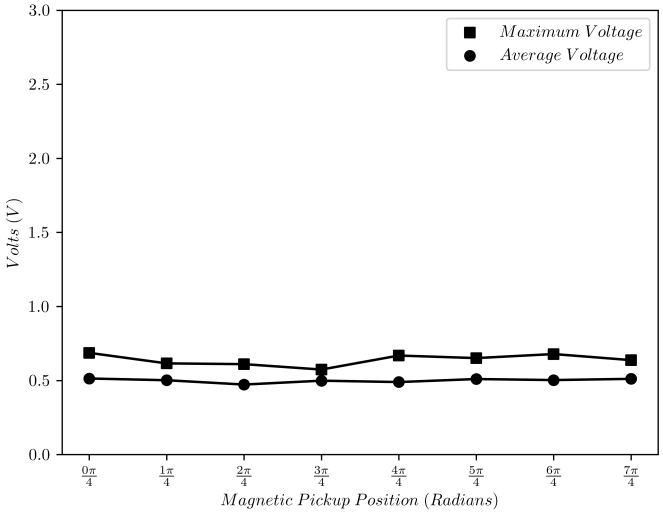


Figure 7.4: Maximum and average voltage outputs of each horizontal optical switch measurement taken during the measurement of the magnetic pickup signal for a specific position for the first iteration of the experiment.

voltage output.

The average voltage outputs for all iterations for all pickup positions display, understandably, lower values. Looking to the same figures, the average voltages of positions, $\frac{0\pi}{4}$, $\frac{4\pi}{4}$, $\frac{5\pi}{4}$, and $\frac{7\pi}{4}$, fall within or close to the approximate output range, $0.5 - 1.0$ volts, which is the

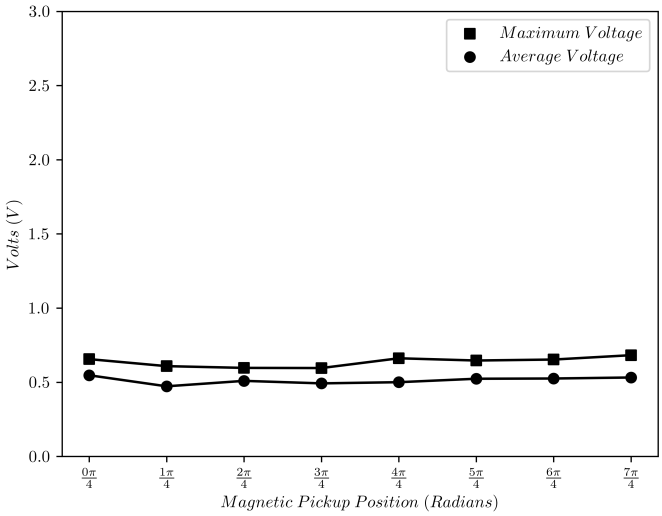


Figure 7.5: Maximum and average voltage outputs of each horizontal optical switch measurement taken during the measurement of the magnetic pickup signal for a specific position for the second iteration of the experiment.

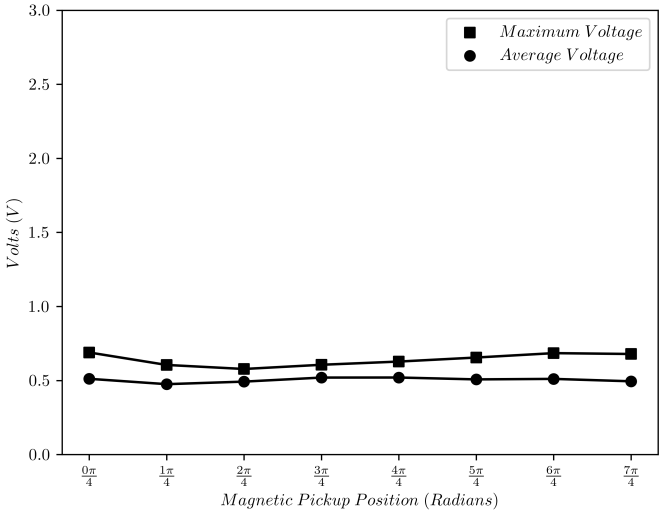


Figure 7.6: Maximum and average voltage outputs of each horizontal optical switch measurement taken during the measurement of the magnetic pickup signal for a specific position for the third iteration of the experiment.

expectation for voltage seen in Sec. 6.6.

Both the maximum and average voltage outputs show what sort of pickup positions produce favorable voltage outputs for the purpose of bowed instrument amplification. It was

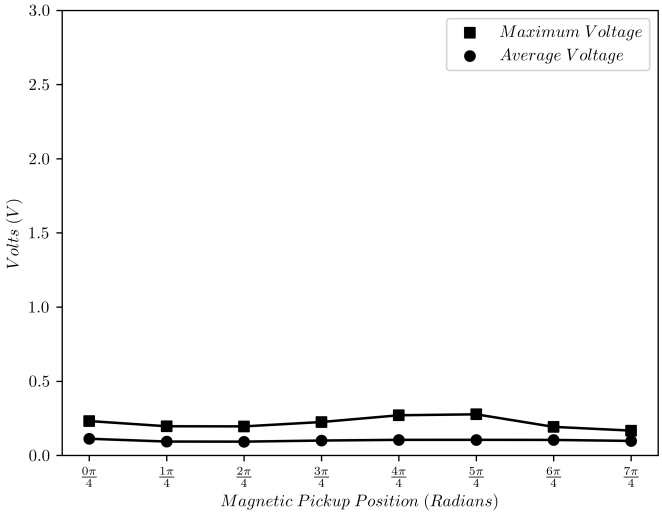


Figure 7.7: Maximum and average voltage outputs of each vertical optical switch measurement taken during the measurement of the magnetic pickup signal for a specific position for the first iteration of the experiment.

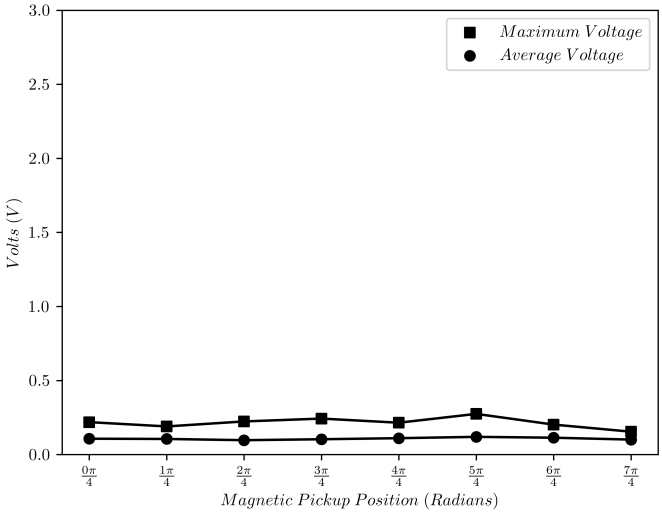


Figure 7.8: Maximum and average voltage outputs of each vertical optical switch measurement taken during the measurement of the magnetic pickup signal for a specific position for the second iteration of the experiment.

hypothesized that the pickup when placed horizontally at either $\frac{0\pi}{4}$ or $\frac{4\pi}{4}$ would produce the greatest voltage outputs. This turned out to be incorrect, despite significant outputs from the pickup at both positions, but it is due to an unaccounted for bias from downward bow

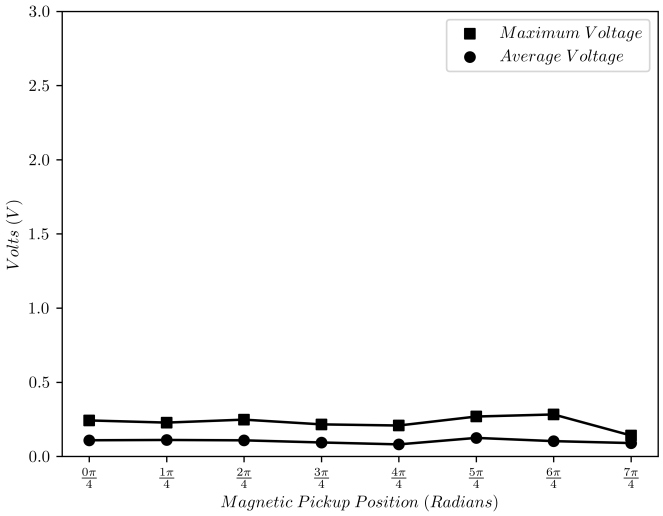


Figure 7.9: Maximum and average voltage outputs of each vertical optical switch measurement taken during the measurement of the magnetic pickup signal for a specific position for the third iteration of the experiment.

force. This will be addressed later in this section. Across all iterations of the experiment, the pickup at $\frac{7\pi}{4}$ produced the highest maximum and average voltage outputs. The pickup signal's maximum and average outputs for positions $\frac{0\pi}{4}$, $\frac{4\pi}{4}$, and $\frac{5\pi}{4}$ are also high, though not as great as for the $\frac{7\pi}{4}$ position. The pickup at the two vertical positions, $\frac{2\pi}{4}$ and $\frac{6\pi}{4}$ accounted for the two lowest outputs for both voltage types. These results for when the pickup was positioned vertically is evidence for the arguments put forward in Sec. 2.4 and the need for an update of Eq. 2.1.14 to account for the dampening effects onto the vertical string oscillations by the bow hair. And the middling outputs came from the two top diagonal positions, $\frac{1\pi}{4}$ and $\frac{3\pi}{4}$.

It is observed that the maximum and average voltage outputs of the pickup are most dominant when located at the bottom diagonals and the right horizontal positions (assuming the $y-z$ axis is defined such that the positive y axis is to the right of the string as it passes through the origin along the x-axis, where one may look down the string from the bridge to the nut). The vertical positions produce little signal because of the lack of a presence of vertical string oscillations over time, which will be explored further through

Chapter 7. One might expect similar voltage results between mirrored positions, vertical-to-vertical, horizontal-to-horizontal, and diagonal-to-diagonal, but this was not the case. The discrepancies between mirrored positions has to do with the directions of bow forces in relation to the orientation of the magnetic field of the pickup.

The bow experienced a downward bow force with a weight attached to the tip. Stationary, the bow with the weight in this position is a third class lever with the fulcrum being the string. Instead of applying a vertical force to the lever, the bow stroke mechanism simply moves this lever horizontally, effectively moving the fulcrum, the string, closer to the weight. With that being said, this downward bow force, from the start of the experiment repetition to the end, displaces the string downward. This in effect changes the equilibrium of the string for both its horizontal and vertical waves. If the string vibrates closer to the magnetic pole face, greater magnetic flux density and magnetic flux will be generated, which creates a larger voltage signal. Fig. 6.5 supports this explanation. In some cases during testing, the downward force of the bow in combination with both the initial distance between the string and magnetic pole face and the tension of the string tuned to 196 Hz, G, caused enough string displacement causing the string to physically hit the magnet during oscillation.

For the purpose of future pickup design, a greater vertical distance between the string and magnet may be needed. With the string oscillating closer to the magnetic pole face, the voltages will be greater. This is why the pickup at the top diagonal positions produces much lower voltages. The downward bow force displaces the string away from the magnet pole face, which will reduce magnetic flux and magnetic flux density when the string is excited with its equilibrium being further away. This is also one reason why the pickup at the bottom vertical position is slightly greater than that of the top vertical position. The right diagonal position, $\frac{7\pi}{4}$, experiences the greatest voltage outputs due to the great string equilibrium displacement towards the magnet pole face and also because of the influence of the horizontal bow force. The experiment simulates a simplified down bow, where the bow moves across the string from left to right, given the previously defined axes of the experiment.

The string oscillations operate under a stick-slip regime, where the bow excites the string in the stick regime and causes vibration during the slip regime. The horizontal bow force of a down bow, particularly as the downward bow force brings the string closer to the magnet in rest and through its equilibrium during oscillations, will provide a fuller capture of the string oscillations by the magnetic pickup, which will produce a much greater voltage signal than if it were at other positions. Note that for these increased voltage outputs for the magnetic pickup signals of bottom positions, downward bow force affected the increase due to the vertical displacement of the string's equilibrium. It is possible that the downward bow force added to the static friction between the bow and the string as well. Another consideration that can be explored for a pickup signal of any diagonal position is to see how the frequency spectrum is influenced by both the horizontal and vertical string oscillation components being captured by the diagonal pickup.

For a design of a magnetic pickup for a bowed instrument, one would need to account for both bowing directions, up and down. Ideally, to preserve a consist signal output, two magnets and coils would be needed per string to provide a consistent signal for both bowing directions.

The maximum and average voltages of the optical switch signals were also recorded. These can be seen in figures, Fig. 7.4, Fig. 7.5, and Fig. 7.6 for the horizontal switch and in figures, Fig. 7.7, Fig. 7.8, and Fig. 7.9 for the vertical switch. The scaling of these figures are kept the same as for figures, Fig. 7.1, Fig. 7.2, and Fig. 7.3 to emphasize the difference in voltage output between the magnetic pickup signals and the optical switches' signals. Both switches remained stationary for the entirety of the experiment for all three iterations. When a magnetic pickup signal was recorded for a specific position, the signals of both optical switches were recorded too. Recall that the horizontal optical switch records a voltage signal related to horizontal string displacement and the vertical optical switch records a voltage signal related to vertical string displacement. The first result to notice for the horizontal optical switch signals is that they remain very consistent between experiment

iterations and between all eight repetitions per iteration. This indicates that the bow stroke mechanism demonstrates good consistency for downward and horizontal bow force between every stroke. This can also be demonstrated by the similar results between iterations for the magnetic pickup signals. The voltage outputs for the horizontal optical switch are not as large as the ones of the magnetic pickup, but it is designed more for measurement than for amplitude. With that being said, the average voltage output is around 0.5 volts, with its maximum voltages not being much greater than its averages.

Considering the vertical optical switch outputs, it is clear that they are much smaller in comparison to those of the horizontal optical switch signals. For both the maximum and average signals, the vertical optical switch signals are about 50% or less of the volts produced by the horizontal optical switch signals. This is further evidence towards demonstrating the dampening effect on vertical waves of a bowed string. This is evidence for adding a new term to the governing bowed string equation, Eq. 2.1.14, and strengthens the arguments put forward in Sec. 2.4. The vertical optical switch's signals also demonstrate the reliable consistency of the bow stroke mechanism with respect to consistent downward bow force and bow velocity between bow strokes.

7.2 Frequency Spectra and Timbre: comparing spectra between magnetic pickup positions

For acoustics and particularly better understanding the relationship between a magnetic pickup and a bowed string, frequency analysis is imperative. One of the considerable aims of this work is to inform the design of a magnetic pickup for a bowed instrument. In this aim is producing an agreeable sound and tone. When considering tonal quality, or "timbre," of an instrument's sound, one imposes subjective terms and concepts onto the frequency distribution present in such sound. This is to say that frequency analysis can aid in understanding whether or not a signal is acceptable tonally. With this, design decisions

of a magnetic pickup can be supported or rejected.

In the scope of this work, frequency spectra were obtained for each magnetic pickup signal at each position. The signals of the main experiment repetitions are 0.5 seconds long. It should be noted that the start and end of the signals have the potential to exhibit non-harmonic frequencies and non-periodicity. This is partially due to the fact that the bow must get up to speed initially and quickly decelerate when the bow stroke ends. During the initial period, it is possible for there to be deficient static friction at the bow-string interface such that, the expected stick-slip regime of Helmholtz motion has yet to be realized. While cognizant of this, many of the main results still exhibited expected results such as key frequency characteristics, despite the realities of using the entire 0.5 second signal which invites potential non-harmonic frequencies and non-periodicity in part. This decision to maintain the initial and final portions of the signals was also recognized in Sec. 7.4. With these considerations in mind, the frequency spectra of all the signals of the magnetic pickup in the various positions can be analyzed and be used to inform design decisions for the development of a bowed instrument magnetic pickup.

When speaking of timbre for instruments, one can suppose there is a unique tonal color to each instrument. Instruments of the same species, of the same family, or simply of the instrumental genus, all possess timbre. When the A_4 (440 Hz) note is played on both a violin and a trumpet, it is evident that both instruments are playing the same note, yet the violin and trumpet do not sound the same. They possess different tonal character or tonal color called timbre. Mathematically, timbre relates primarily to the frequency distribution or "spectral envelope" produced by an instrument [7]. Both the violin and trumpet play the A_4 note, but along with both instruments producing a fundamental frequency (the lowest, present harmonic in the signal) of 440 Hz, their spectra reveal very different and unique presences of harmonics of varying amplitudes. It is the combination of the fundamental frequency and various harmonics of varying amplitudes that gives tonal color or unique timbre to two different instruments. This area of study, again, is called "psychoacoustics", where

objective analysis of acoustics is connected to the more approachable realm of describing one's experience when hearing music or the sounds of an instrument.

For bowed instruments, including the violin, a good tonal quality would have a frequency spectrum that has the fundamental frequency being most amplified. But it should be noted that some instruments may not follow this standard. In addition to that attribute of a good bowed instrument frequency spectrum, a higher number of following harmonics in the spectrum indicates a full, rich sound. A beneficial analogy to explain why having more harmonics is a pleasant attribute is to imagine an orchestra playing an A note of each octave from $A_1 - A_7$ in contrast to a section of violins of the same number of players as the orchestra only playing one A note from one octave, A_4. The orchestra with the wide range of harmonics undoubtedly produces a more brilliant sound. Much is the same when considering the frequency spectrum of a sound produced by a single instrument. Another aspect of a good frequency spectrum of a bowed instrument would be that the amplitudes of a wide range of harmonics are large. For violins, brightness, or high amplitudes of higher harmonics is another acceptable characteristic.

When musicians refer to "bass," "middle," and "treble" for an equalizer, pre-amplifier, or amplifier they are generally referring to the low (41 Hz to 200 Hz), medium (200 Hz to 1000 Hz), and high (1000 Hz to 3000 Hz) frequency bands of standard instruments like bass, guitar, violin, saxophone, etc. A problem that piezo-electric pickups for violins face is that they produce signals that greatly favor treble frequencies with respect to increasing amplitude. They are known for producing very "sharp," top-end frequency range biased sounds. In the area of live music, in a band, it is practically industry standard for most violins to use a "pre-amplifier" in conjunction with the piezo-electric pickup to better balance the frequency distribution of the signal. For the purposes of amplification and amplifying a pleasant sound from a violin, one may very well need to purchase a pre-amplifier that costs upwards of 200 US dollars. Avoiding the financial burden of a pre-amplifier or equalizer for a piezo-electric pickup would be a good benefit to the musician. A magnetic pickup can be designed to be

"warmer" (greater presence of lower harmonics) or "brighter" (greater presence of higher harmonics) at a price relatively close to that of a piezoelectric pickup, yet without there being a need to purchase a pre-amplifier or equalizer. This work aims to demonstrate this sort of characteristic of a magnetic pickup of a bowed string. And with the aforementioned considerations on tonal quality in mind, there is now a good and accessible point to discuss the frequency spectra results.

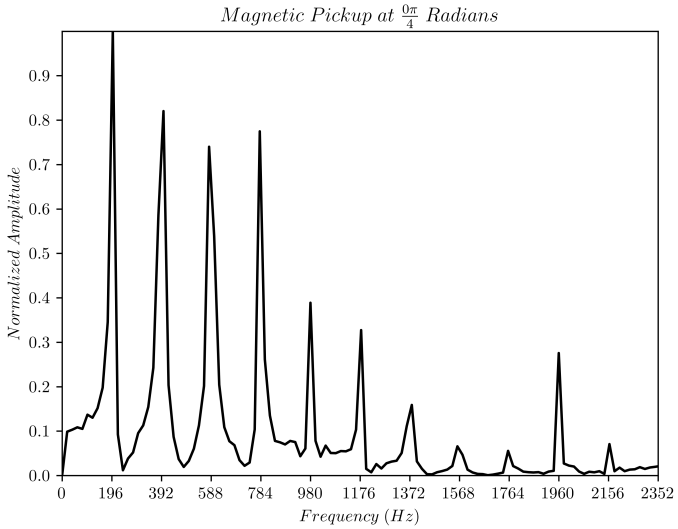


Figure 7.10: Normalized amplitude frequency spectrum of the signal from the magnetic pickup at the first position for a total time period of 0.05 seconds.

A frequency spectrum for the magnetic pickup signal at the $\frac{0\pi}{4}$ position for a time period of 0.05 seconds is given in the results initially before the following figures, which detail the frequency spectra of the main experiment repetition signals. This is shown in Fig. 7.10. The signal obtained by the oscilloscope was discretized into 937 points of data. But for the frequency spectra of the magnetic pickup signals at each position for a time period of 0.5 seconds were based off of a signal discretization of 1000 points of data. This is to say that, due to the limitations of the oscilloscope used, wave information is not as precise for the magnetic pickup signals that were 0.5 seconds long. It may appear that the signals for 0.5 seconds only produce frequency distributions up to 980 Hz with 196 Hz as the fundamental frequency, but it is argued that this is merely a limitation due to the oscilloscope's lower

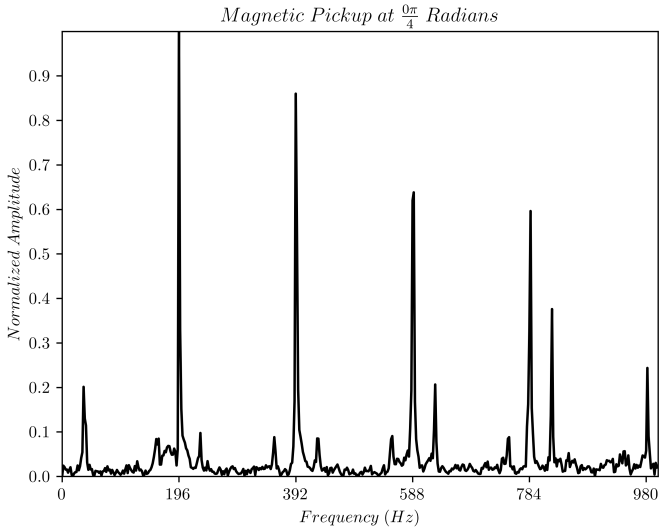


Figure 7.11: Normalized amplitude frequency spectrum of the signal from the magnetic pickup at the first position for a total time period of 0.5 seconds.

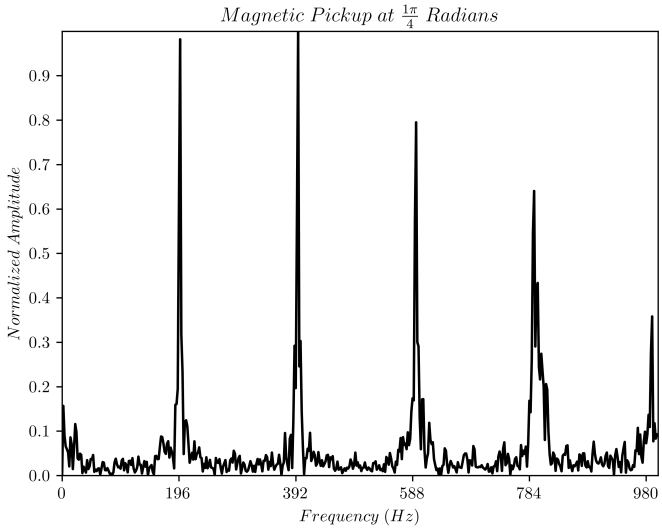


Figure 7.12: Normalized amplitude frequency spectrum of the signal from the magnetic pickup at the second position for a total time period of 0.5 seconds.

resolution discretization of signals over a longer period on time. Fig. 7.10 is based off the same bow stroke velocity and bow forces used for all signals recorded for this thesis. It shows that with a higher resolution signal, a more complete frequency spectrum of magnetic pickup signal can be achieved and does exist. It shows at least three extra harmonics present in the

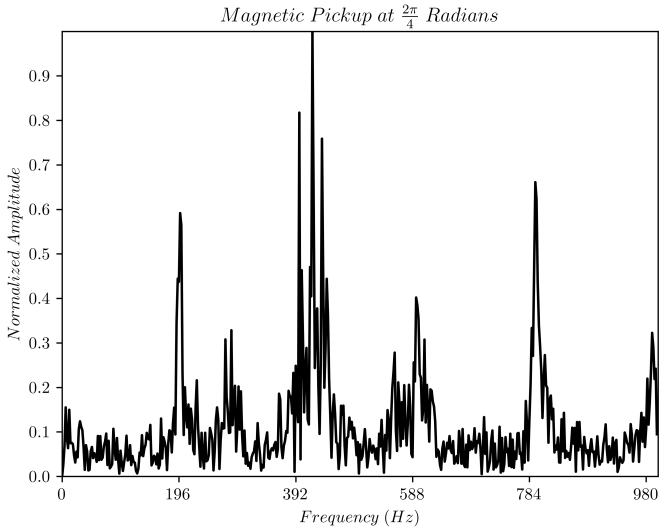


Figure 7.13: Normalized amplitude frequency spectrum of the signal from the magnetic pickup at the third position for a total time period of 0.5 seconds.

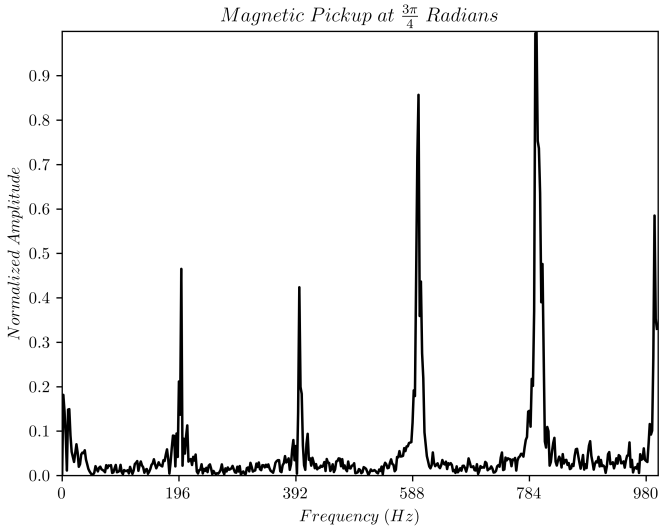


Figure 7.14: Normalized amplitude frequency spectrum of the signal from the magnetic pickup at the fourth position for a total time period of 0.5 seconds.

signal (1176 Hz, 1372 Hz, and 1960 Hz), which could not be seen in signals that were 0.5 seconds long with an only marginally higher discretization.

With basic tonal theory in mind, figures, Fig. 7.11, Fig. 7.12, Fig. 7.15, and Fig. 7.18 maintain the fundamental frequency, 196 Hz, as the most amplified frequency in each of

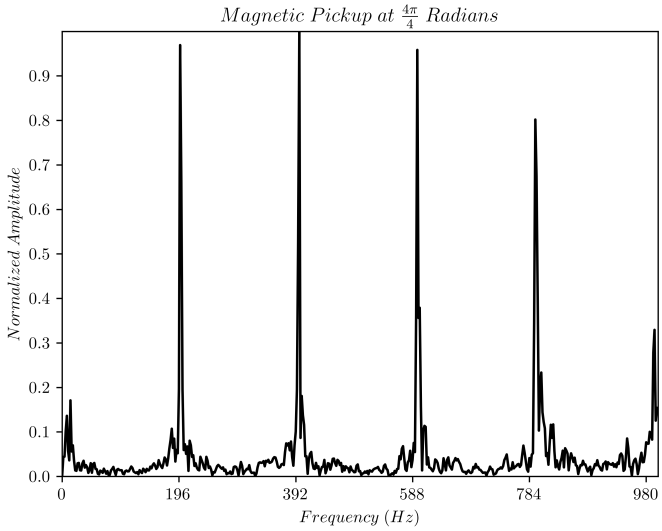


Figure 7.15: Normalized amplitude frequency spectrum of the signal from the magnetic pickup at the fifth position for a total time period of 0.5 seconds.

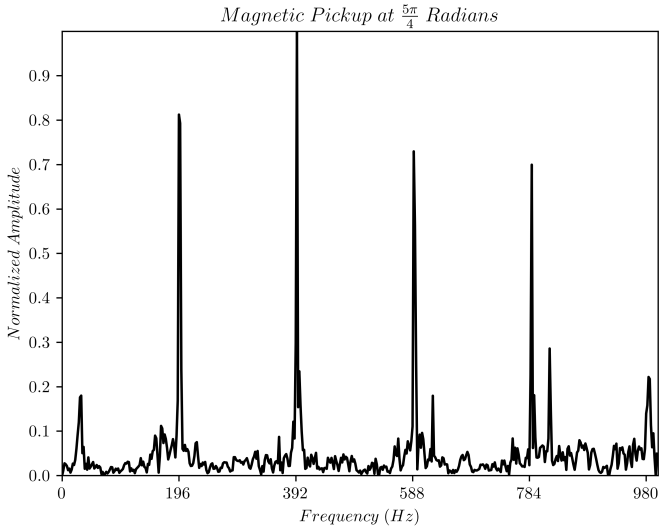


Figure 7.16: Normalized amplitude frequency spectrum of the signal from the magnetic pickup at the sixth position for a total time period of 0.5 seconds.

the distributions. In all these figures, the following three harmonics, 392 Hz, 588 Hz, and 784 Hz, have amplitudes that are at least 50% of the fundamental frequency amplitude. These are high harmonic-to-fundamental-frequency ratios, which indicate a fuller sound and a brightness to the sound. At the same time, the fundamental frequency is still the most

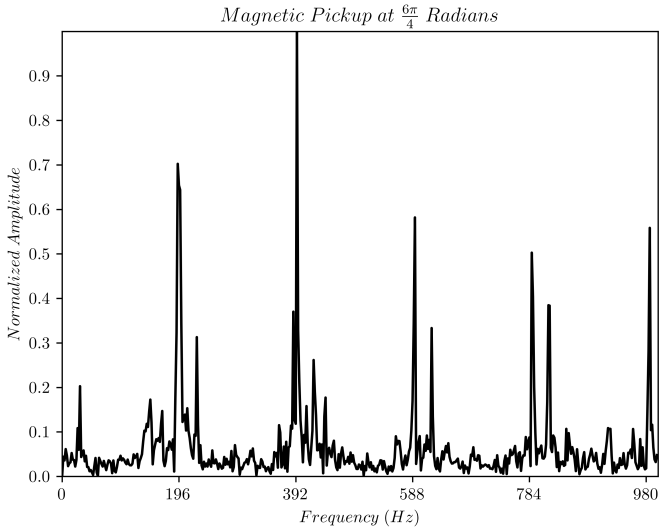


Figure 7.17: Normalized amplitude frequency spectrum of the signal from the magnetic pickup at the seventh position for a total time period of 0.5 seconds.

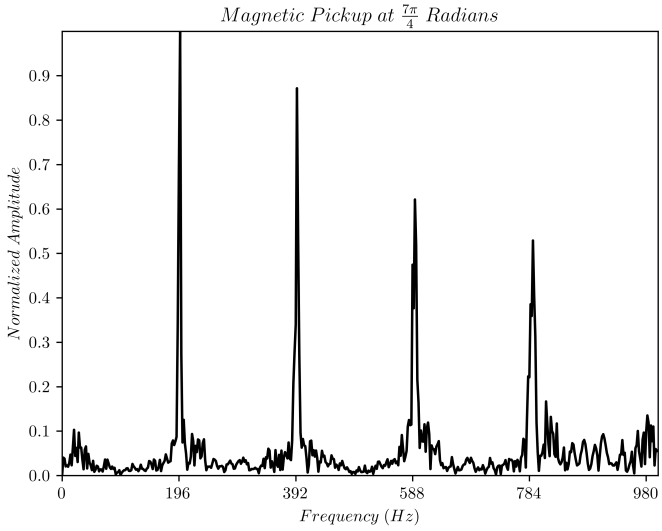


Figure 7.18: Normalized amplitude frequency spectrum of the signal from the magnetic pickup at the eighth position for a total time period of 0.5 seconds.

dominant frequency in each respective spectrum.

Fig. 7.14 shows the frequency spectrum of the magnetic pickup signal in the top left diagonal position. It exhibits expected behavior of a string, in that the correct harmonics are more or less present, but the fundamental frequency, 196 Hz, is not the dominant frequency

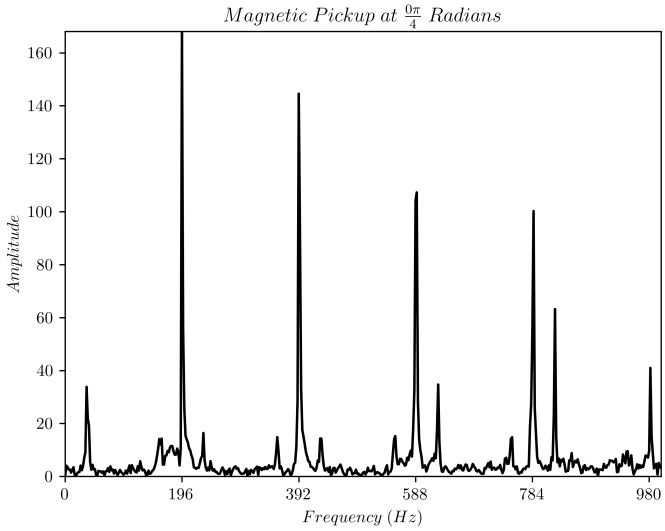


Figure 7.19: Linear amplitude frequency spectrum of the signal from the magnetic pickup at the eighth position for a total time period of 0.5 seconds.

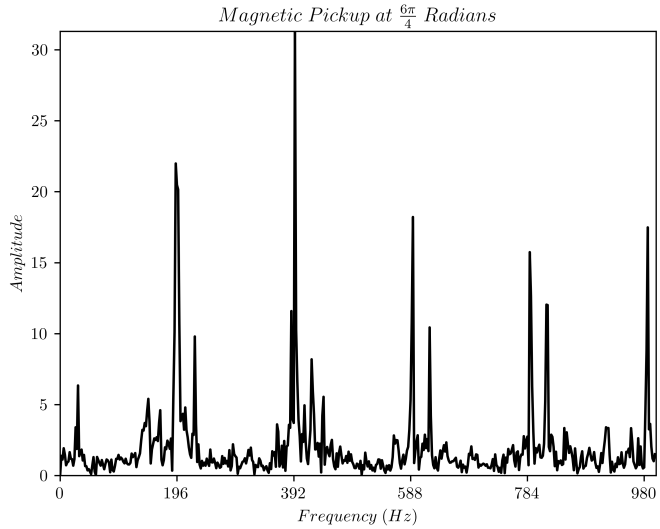


Figure 7.20: Linear amplitude frequency spectrum of the signal from the magnetic pickup at the eighth position for a total time period of 0.5 seconds.

in the spectrum. It should be noted that the most amplified frequencies in this spectrum are slightly higher than 196 Hz or the following harmonics. It is possible that this is an instance of pitch glide due to nonlinear string-barrier interaction and the effects of nonlinear string tension, where the frequency "glides" higher during the initial moments in time immediately

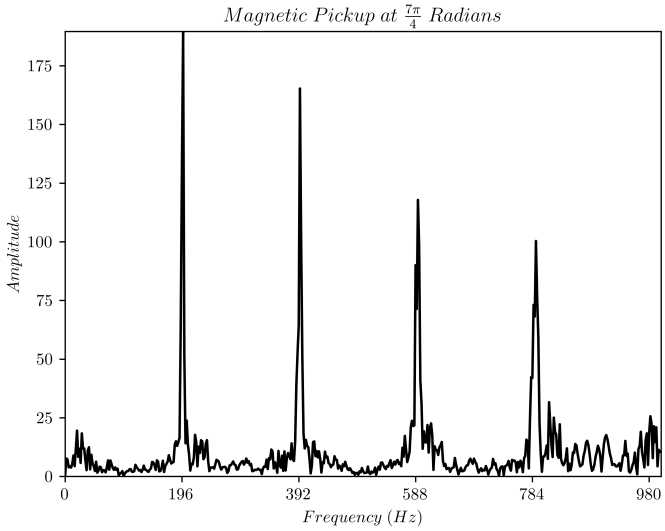


Figure 7.21: Linear amplitude frequency spectrum of the signal from the magnetic pickup at the eighth position for a total time period of 0.5 seconds.

after excitation [14]. But these are very small changes in frequency. Another consideration is that the string may have changed tuning due to changes in temperature. The latter consideration is the more probable and small variations in pitch like that can go unnoticed, even to trained professionals. For the spectra that exhibit good tonal behavior and have instances of amplitude peaks near expected harmonics, pitch glide could potentially be an explanation. Consider again Fig. 7.14 for the signal of the magnetic pickup at position, $\frac{3\pi}{4}$. The peak amplitudes occur at frequencies, 198 Hz, 396 Hz, 796 Hz, and 990 Hz. For the frequencies, the nominal percent difference from their corresponding expected harmonics are respectively, 1.01%, 1.01%, 1.51%, and 1.01%. Aside from the percent difference for 784 Hz, the consistency in percent differences for the other frequencies is probably due to the constant geometry of the bridge and nut for the one repetition of the experiment. This would be the case such that the bridge and string and the nut and string present two nonlinear string-barrier instances. The bridge and nut have small radii when considered as barriers and larger barriers induce greater percent difference in pitch, or pitch gliding. The fact that for these spectra the percent differences are high, but the barrier radii are small, change in string tuning due to temperature and long durations of play time are probably also factors.

If one considers the end point fixtures as barriers which change the wave behavior of the string when it is oscillating near and against them, it is also possible to consider a similar effect from the bow hairs, assumed they can be treated as a barrier where wave behavior of string displacement is affected. Looking to the corresponding spectrogram, Fig. 7.30, it can be seen that for the most prominent frequencies near 588 Hz and 784 Hz maintain consistent frequency amplitude across time segments. In Kartofelev et al.'s work, pitch glide reached a maximum near the time of excitation, as shown in their Fig. 2 [14]. Similar work is found in the research conducted by Lee et al. as well and the results of this thesis can be compared to the results of that previous study [19]. But for a bowed string, excitation is approximately continuous, so the percent differences for the frequencies of the signal should be sustained as long as the bow excites the string. In contrast, a spectrogram for a plucked string, if it experienced pitch glide, should exhibit a frequency amplitude presence at the pitch glided frequency initially, then fall back down to the nominal, expected frequency. So pitch glide and a sightly out of tune string due to short term temperature drop may explain why the most amplified frequencies are only approximately 1% higher than the expected nominal frequencies. This effect can be seen in various other frequency spectra.

Fig. 7.16, which shows the frequency spectrum of the bottom left diagonal position of the magnetic pickup, also does not feature the fundamental frequency as the dominant frequency. With the magnetic pickup position at $\frac{5\pi}{4}$, 392 Hz is the most dominant frequency. The spectrum also does not exhibit the same behavior of higher frequencies with large amplitudes being near the expected harmonics, multiples of 196, but are not results of pitch glide. Fig. 7.13 shows the spectrum of the magnetic pickup signal with the pickup at the top vertical position, $\frac{2\pi}{4}$. There is a vague semblance of an expected frequency distribution with peaks at the multiples of 196 Hz, but the signal is very noisy, has a weak amplitude for the fundamental frequency, 196 Hz, and demonstrates that the signal has a very poor frequency distribution. Looking to the result of the magnetic pickup signal at the bottom vertical position, $\frac{6\pi}{4}$, Fig. 7.17 displays a distribution not entirely dissimilar to that of Fig.

7.16. It appears to be a little noisier and has comparatively (to that of the signal from the $\frac{5\pi}{4}$ position) greater peaks at unexpected frequencies near harmonics, which can be observed in Fig. 7.11 and Fig. 7.16.

Looking specifically to figures, Fig. 7.19, Fig. 7.20, and Fig. 7.21, the frequency spectra of linear amplitude for signals of a magnetic pickup at positions, $\frac{0\pi}{4}$, $\frac{6\pi}{4}$, and $\frac{7\pi}{4}$ are given. In relation to the results of Sec. 7.1, these figures show how the vertical string oscillations for a bowed string are greatly dampened. The bottom vertical and bottom right diagonal positions are dependent on downward bow force, further amplifying their signal. The bottom right diagonal and right horizontal positions both have horizontal string oscillations exciting the magnetic field of the pickup in those respective positions. Simply looking to the amplitudes of the fundamental frequency for each, the results show that the amplitude for the bottom vertical position is approximately 8.5× smaller than the amplitude for the bottom right diagonal position and approximately 7.5× smaller than the amplitude for the right horizontal position. For the magnetic pickup signal from the better of the two vertical positions, the frequency amplitudes are significantly smaller in comparison to those of horizontal and diagonal positions. This coincides with the voltage amplitude results of Sec. 7.1 and demonstrates how vertical string oscillations are much weaker, even when transformed and viewed in the frequency domain. This strengthens the proposal in Sec. 2.4 to add a new damping factor or external force term to the vertical transverse bowed string equation, Eq. 2.1.14, which occurs in the interaction between the vertical bow oscillations and the vertical string oscillations.

7.3 Frequency Spectra: pickup position-string polarization comparisons

Results similar to those of Sec. 7.2 were achieved for signals coming from either optical switch. These results serve as helpful benchmarks to compare to the good spectra from

pickup signals. Recall the optical switch signals are related to the transverse string displacements as opposed to the string velocity which is captured by the magnetic pickup. Being able to capture the frequencies of these signals or enhancing them will show that a magnetic pickup for a specific position is a viable alternative to other amplification methods for a bowed instrument.

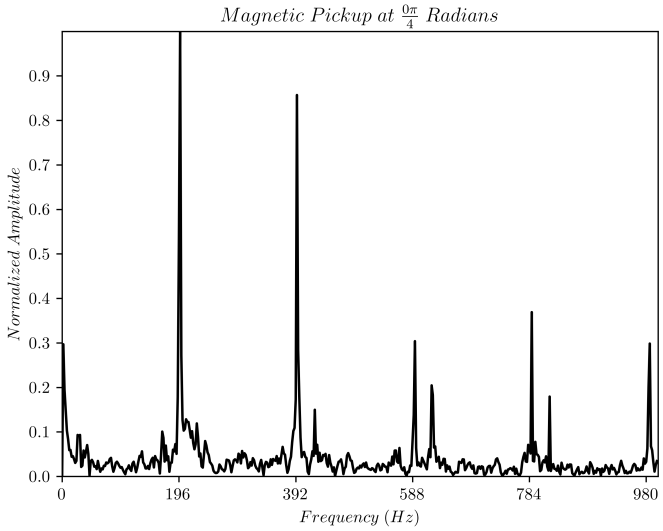


Figure 7.22: Normalized amplitude frequency spectrum of a horizontal optical switch signal for a total time period of 0.5 seconds.

It should be reiterated that the frequency spectra of the experiment results was for signals of lower resolution, leading to a smaller sampling rate and thus simpler frequency distributions reaching only up to around 1000 Hz. When comparing these results to Fig. 7.10 for a signal of 0.05 seconds, one can see a fuller frequency distribution present in a magnetic pickup signal. The results of the experiment for the signals of the magnetic pickup at all positions for a time period of 0.5 seconds can also be compared to the signals of the horizontal and vertical optical switches. The voltage signals captured by the optical switches are proportional to the two transverse string displacements, respectively. Comparing the frequency results of the magnetic pickup signals to the results of the optical switch signals can shed light on the relationship between the actual string displacement and what the magnetic pickup is "picking up" from the overall string velocity.

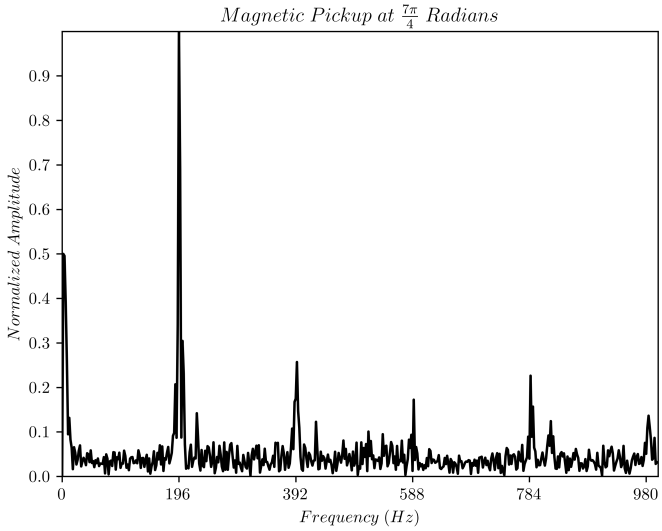


Figure 7.23: Normalized amplitude frequency spectrum of a vertical optical switch signal for a total time period of 0.5 seconds.

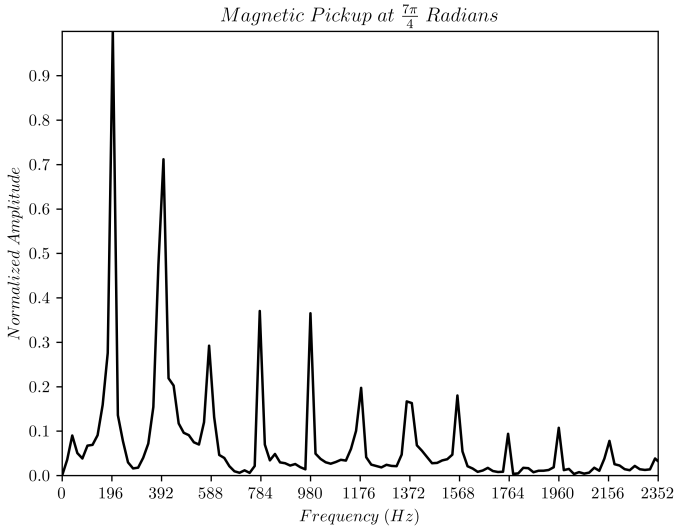


Figure 7.24: Normalized amplitude frequency spectrum of a horizontal optical switch signal for a total time period of 0.05 seconds.

The frequency spectra for the signals of the horizontal optical switch are shown in figures, Fig. 7.22 and Fig. 7.24. Fig. 7.24 displays a fuller, encapsulating frequency distribution. Signals of both time periods, 0.5 seconds and 0.05 seconds display similar amplitudes for the peaking frequencies. For figures, Fig. 7.11, Fig. 7.16, and Fig. 7.17, the appearance

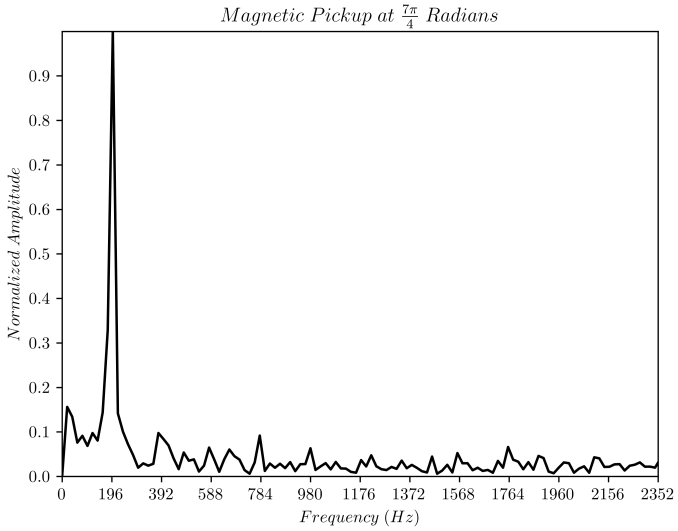


Figure 7.25: Normalized amplitude frequency spectrum of a vertical optical switch signal for a total time period of 0.05 seconds.

of twin peaks near high amplitude harmonics was unexpected. Comparing these results to that of Fig. 7.24, the frequency spectrum for the horizontal optical switch, the same characteristic is observed. There is a potential to rule out the influence of the magnetic pickup on this frequency domain result, given it occurred for both the magnetic pickup and the optical switch signals. This opens the opportunity to future research in deriving the source of this frequency characteristic and attempting to replicate it. When considering the signals of the magnetic pickup at specific positions that produce favorable frequency spectra with a dominating fundamental frequency, high number of present harmonics, and high amplitudes of those harmonics, Fig. 7.22 and Fig. 7.24 seems to lack in comparison. The horizontal optical switch signals exhibit the presence of many harmonics and have the fundamental frequency as the most dominant in amplitude, but after the first two harmonics, the amplitudes decrease for the harmonics, 588, Hz and on. Though they are still there. With the pickup in the best positions for tone, the $\frac{0\pi}{4}$, $\frac{4\pi}{4}$, and $\frac{7\pi}{4}$ positions, harmonics from mechanical string vibrations, which were initially weak in amplitude, were amplified when captured using the magnetic pickup. This is in part related to the reception of a new amplitude scalar to string velocity, given the nature of the derivative of string displacement,

which is a waveform (one can imagine how the chain rule is applied to a sinusoidal function where the derivative gains in amplitude). Much like how the violin's material types and geometries are able to resonant with certain frequencies to amplify them, it is observed that the magnetic pickup can also heighten certain frequency amplitudes to bring out a more excellent sound.

The frequency spectrum for the vertical optical switch signal for 0.5 seconds, shown in Fig. 7.23, is noisy like the spectra for the signals of magnetic pickup placed in either vertical positions. Smaller amplitude frequency peaks can be seen at the harmonics of 196 Hz, but are all very shallow. Fig. 7.25 shows the vertical optical switch signal for 0.05 seconds. This reveals that the most dominant frequency is the fundamental frequency and that the harmonics have very low amplitude. They are surrounded by noisy frequencies of similar low amplitude.

7.4 Spectrograms Between Positions: Frequency Over Time

Additional frequency analysis was conducted on the experiment data by looking at spectrograms. By looking at frequency amplitudes over time for various frequencies, better insight into the use of a magnetic pickup for a bowed string can be achieved. Ideally, for an arbitrary frequency spectrum from the magnetic pickup at a specific position, the associated spectrogram should produce a frequency amplitude that is very close to the normalized amplitudes of the spectrum for all time segments. This is to say that frequency distribution should be consistent over time. This would indicate that frequencies vary little over time. Though, note that signals for this work are both quite short, 0.05 seconds and 0.5 seconds, respectively. Even then, spectrograms are an excellent analysis tool to review the efficacy of magnetic pickups for bowed instruments.

For the start of the results, Fig. 7.26 is given, which is the spectrogram of the magnetic

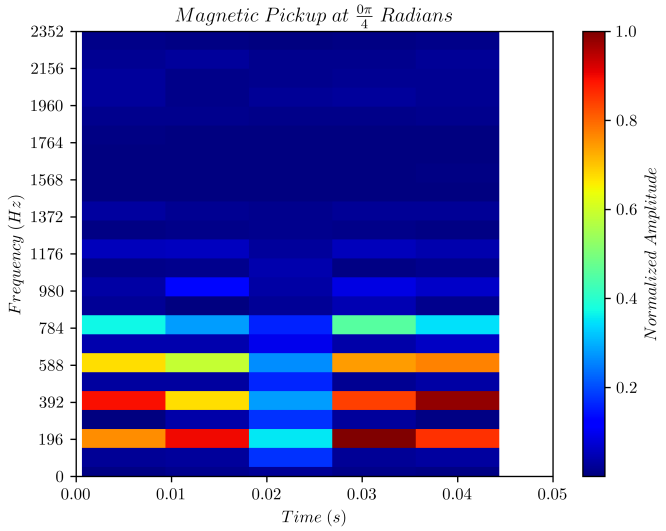


Figure 7.26: Normalized amplitude spectrogram of the signal from the magnetic pickup at the first position for a total time period of 0.05 seconds.

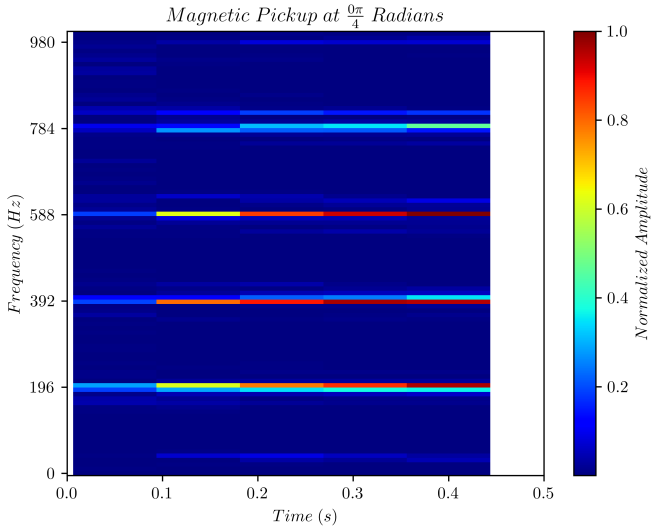


Figure 7.27: Normalized amplitude spectrogram of the signal from the magnetic pickup at the first position for a total time period of 0.5 seconds.

pickup at the $\frac{0\pi}{4}$ position for a total time period of 0.05 seconds. Looking to it, one can see some variability between what frequency is most prominent over time, particularly for 196 Hz and 392 Hz. From 0.02 seconds to 0.03 seconds, there is a drop in overall frequency amplitude across all frequencies, once previously present, but immediately after, the frequencies appear

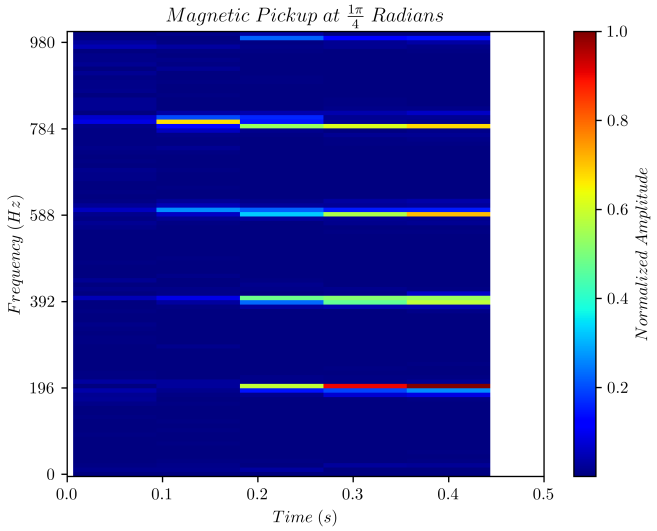


Figure 7.28: Normalized amplitude spectrogram of the signal from the magnetic pickup at the second position for a total time period of 0.5 seconds.

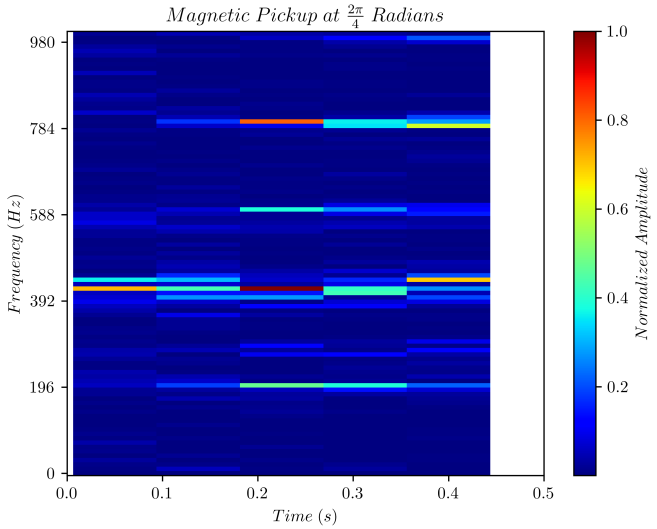


Figure 7.29: Normalized amplitude spectrogram of the signal from the magnetic pickup at the third position for a total time period of 0.5 seconds.

again. This is such a short span of time, it calls into question whether or not such a drop in frequency can be detected by the average listener.

For the experiment results with 0.5 seconds, the results are better fit for the use of spectrograms as analysis tools. Fig. 7.27 is a good spectrogram given that the amplitude of

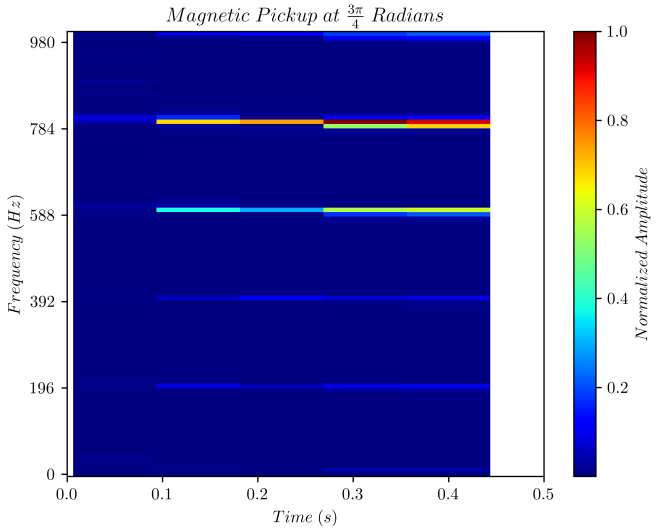


Figure 7.30: Normalized amplitude spectrogram of the signal from the magnetic pickup at the fourth position for a total time period of 0.5 seconds.

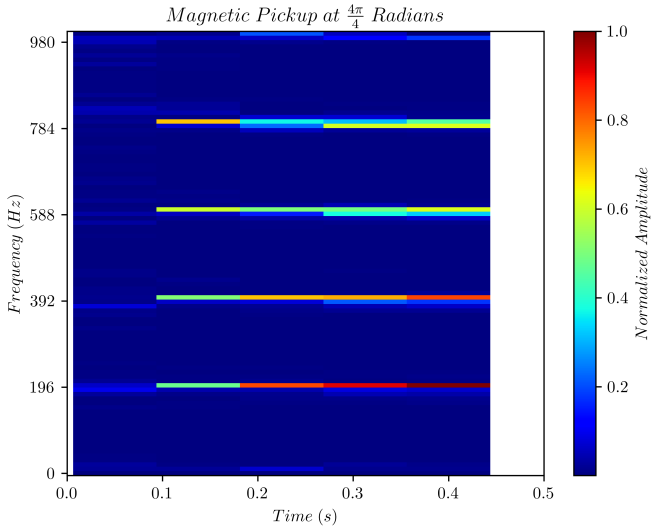


Figure 7.31: Normalized amplitude spectrogram of the signal from the magnetic pickup at the fifth position for a total time period of 0.5 seconds.

the fundamental frequency and three following harmonics is consistent over tenths of seconds respectively. For many of the spectrograms in this section, the first or first two time segments have very low frequency amplitudes and number of frequencies. This is simply the result of no sound being produced as the signal was being recorded by the oscilloscope. Recall that

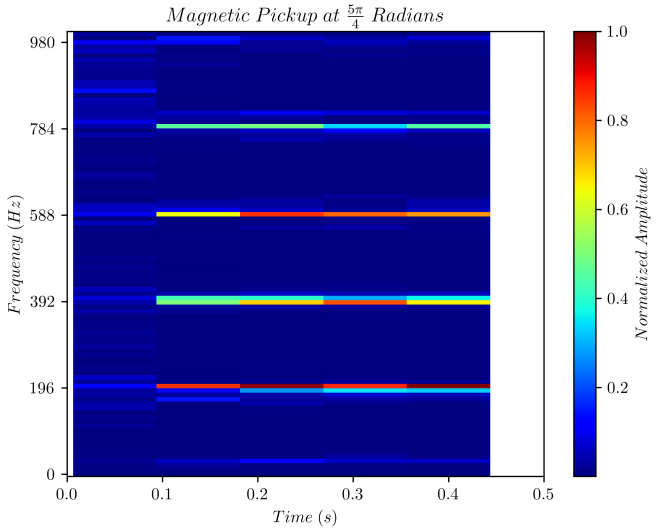


Figure 7.32: Normalized amplitude spectrogram of the signal from the magnetic pickup at the sixth position for a total time period of 0.5 seconds.

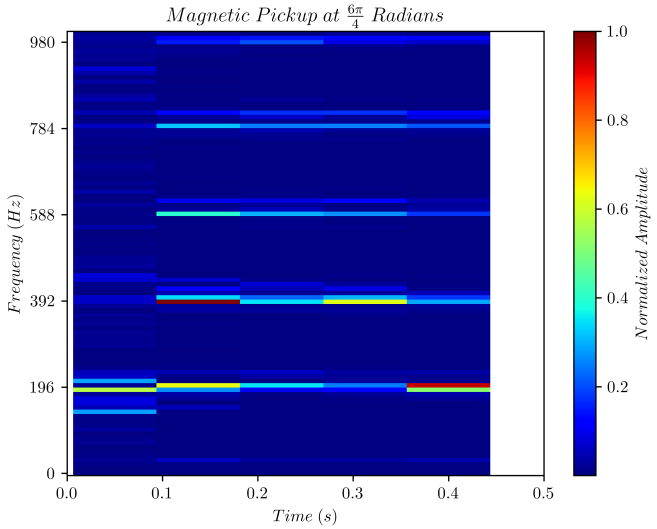


Figure 7.33: Normalized amplitude spectrogram of the signal from the magnetic pickup at the seventh position for a total time period of 0.5 seconds.

the oscilloscope's trigger method used the horizontal optical switch signal channel to trigger recording of 0.5 seconds of data. As the bow stroke mechanism initially moves, the string undergoes the stick regime, where the string's displacement follows the point of the bow in which it is in friction with. That small movement is enough to move the string to change

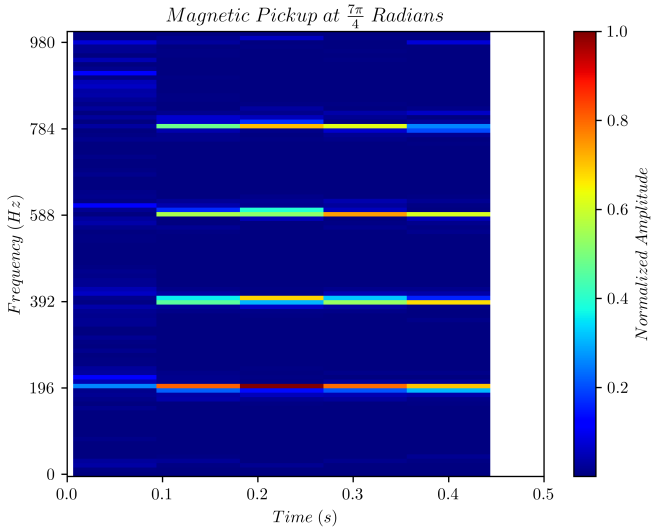


Figure 7.34: Normalized amplitude spectrogram of the signal from the magnetic pickup at the eighth position for a total time period of 0.5 seconds.

the signal of the horizontal optical switch and trigger the oscilloscope to record, but not enough to sufficiently amplify the waveform of the string and thus amplify the associated frequencies of the magnetic pickup signal. No attempt was made to avoid this given that the experiment required consistency between positional data with respect to each signal starting its recording time at the same bow position, not randomly along any bow position as the bow was already in motion. Note that this did not occur for all signals, though. The virtual absence of frequency amplitude among the initial one or two time segments can be expected due to this attempt for inter-positional time consistency and bow stroke location consistency. And given the lower resolution of signals even at a short signal of 0.5 seconds, the signals were not clipped to exclude these portions because for spectrograms, it is beneficial to observe frequency distributions at these longer time segments.

Looking to the signal of the magnetic pickup when it is in the top right diagonal position, $\frac{1\pi}{4}$, its spectrogram, shown in Fig. 7.28, produces good frequency amplitudes for each harmonic in the latter two time segments. This is consistent with the corresponding non-time-dependent frequency spectrum shown in Fig. 7.12. In contrast, when the magnetic pickup is in the top left diagonal position, $\frac{3\pi}{4}$, its spectrogram, shown in Fig. 7.30, reveals

that the fundamental frequency has a very low amplitude over the whole time period. In fact, the harmonic, 784 Hz, is the most amplified overall and over the 0.5 second time period. This is in agreement with the corresponding frequency spectrum shown in Fig. 7.14. Note that in Sec. 7.2, pitch glide considering Fig. 7.30 was discussed. Potential evidence for continuous pitch glide due to the continuous excitation of the string by the bow can be inferred from other spectrograms of the section.

For the signal of the magnetic pickup at the top vertical position, $\frac{2\pi}{4}$, the spectrogram in Fig. 7.29 shows much inconsistency of frequency amplitudes between time segments and reveals that the signal over time, though somewhat orbiting expected frequencies, multiples of 196, does not maintain any orderly structure. With respect to magnetic pickup position, this is not an optimal position when one wants to have a faithful frequency presence and one consistent over time as well. For the magnetic pickup in the bottom vertical position, $\frac{6\pi}{4}$, its signal's spectrogram, shown in Fig. 7.33, shows inconsistency of frequency density between time segments. From 0.1 to 0.2 seconds, 392 Hz is the frequency of peak amplitude, then towards the end of the signal, 196 Hz is. When comparing this result to Fig. 7.17, there is not an inconsistency between the two results, but the spectrogram reveals more information about the signal's frequencies. Though it is a short time period of 0.5 seconds, when the magnetic pickup is in either vertical position, the frequency distribution over time is not very consistent. Given music occurs over time, this would be a problem for the violinist using a magnetic pickup in such a way.

The signal for when the magnetic pickup is in the left horizontal position, $\frac{4\pi}{4}$, produces a good and consistent frequency distribution over time. As seen in Fig. 7.31, each harmonic is consistent between time segments. Additionally, it correlates with the corresponding frequency spectrum seen in Fig. 7.15. Both the spectrograms of the signal of the magnetic pickup in both bottom diagonal positions, $\frac{5\pi}{4}$ and $\frac{7\pi}{4}$ (left and right), are also fairly consistent over time as well.

7.5 Spectrograms of Transverse String Displacements: Frequency Over Time

The spectrograms of the optical switch signals will also be evaluated and discussed. This help provides a reference for the magnetic pickup spectrograms, so that the magnetic pickup signal results can be compared to the optical switches' results.

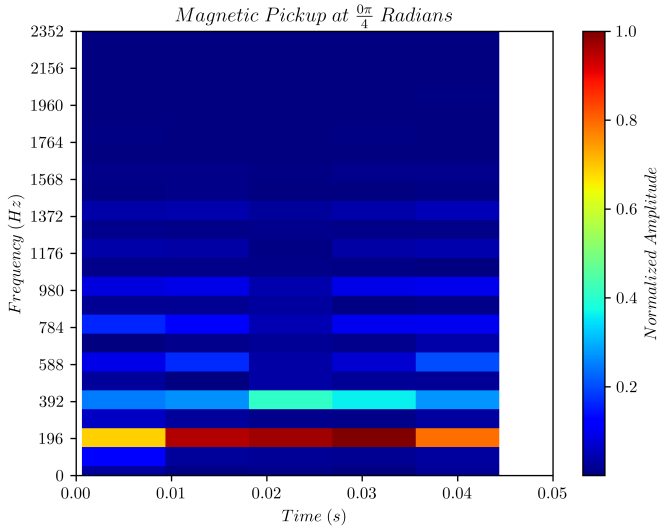


Figure 7.35: Normalized amplitude spectrogram of a horizontal optical switch signal for a total time period of 0.05 seconds.

Figures, Fig. 7.35 and Fig. 7.37, show the spectrograms for the horizontal optical switch signals for time periods, 0.05 seconds and 0.5 seconds respectively. Fig. 7.35 shows a strong continuity of the fundamental frequency's amplitude across all time segments. The same can be said for the 392 Hz harmonic as well. Looking to Fig. 7.37, the same is true, but for a time period of 0.5 seconds. In both figures, there is also the lesser presence of higher harmonics as well, which coincides with the results for the corresponding frequency spectra for the horizontal switch signals shown in figures, Fig. 7.24 and Fig. 7.22.

Figures, Fig. 7.37 and Fig. 7.38, show the spectrograms for the vertical optical switch signals for time periods, 0.05 seconds and 0.5 seconds respectively. The spectrogram for the short time period signal of the vertical optical switch reveals frequency amplitude consistency

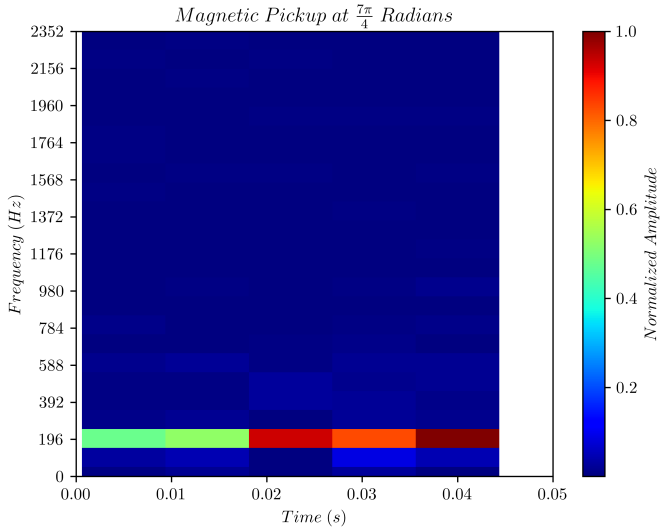


Figure 7.36: Normalized amplitude spectrogram of a vertical optical switch signal for a total time period of 0.05 seconds.

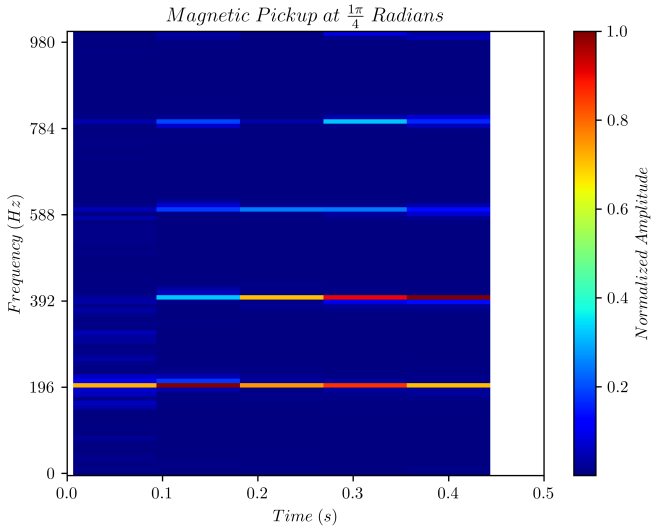


Figure 7.37: Normalized amplitude spectrogram of a horizontal optical switch signal for a total time period of 0.5 seconds.

in the latter time segments, but not the first two. A similar result is found in Fig. 7.38. In addition, the frequency amplitude of the fundamental frequency slightly diminishes towards the end of the signal's time.

The spectrograms of the horizontal optical switch signals correlate most with the spectro-

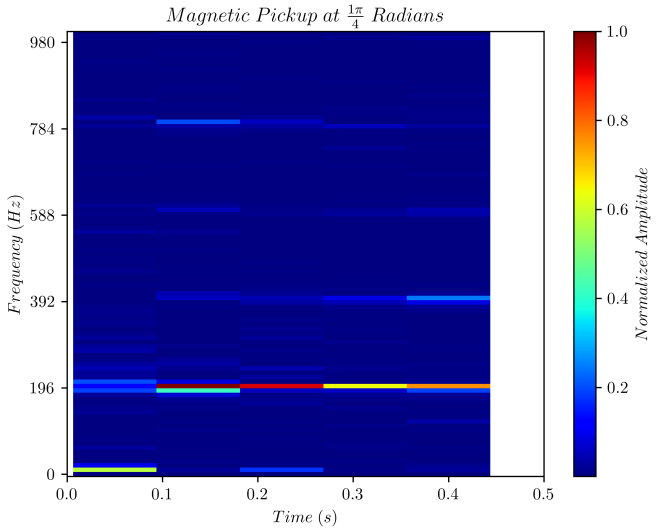


Figure 7.38: Normalized amplitude spectrogram of a vertical optical switch signal for a total time period of 0.5 seconds.

grams of the signals of the magnetic pickup for the positions, $\frac{0\pi}{4}$, $\frac{4\pi}{4}$, $\frac{5\pi}{4}$, and $\frac{7\pi}{4}$. The number of frequencies in these magnetic pickup spectrograms do not reach the same number as in the horizontal optical switch's for a 0.05 signal, but this is only due to the signal resolution automatically generated by the specific oscilloscope used. This result was expected because the magnetic pickup in the horizontal positions and the bottom diagonal positions make it to where the magnetic field can be excited through its horizontal components (and the diagonal positions allow the smaller influences of the vertical oscillations of the string to affect the vertical components of the field). For these more optimal magnetic pickup positions, the spectrograms show that the tone of a note can be reliably maintained over time. A more effective method for the future would be to apply the same spectrogram technique to a much longer signal on a time period that envelops typical note length for common time signatures and tempos in sheet music.

7.6 Magnetic Flux Density Over Time

Based on the assumptions made regarding the construction of the magnetic pickup in Sec. 3.4, the assumptions regarding the magnetic field in Sec. 2.2 and Sec. 5.5, and initial conditions for magnetic flux density of the magnetic pickup's magnet, Faraday's Law of Induction was solved for with respect to time. The initial conditions were taken with a Gaussmeter and were applied to the magnet pole face facing the string. It was discussed in Sec. 7.1 that voltage outputs were greater for the magnetic pickup signals when the pickup was in the bottom diagonal positions and the right horizontal position. This was due to the initial displacement of the string due to downward bow force. A similar result was found when taking the initial conditions for the signal at each position. The initial conditions of all the signals for when the pickup was in the bottom positions, were comparatively higher than when the pickup was located horizontally or above. This had to do with the magnetized string being closer to the magnet pole face. It stands to reason that with this extra initial string displacement due to the weight on the tip of the bow, which was approximately the length of the bow away from the inward facing magnet pole face, the number of field lines of the magnetic field passing through the cross-sectional area of the coils would be much greater, affecting thus magnetic flux density. For future work, using different amounts of downward bow force and horizontal bow force would be a fruitful exploration when measuring magnetic flux density over time. To reiterate, this experiment erred on the side of greater downward bow force to ensure realistic frequency distributions of the bowed string.

One of the most interesting results for magnetic flux density over time can be seen in figures, Fig. 7.39, Fig. 7.40, Fig. 7.41, and Fig. 7.42. Before discussing the main feature of these, one ought to look to a plot of magnetic flux density over time for a shorter signal time. Fig. 7.39 maintains a higher resolution because it has nearly the same discretization size as the experiment signals but covers a tenth of the time elapsed. Looking first to this figure, it strongly exhibits a sawtooth wave pattern. In fact, all the figures for the magnetic pickup at a horizontal or bottom diagonal position display a variant of the sawtooth wave

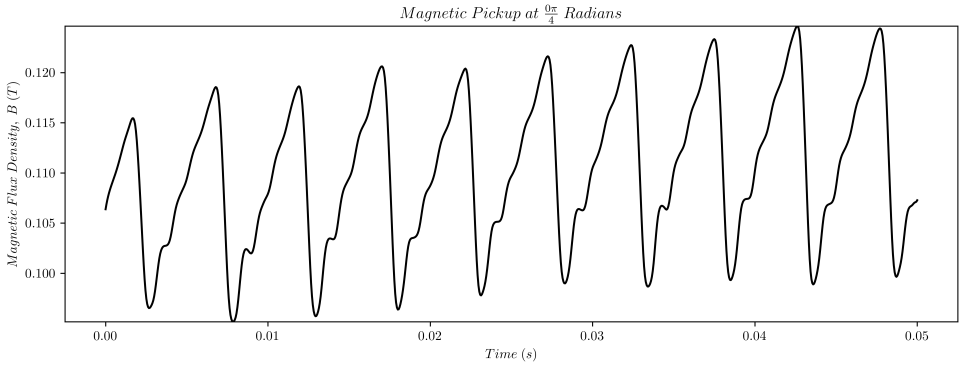


Figure 7.39: Magnetic flux density over time for the signal from the magnetic pickup at the first position for a total time period of 0.05 seconds.

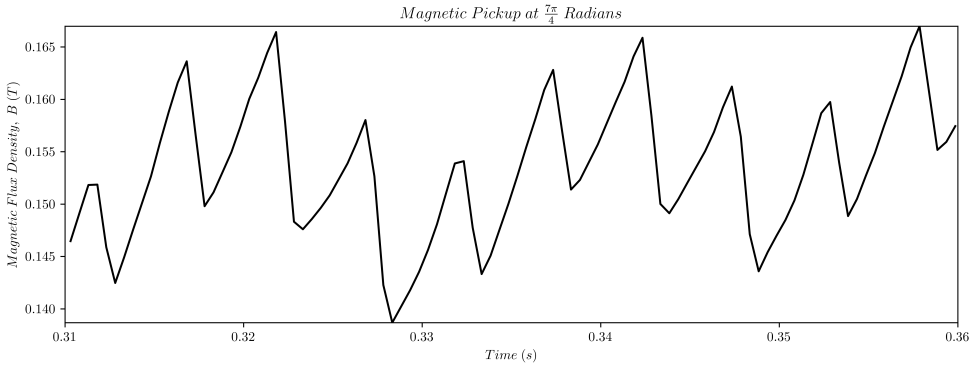


Figure 7.40: Magnetic flux density over time for the signal from the magnetic pickup at the eighth position for a total time period of 0.05 seconds. This was from the third iteration of the experiment.

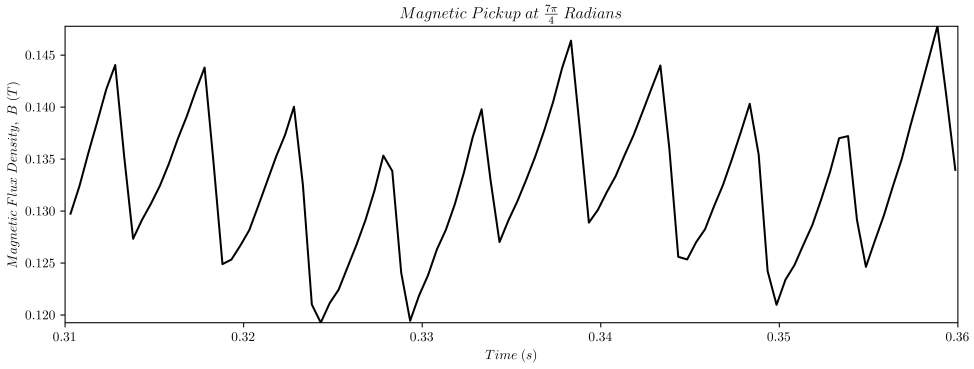


Figure 7.41: Magnetic flux density over time for the signal from the magnetic pickup at the eighth position for a total time period of 0.05 seconds. This was from the second iteration of the experiment.

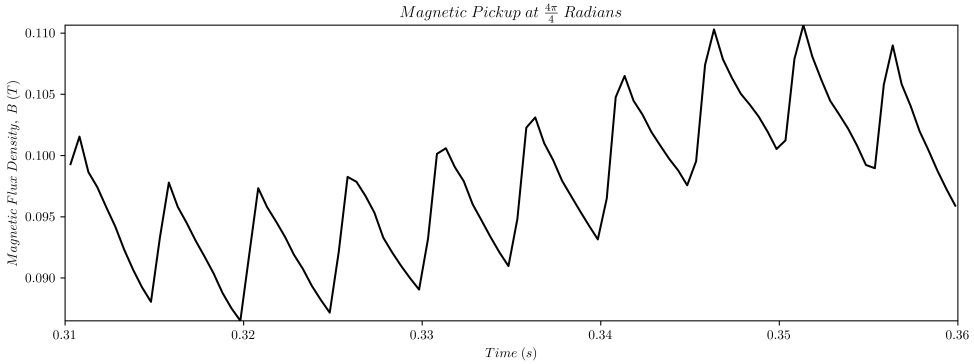


Figure 7.42: Magnetic flux density over time for the signal from the magnetic pickup at the fifth position for a total time period of 0.05 seconds. This was from the second iteration of the experiment.

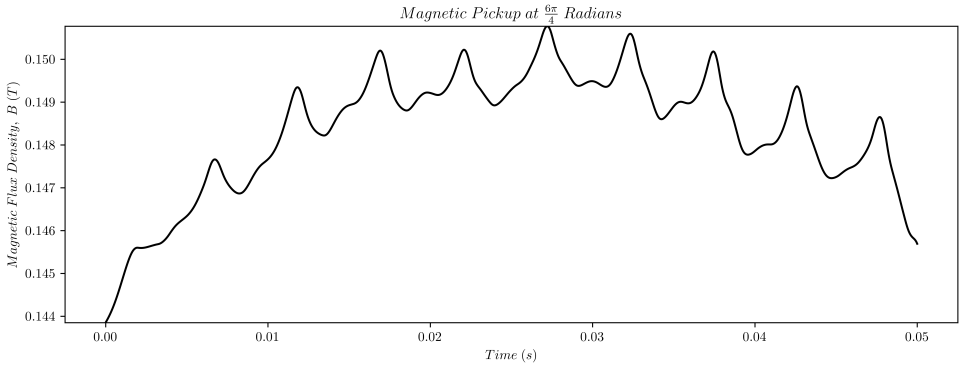


Figure 7.43: Magnetic flux density over time for the signal from the magnetic pickup at the seventh position for a total time period of 0.05 seconds.

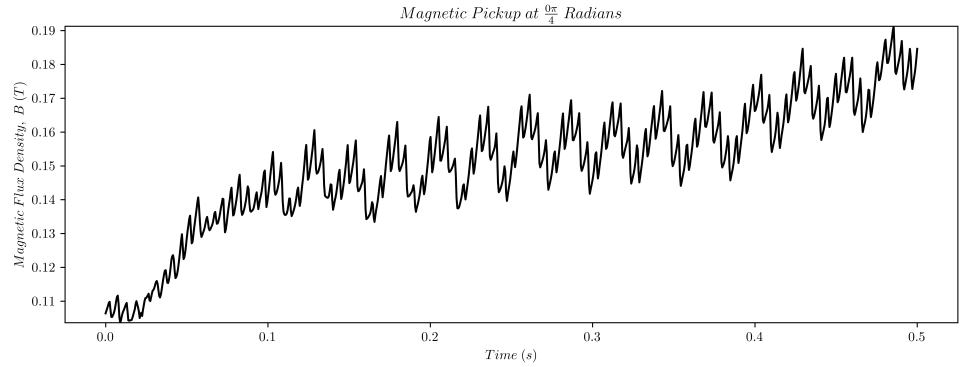


Figure 7.44: Magnetic flux density over time for the signal from the magnetic pickup at the first position for a total time period of 0.5 seconds.

pattern. The reason for this pattern is because of the wave pattern of the horizontal string displacement of a bowed string. As it was discussed in Sec. 2.1, for the horizontal trans-

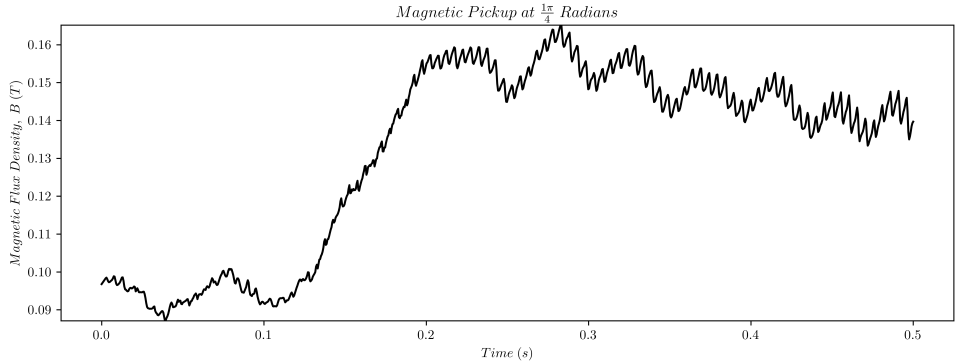


Figure 7.45: Magnetic flux density over time for the signal from the magnetic pickup at the second position for a total time period of 0.5 seconds.

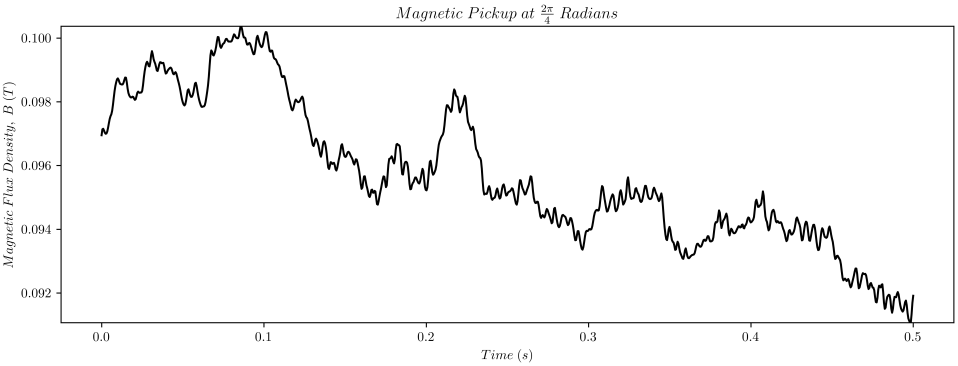


Figure 7.46: Magnetic flux density over time for the signal from the magnetic pickup at the third position for a total time period of 0.5 seconds.

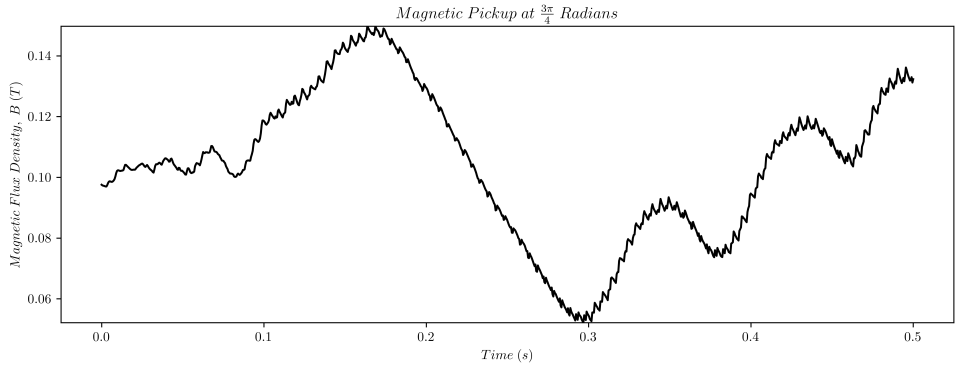


Figure 7.47: Magnetic flux density over time for the signal from the magnetic pickup at the fourth position for a total time period of 0.5 seconds.

verse string displacement of a bowed string, assuming the string is producing Helmholtz motion, the displacement should resemble a very orderly sawtooth pattern. Fig. 7.39 seems

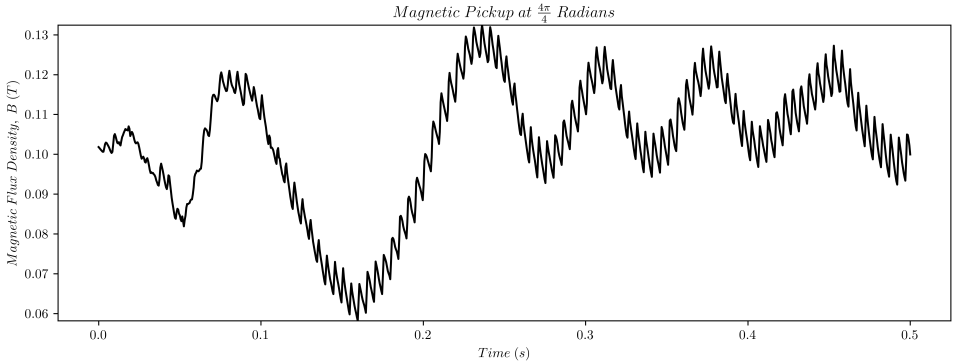


Figure 7.48: Magnetic flux density over time for the signal from the magnetic pickup at the fifth position for a total time period of 0.5 seconds.

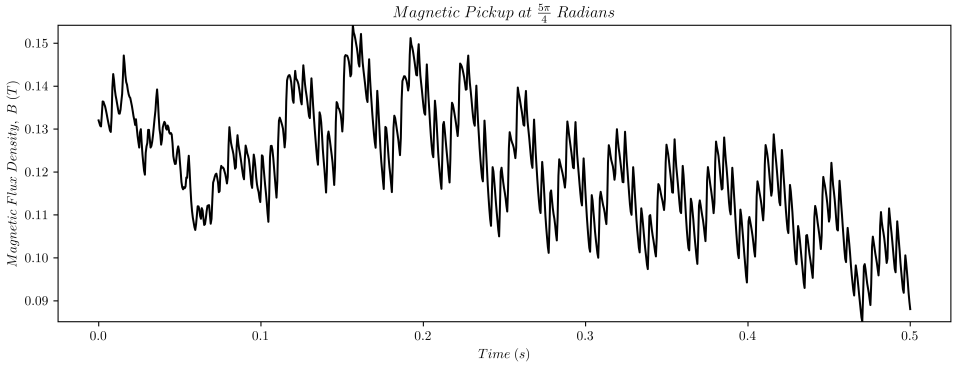


Figure 7.49: Magnetic flux density over time for the signal from the magnetic pickup at the sixth position for a total time period of 0.5 seconds.

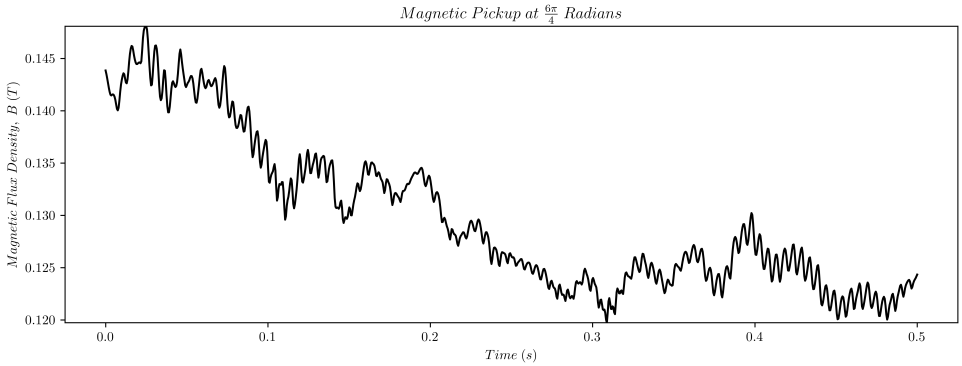


Figure 7.50: Magnetic flux density over time for the signal from the magnetic pickup at the seventh position for a total time period of 0.5 seconds.

to demonstrate Helmholtz motion displacement [1]. This also correlates with the results of the horizontal optical switch, triangular wave displacement from Cremer, and the horizontal

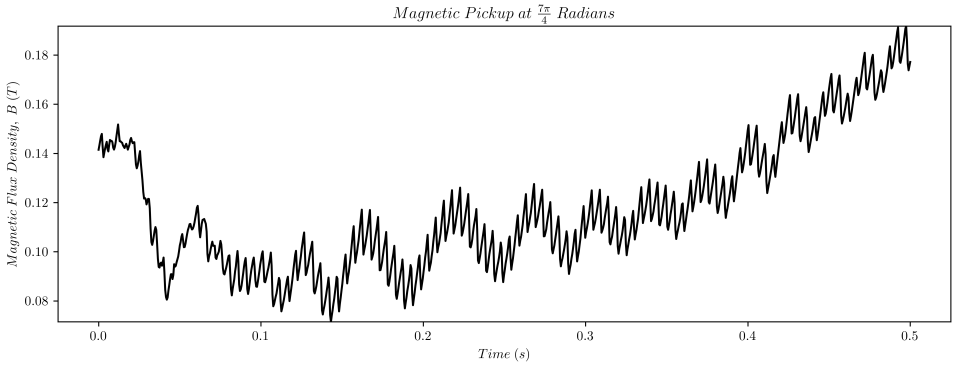


Figure 7.51: Magnetic flux density over time for the signal from the magnetic pickup at the eighth position for a total time period of 0.5 seconds.

bowed string displacement simulation [4, 2]. Over time, the waveform climbs, indicating a continuous change in amplitude. Though, the plot indicates it is quasi-periodic on this short time period. Looking to the stick phases of the displacement, the sloped sections, it does not exhibit a straight line as would be expected for Helmholtz motion displacement. Near the start of each stick phase, there is a second corner developed and then two extremely shallow corners (analogous to a sloped wave of long wavelength) before each local maximum crest. Considering the Schelleng diagram again, as mentioned in Sec. 3.6, the bow position is in the *sul tasto* range, around 66 mm from the bridge end point, and that the downward bow force is qualitatively high along with the horizontal bow force, as evidenced by the calibration of the experiment's bow forces and the results in Sec. 7.1 [32, 1]. There are qualitative indications in bow forces with respect to bow position that indicate the expected motion of the experiment's bow stroke mechanism should be that of Helmholtz motion or even slightly non-periodic motion. With the Schelleng diagram, this specific result indicates that, due to an insufficiently high horizontal bow force, there should be multiple-slip motion displacement where small spikes appear along the main stick phase slope of Helmholtz motion displacement. Though, consider that horizontal bow force is only a sufficient cause of multiple-slip motion displacement. This type of motion and displacement qualitatively indicates an insufficiently high enough static friction coefficient or an excessively high slipping friction coefficient for the bow-string interface. One way other than the application of

insufficient bow forces to effect either of these is to have a lack of rosin on the bow, which decreases the static friction. It is possible to then have both the presence of high bow forces and instances of multiple-slips in the bowed string motion's displacement. The lack of sufficient amount of rosin applied to the bow is a plausible explanation for the inter-stick phase slips as seen in Fig. 7.39. Despite this, many of the characteristics of this displacement are indicative of Helmholtz motion and its displacement. Note also that this plot, along with the others of this section, denotes magnetic flux over time, not explicitly the displacement of the string. There are many other factors to consider in describing its characteristics such as the other independent variables and scalars in Faraday's Law of Induction, Eq. 2.2.11, or particularly the methods used to reduce Faraday's Law and model a non-uniform magnetic field. For this short time period, the reduction of Faraday's Law of Induction and rudimentary modeling of the non-uniform magnetic field are sufficient. This is supported by the observed Helmholtz motion displacement sawtooth waveform, existence of explainable minor slips in the stick phase of the displacement, the quasi-periodicity of the waveform, and the value range of magnetic flux density falling within or near the expected range as mentioned in Sec. 6.6.

For figures, Fig. 7.40, Fig. 7.41, and Fig. 7.42, there are qualitative characteristics of Helmholtz motion displacement with the appearance of the sawtooth waveform. They are also quasi-periodic, but to a lesser degree qualitatively. Recall that for these figures, they are derived from a longer time signal of 0.5 seconds. The full plots of magnetic flux density over time for the magnetic pickup signals at each position are depicted in figures, Fig. 7.44 – Fig. 7.51. More discussion of periodicity and accuracy of the reduction and model with respect to the signals and magnetic flux density over time plots in the associated figures will be provided later in this section.

Looking to magnetic flux density over time for when the pickup is in a vertical position, as seen in Fig. 7.43, it does not exhibit similar characteristics to displacement due to horizontal string oscillations. Recall that Helmholtz motion is derived from the stick-slip

regime of the bow and string. The static and slipping frictions that cause that type of motion and thus displacement are in horizontal directions, not vertical ones, assuming the string is excited transversely in the positive y-direction (simulating a down bow). The bowed string will vibrate vertically due to transverse displacement, downward bow force, and transfer of energy from horizontal vibrations, but the string does not experience the same type of friction as it would horizontally. As it was demonstrated in Sec. 2.2, electromotive force or voltage and the components of the magnetic field are dependent on string displacement in both transverse directions, even as the magnetic field is rotated as the magnetic pickup is rotated from position to position (noted in Sec. 2.3). So, it would be sensible to think that bowed string motion appears in magnetic flux density over time. And at least for short time signals, this occurrence also provides more justification for the assumptions made regarding Faraday's Law of Induction for this specific design of magnetic pickup and the design of the experiment.

Fig. 7.42 is the magnetic flux density over time for the signal of the magnetic pickup when it is located in the left horizontal position. Notice that it is a sawtooth pattern, but in the other direction. Most overviews of displacement of horizontal bowed string motion shows it in the other direction. But in this figure, this is the result of the magnetic pickup point in the same direction of the bowing direction. This same result can be seen for when the pickup is in the left horizontal position as well.

On the shorter time period, as for Fig. 7.39, for certain signals of specific pickup positions, magnetic flux density over time exhibits the displacement of Helmholtz motion apart from minor slips due to lower static friction from a lack of rosin on the bow and only strong quasi-periodicity as opposed to pure periodicity of the waveforms. This is the most significant result of Sec. 7.6. Quasi-periodicity was observed in figures, Fig. 7.42 – Fig. 7.41, but to a lesser extent. Those plots were derived from pickup signals of 0.5 seconds as opposed to 0.05 seconds. Looking at the totality of these signals in figures, Fig. 7.44 – Fig. 7.51, there are many differences from signals of 0.05 seconds like that shown in Fig. 7.39. First

recall in Sec. 7.4 the issue of time consistency between experiment repetitions of the main experiment. This compromise allowed for inter-repetition synchronicity in time with the same starting bow position at the expense of having around 0.2 seconds of initial signal that would not be representative of a genuine bow stroke. With this in mind, for all signals of the main experiment repetitions, within the first 0.1– 0.2 seconds, magnetic flux density over time generally did not display any meaningful sense of order or periodicity. All signals except for the signals when the pickup was placed vertically as seen in figures, Fig. 7.46 and Fig. 7.50, displayed generally unique signal envelopes. Magnetic flux density over time was somewhat similar for when the pickup was in positions, $\frac{0\pi}{4}$, $\frac{5\pi}{4}$, and $\frac{7\pi}{4}$, in that when applying a periodic window to each, the waveforms were qualitatively shaped similarly. Local extrema amplitudes of magnetic flux density over time for positions $\frac{1\pi}{4}$ and $\frac{3\pi}{4}$ as shown in figures, Fig. 7.45 and Fig. 7.47, were comparatively smaller than those of other positions, excluding those of vertical positions. As it was shown in figures, Fig. 7.42 – Fig. 7.41, sawtooth waveforms, indicative of bowed string motion displacement, are exhibited in a shorter time period for magnetic flux density over time for the signals in all positions except the vertical ones. This is observed for figures, Fig. 7.44 – Fig. 7.51, except for figures, Fig. 7.45 and Fig. 7.47. It is perhaps possible to argue there is local periodicity, but for these pickup positions' signals and figures, the sawtooth waveform appears similarly to wave composition of a low frequency wave and high frequency wave.

When looking to the longer signals and deriving magnetic flux density, there are sawtooth wave forms locally, but weak local quasi-periodicity and definitive global non-periodicity. And for some signals, particularly for pickup positions, $\frac{3\pi}{4}$, $\frac{4\pi}{4}$, and $\frac{7\pi}{4}$, magnetic flux density falls below the expected range as detailed in Sec. 6.6. But, This must also be compared to the figure showing magnetic flux density as a function of vertical distance from the magnet pole face, Fig. 6.5. This would indicate that the magnetic flux density values for the signals of the specified positions are not as low when taking into account vertical distance of a probe and the position of the string segments altering the magnetic field over time. The global

non-periodicity of magnetic flux density over time and weak local quasi-periodicity of the sawtooth waves of the aforementioned figures for the specific signals could be the result of one of two or both causes to be discussed. First, the reduction of Faraday's Law of Induction and or the rudimentary modeling of the non-uniform magnetic field, both being based on certain simple assumptions, may be inherently unable to accurately capture magnetic flux density for longer periods of time. Recall that for magnetic flux density over time for short signals, there are many characteristics that argue in favor of the approximations' accuracy in a short time period. Future areas of research could be applied to utilizing and improving on different models of magnetic pickups to then capture magnetic flux density over time for pickup signals derivative of a bowed string. Another potential cause or explanation is that magnetic flux density is not identical with Helmholtz motion displacement or displacement of bowed sting motion in general. String displacements in both transverse directions are independent variables of the pickup's magnetic field, as shown in equations, Eq. 2.3.1 and Eq. 2.3.2, so it would make sense some form of displacement will appear in magnetic flux density over time. When tuning the approximation of Faraday's Law of Induction and the magnetic field in Sec. 2.2 and Sec. 5.5, frequency spectra were used to help calibrate the approximations and used to see how much magnetic flux density over time was influenced by string displacement. These specific results were not provided, but many of the spectra for signals of both 0.05 seconds and 0.5 seconds did in fact exhibit amplitude peaks at 196 Hz and following harmonics, but also sometimes at 20 Hz. For the longer signals, the string and string velocity harmonics were present but with a maximum amplitude at typically 20 Hz and much noise in the range up to about 100 Hz. With this aside about frequency spectra in this application, wave composition should be considered when considering magnetic flux density over time. This would explain the presence of bowed string motion displacement with the sawtooth waveform locally and its associated weak quasi-periodicity, which would be dependent on the structure of lower frequency waves present in the result. With these two causes or explanations in mind, it can be argued that it is likely that, with respect to searching

for the displacement of Helmholtz motion in magnetic flux density over time, the causes of weak local quasi-periodicity and global non-periodicity are a non-exclusive combination, first, of the reduction of Faraday's Law of Induction and basic magnetic field modeling being inherently unable to accurately capture magnetic flux density over longer time periods and second, of the structure of magnetic flux density over time being only partially dependent on the horizontal transverse string displacement of the bowed string. For the latter possible explanation, consider that for Fig. 7.39 and Fig. 7.44, which represent magnetic flux density over time for the $\frac{0\pi}{4}$ position but for a 0.05 second and 0.5 second signal respectively, the magnetic flux density range was approximately 0.02 Tesla wide for both the 0.05 second plot and a 0.05 second window from 0.2 seconds to 0.25 seconds for the 0.5 second plot. The local extrema of these two windows, the crests of the sawtooth waveforms, differed in that those of the latter window do not exhibit the same approximation of periodicity of the first. Acknowledging these similarities and differences specifically inform the plausibility of the magnetic flux density realistically having a waveform beyond just that of a function of horizontal string displacement. There is potential for magnetic flux density over time to be globally quasi-periodic with a sawtooth waveform of Helmholtz motion displacement or general bowed string motion displacement. But, again, this topic can be, instead, explored further in future research with respect to using better modeling for the magnetic field and exploring the presence of Helmholtz motion displacement with respect to magnetic flux density.

7.7 Subjectively Bowed String

After the survey of the main experiment results and discussion of these results, it would also prove to be beneficial to compare these results to those of a plucked string of subjective excitation force and those of a bowed string of subjective excitation force. Subjective excitation force on the string refers to an arbitrary amount of plucking or bowing force being applied

to the string. For the experiment, a constant bow velocity and downward bow force was necessary to compare the results of the magnetic pickup signals for each position from one to another. This standard need not apply for capturing the results of this section and the next. To reiterate, the author is a classically trained violinist of over 20 years of experience. The plucked string and bowed string experienced forces which would elicit a sound whose loudness would be considered *mezzo forte*, which is the formal musical term for "moderately loud." For both subjective results, it was decided to only look at the results for the magnetic pickup at three positions, $\frac{0\pi}{4}$, $\frac{6\pi}{4}$, and $\frac{7\pi}{4}$, which are the right horizontal, bottom vertical, and bottom right diagonal positions.

7.7.1 Waveforms And Voltage Outputs

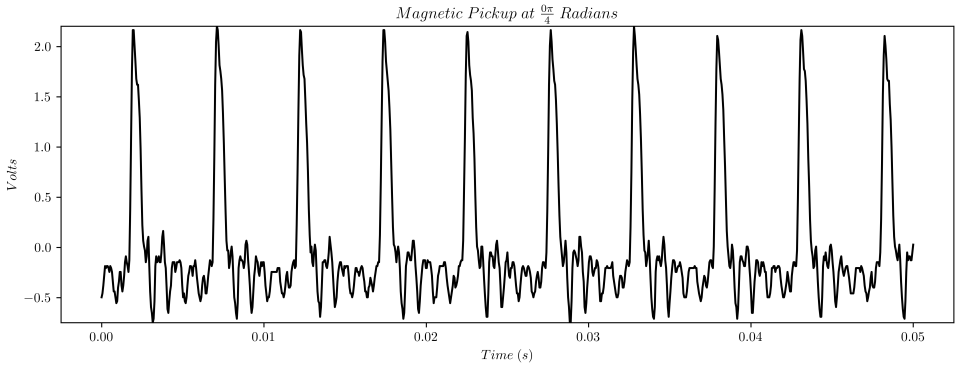


Figure 7.52: Magnetic pickup signal waveform of a bowed string of subjective force at the specified pickup position.

Looking at waveforms of the magnetic pickup signals for the three positions, the maximums and averages are compared respectively. For position, $\frac{0\pi}{4}$, Fig. 7.52 shows that the maximum voltage output is 2.2 volts. The average voltage output is 0.66 volts. For position, $\frac{6\pi}{4}$, Fig. 7.53 shows that the maximum voltage output is 0.15 volts. The average voltage output is 0.06 volts. And for position, $\frac{7\pi}{4}$, Fig. 7.53 shows that the maximum voltage output is 1.24 volts. The average voltage output is 0.4 volts. After a quick comparison of these voltage values to those shown in Sec. 7.1, these are decidedly lower. Even with a middling bow

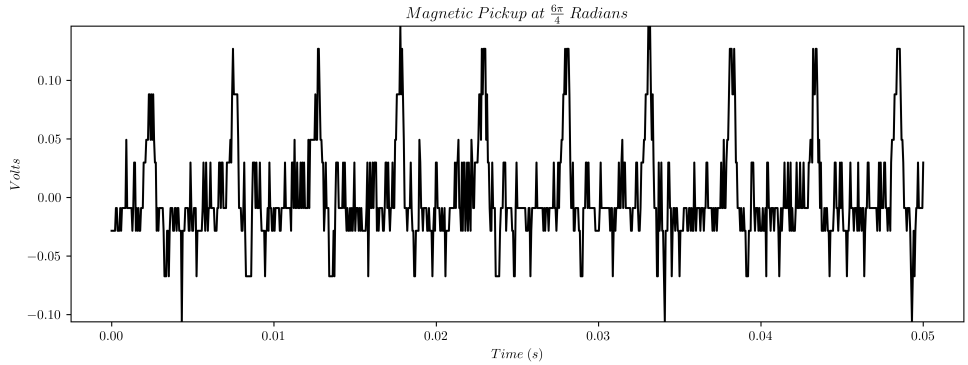


Figure 7.53: Magnetic pickup signal waveform of a bowed string of subjective force at the specified pickup position.

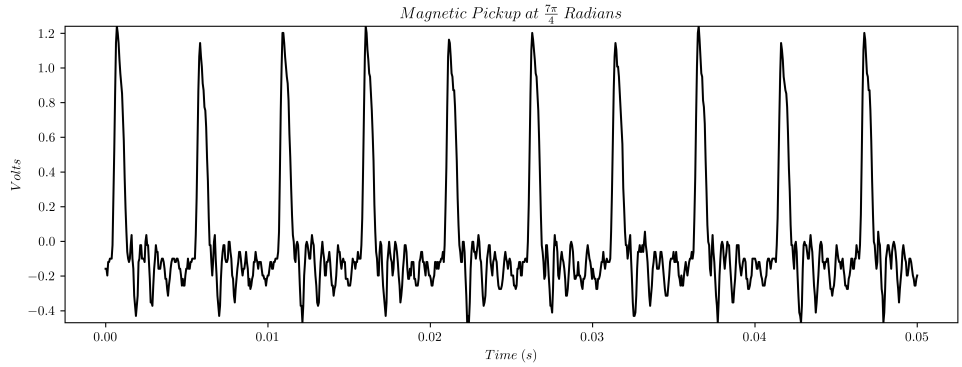


Figure 7.54: Magnetic pickup signal waveform of a bowed string of subjective force at the specified pickup position.

force applied, these voltage ranges for the pickup in the horizontal and diagonal positions are entirely sufficient for amplification's sake. As expected, the maximum voltage output of the magnetic pickup signal in the vertical position is comparatively lower, similar to the results for vertically placed pickups in Sec. 7.1.

7.7.2 Frequency Spectra

When looking at the frequency spectra of the magnetic pickup signals for when the string is bowed with subjective bow forces, there are the favorable results in accordance with good tonal quality. For all spectra, shown in figures, Fig. 7.55, Fig. 7.56, and Fig. 7.57, the fundamental frequency, 196 Hz, G_3, is the most amplified frequency. For all spectra, there is

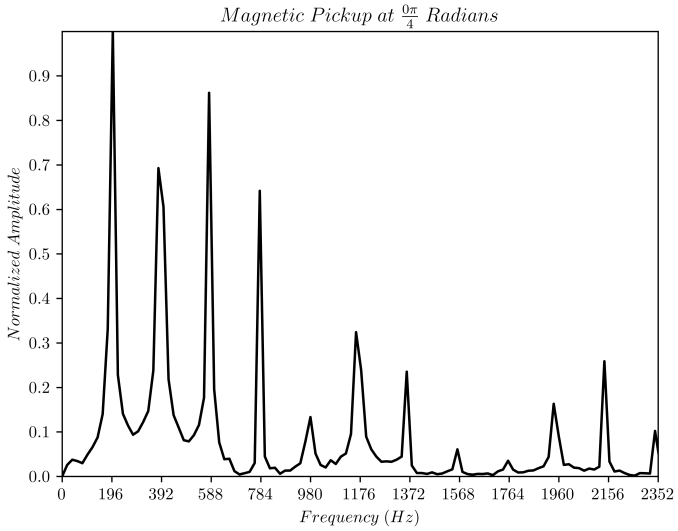


Figure 7.55: The frequency spectrum of the magnetic pickup signal of a bowed string of subjective force at the specified pickup position.

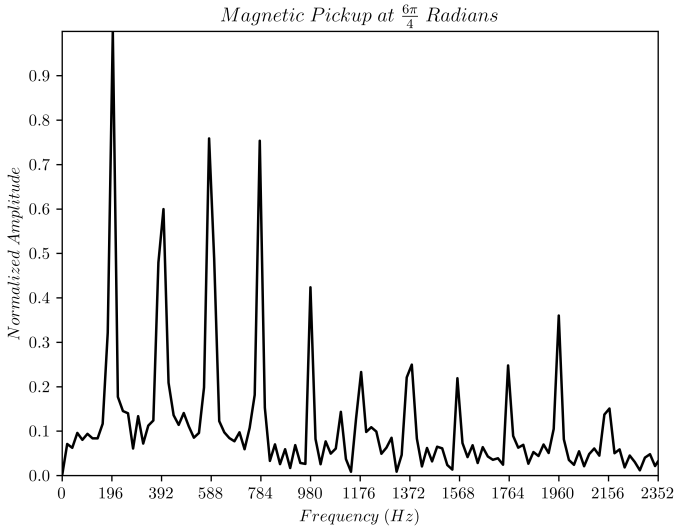


Figure 7.56: The frequency spectrum of the magnetic pickup signal of a bowed string of subjective force at the specified pickup position.

a healthy presence of following harmonics in both amount and their respective amplitudes. Though the amplitudes are small, ranging from 0.2 to 0.3, the spectra for the magnetic pickup in the bottom vertical position as seen in Fig. 7.56 has the most following harmonics between the three spectra (though this is not to disregard that for a non-normalized linear

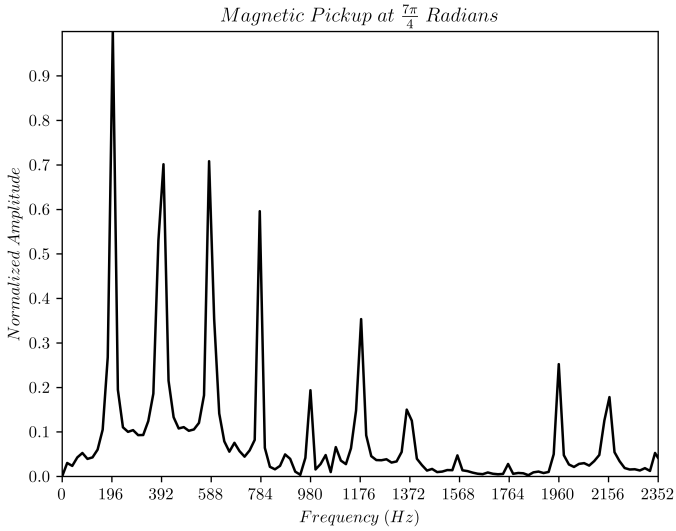


Figure 7.57: The frequency spectrum of the magnetic pickup signal of a bowed string of subjective force at the specified pickup position.

scaling, the modal amplitudes are decidedly smaller than the modal amplitudes of a spectrum of a signal receiving significant influence from horizontal string displacement). Comparing these results to those shown in Sec. 7.2 and Sec. 7.3, these frequency spectra results match well with the better results in those sections.

7.7.3 Spectrograms

In figures, Fig. 7.58 and Fig. 7.60, the frequency amplitudes across time segments are fairly consistent, indicating a steady sound across the short time period. These results for a subjectively bowed string match well with the results seen in Sec. 7.4 for the corresponding pickup positions. Note that unlike the signals recorded for the main experiment, these signals are not time consistent with one another, meaning that the signals were recorded for 0.05 seconds, but at different bow segments, even if close. Recall Fig. 7.10 and how there is a loss of frequency amplitude for the time segment containing 0.02 seconds along the time axis. Fig. 7.58 and Fig. 7.60 give the same characteristic, but when the pickup is in the $\frac{7\pi}{4}$ position as seen in Fig. 7.59, the spectrogram does not exhibit the same characteristic. It

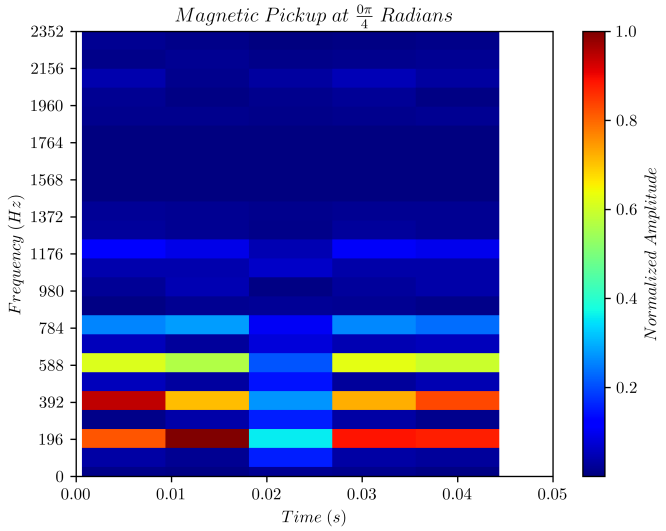


Figure 7.58: The spectrogram of the magnetic pickup signal of a bowed string of subjective force at the specified pickup position.

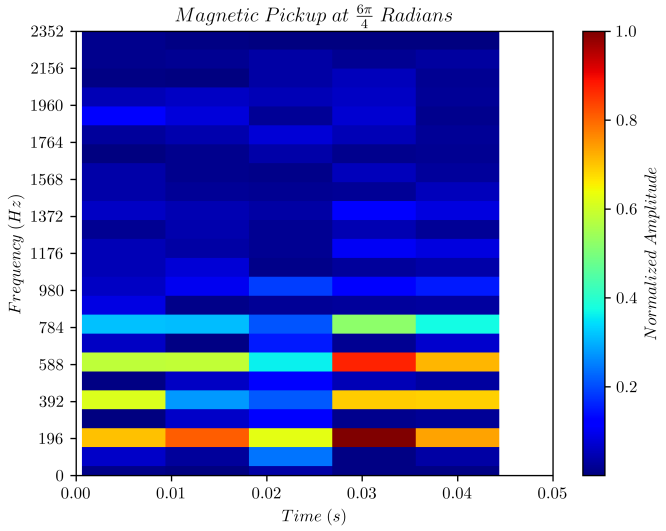


Figure 7.59: The spectrogram of the magnetic pickup signal of a bowed string of subjective force at the specified pickup position.

instead shows a loss in overall frequency amplitude across the 0.03 second time segment. As it was previously stated in Sec. 7.4, it is doubtful that the human listener can detect this short change in frequency over time.

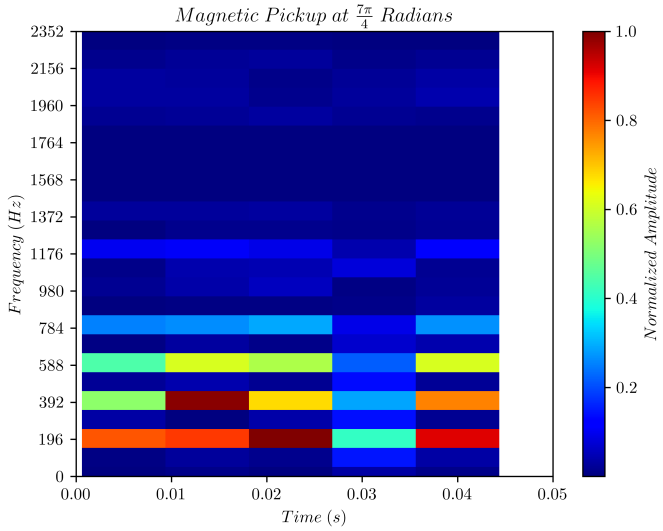


Figure 7.60: The spectrogram of the magnetic pickup signal of a bowed string of subjective force at the specified pickup position.

7.7.4 Magnetic Flux Density Over Time

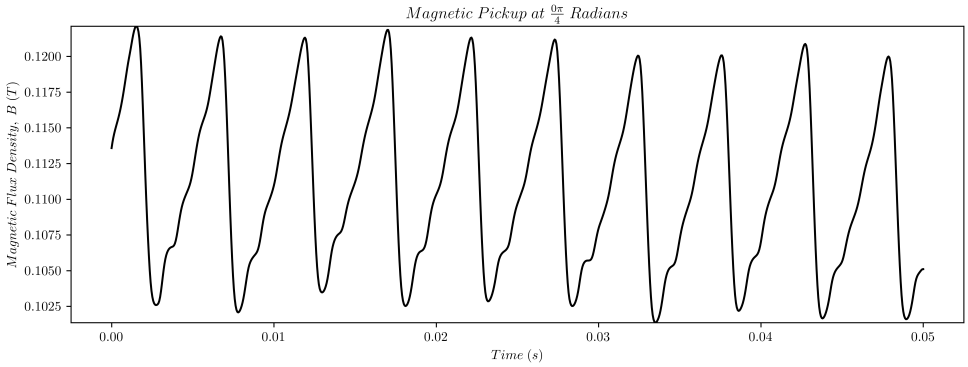


Figure 7.61: The magnetic flux density over time for the magnetic pickup signal of a bowed string of subjective force at the specified pickup position.

Similar to the results of Sec. 7.6 for the signals of the magnetic pickup in horizontal and diagonal positions, Fig. 7.61 and Fig. 7.63 also demonstrate a waveform similar to the bowed string displacement corresponding to Helmholtz motion. So even with varying bow velocities and bow forces, this result is consistent. Exploring this waveform behavior of a magnetic pickup signal from a bowed string proves to be an interesting potential future research area. Though, the same waveform pattern is not present when the magnetic pickup

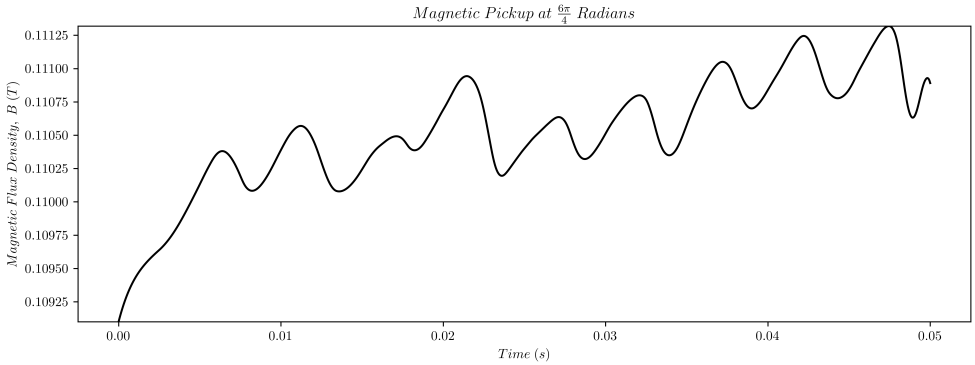


Figure 7.62: The magnetic flux density over time for the magnetic pickup signal of a bowed string of subjective force at the specified pickup position.

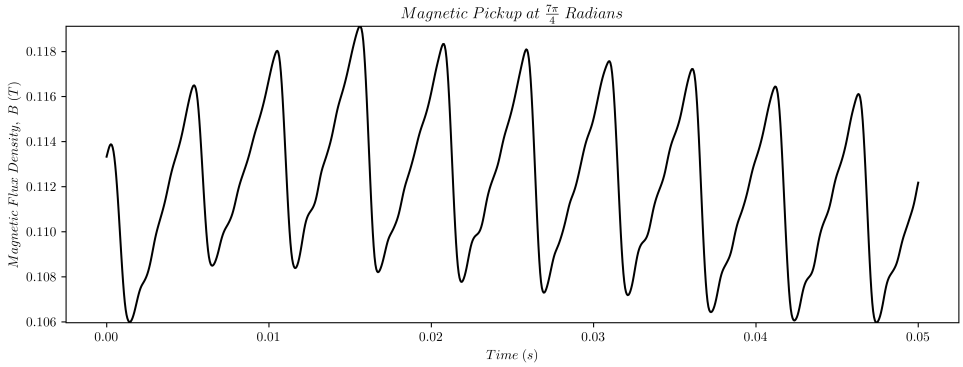


Figure 7.63: The magnetic flux density over time for the magnetic pickup signal of a bowed string of subjective force at the specified pickup position.

was in the vertical position, which can be viewed in Fig. 7.62.

7.8 Subjectively Plucked String

7.8.1 Waveforms and Voltage Outputs

Looking to figures, Fig. 7.64, Fig. 7.65, and Fig. 7.66, the maximum voltages can be observed for the plucked string of subjective force. The same magnetic pickup positions as the subjectively bowed string were used. Like those results, these signals are also not time consistent between each other, in that the standard for applied string force was maintaining a *mezzo forte* level of loudness. For position, $\frac{0\pi}{4}$, the maximum and average voltages, respec-

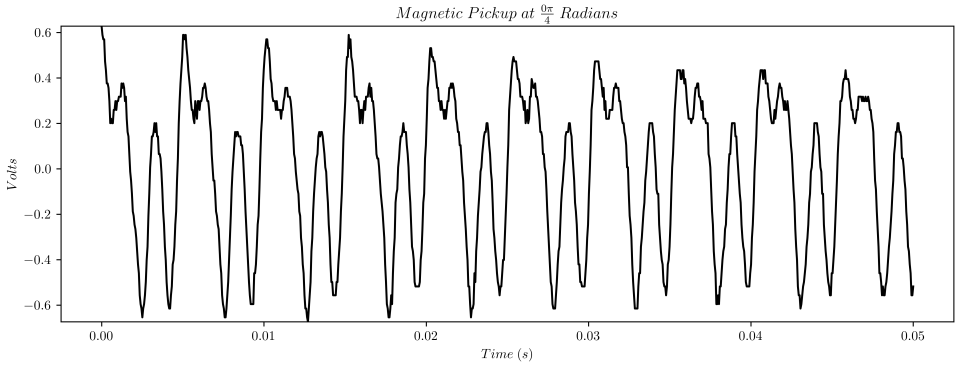


Figure 7.64: Magnetic pickup signal waveform of a plucked string of subjective force at the specified pickup position.

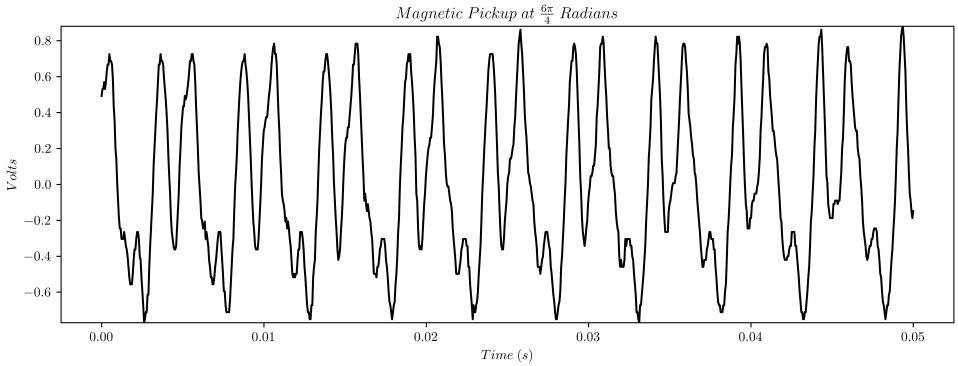


Figure 7.65: Magnetic pickup signal waveform of a plucked string of subjective force at the specified pickup position.

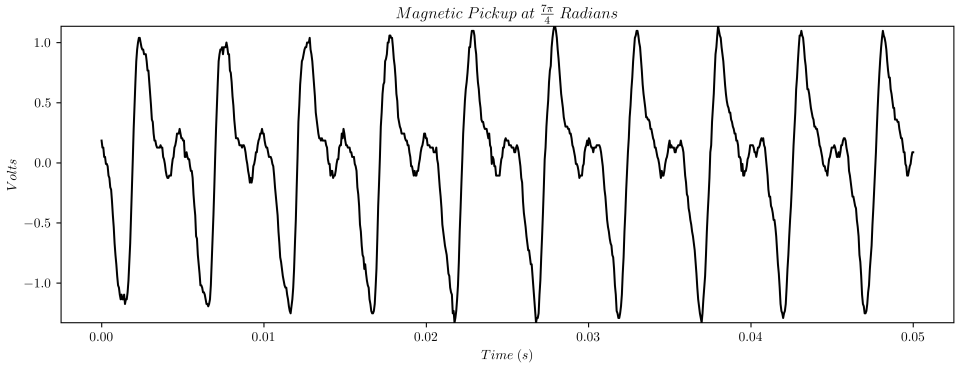


Figure 7.66: Magnetic pickup signal waveform of a plucked string of subjective force at the specified pickup position.

tively, were 0.67 volts and 0.43 volts. For position, $\frac{6\pi}{4}$, the maximum and average voltages, respectively, were 0.88 volts and 0.68 volts. And for position, $\frac{7\pi}{4}$, the maximum and average

voltages, respectively, were 1.33 volts and 0.63 volts. The signal for when the pickup is in the bottom right diagonal position exhibits the highest maximum and average voltage outputs. Note that the waveforms are sinusoidal in nature.

7.8.2 Frequency Spectra

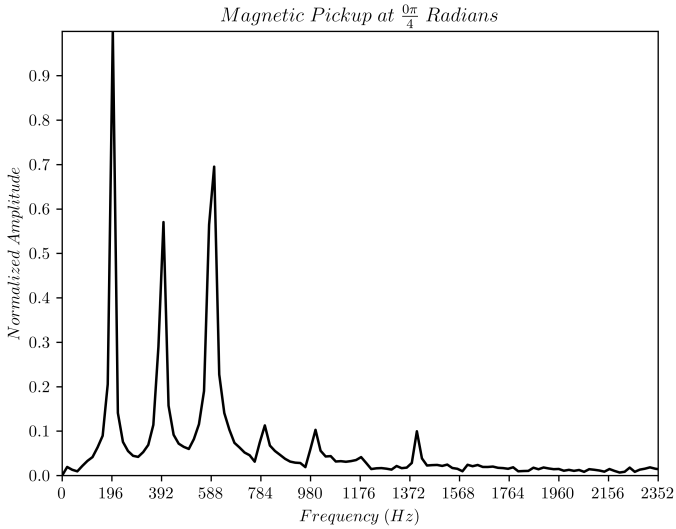


Figure 7.67: The frequency spectrum of the magnetic pickup signal of a plucked string of subjective force at the specified pickup position.

In comparison to the frequency spectra results shown in Sec. 7.2 which featured the experiment results for a bowed string and magnetic pickup in all positions, the frequency spectra of the plucked string are much simpler. The same is true for their comparison to the resulting spectra of the subjectively bowed string in Sec. 7.7.2. The spectra are shown in figures, Fig. 7.67, Fig. 7.68, and Fig. 7.69. For the corresponding pickup positions, the resulting spectra of the plucked string all have a fourth harmonic, 784 Hz, of very low amplitude in contrast to the amplitude of the corresponding harmonic seen for bowed string results. Fig. 7.69 has a significantly lower amplitude for the third harmonic, 588 Hz, which is not the case for the majority of other spectra shown in the result sections. While the 0.05 seconds signal of the experiment shown in Fig. 7.10 and the figures of Sec. 7.7.2 have a

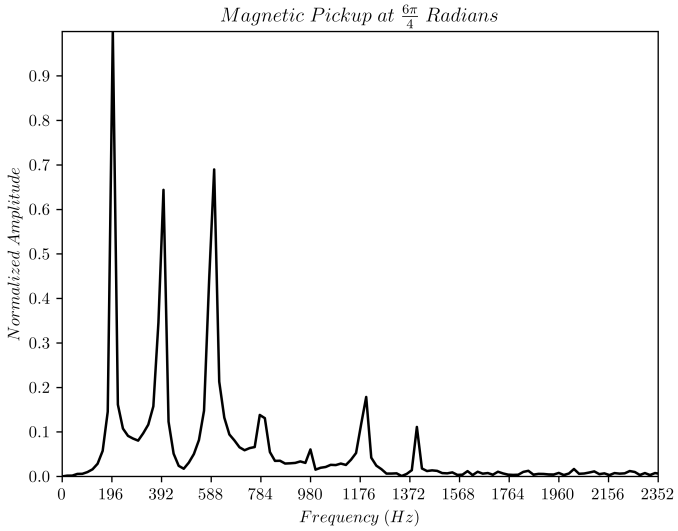


Figure 7.68: The frequency spectrum of the magnetic pickup signal of a plucked string of subjective force at the specified pickup position.

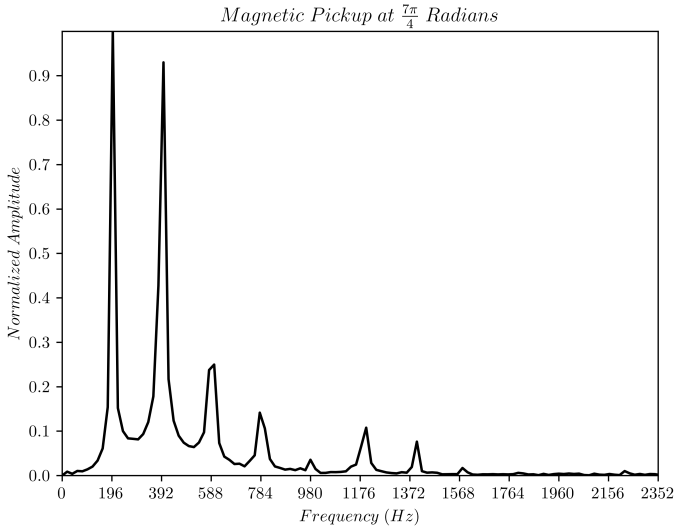


Figure 7.69: The frequency spectrum of the magnetic pickup signal of a plucked string of subjective force at the specified pickup position.

higher number of present harmonics with normalized amplitudes of around 0.2 to 0.3, the same cannot be said of the spectra of the plucked string. And of the present harmonics beyond 588 Hz, none have a normalized amplitude greater than 0.2.

7.8.3 Spectrograms

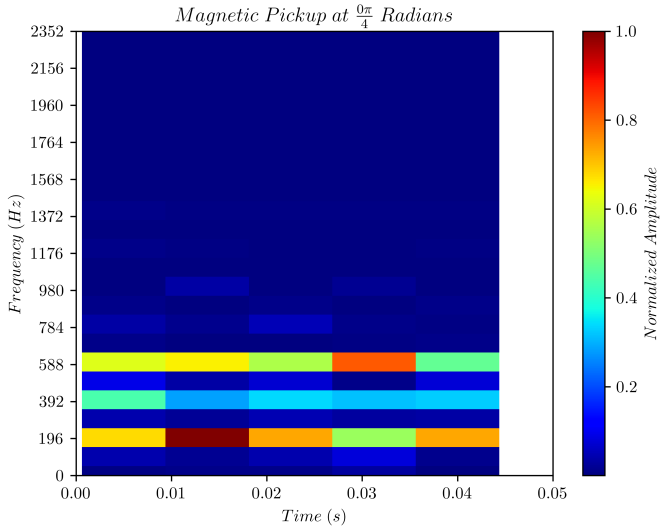


Figure 7.70: The spectrogram of the magnetic pickup signal of a plucked string of subjective force at the specified pickup position.

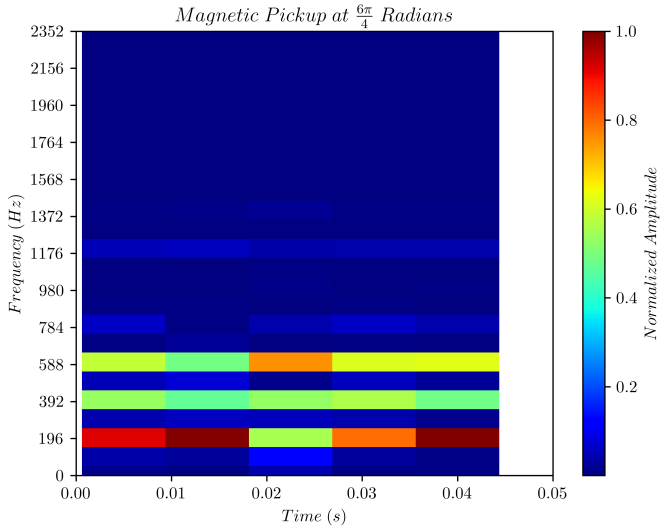


Figure 7.71: The spectrogram of the magnetic pickup signal of a plucked string of subjective force at the specified pickup position.

The spectrograms of the magnetic pickup signals for a plucked string of subjective force produce unexpected results. Fig. 7.70 shows reasonable frequency amplitude consistency across time segments for the first three peaking frequencies, aside from a drop and spike in

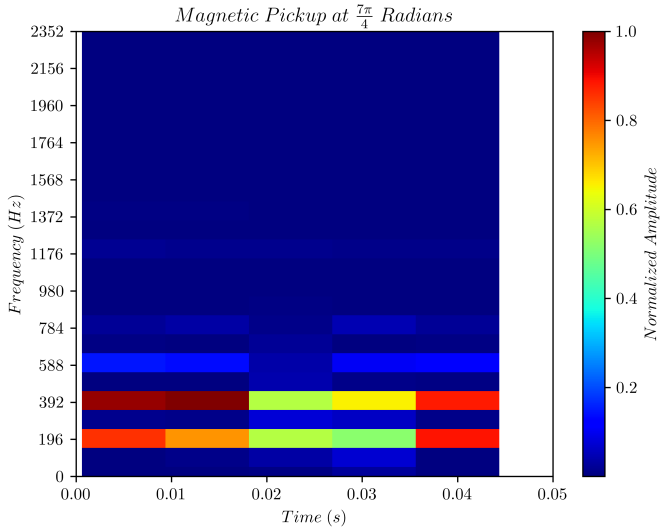


Figure 7.72: The spectrogram of the magnetic pickup signal of a plucked string of subjective force at the specified pickup position.

amplitude of the 0.03 second segment for 196 Hz and 588 Hz respectively. Fig. 7.71 produces good consistency of frequency amplitude across the time segments as well. And Fig. 7.72 drops in frequency amplitude across the 0.02 and 0.03 segments to spike again for 196 Hz and 392 Hz. In comparison to the results of Sec. 7.4 and Sec. 7.5, they are similar except for the occasional drops and spikes in frequency amplitudes at varying time segments.

7.8.4 Magnetic Flux Density Over Time

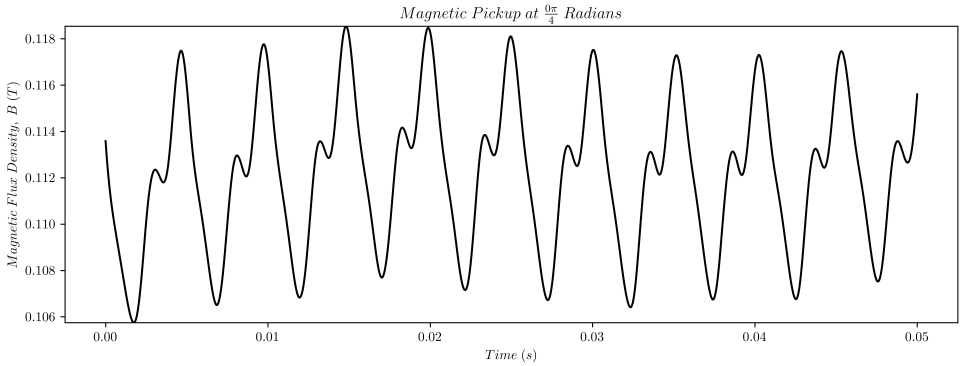


Figure 7.73: The magnetic flux density over time for the magnetic pickup signal of a plucked string of subjective force at the specified pickup position.

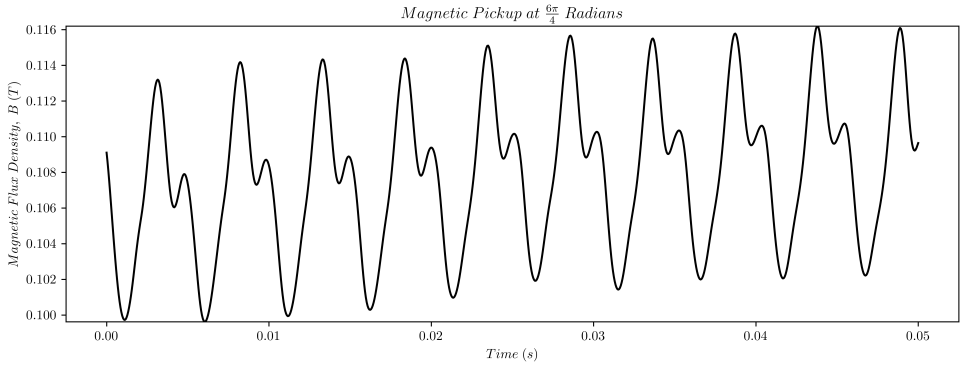


Figure 7.74: The magnetic flux density over time for the magnetic pickup signal of a plucked string of subjective force at the specified pickup position.

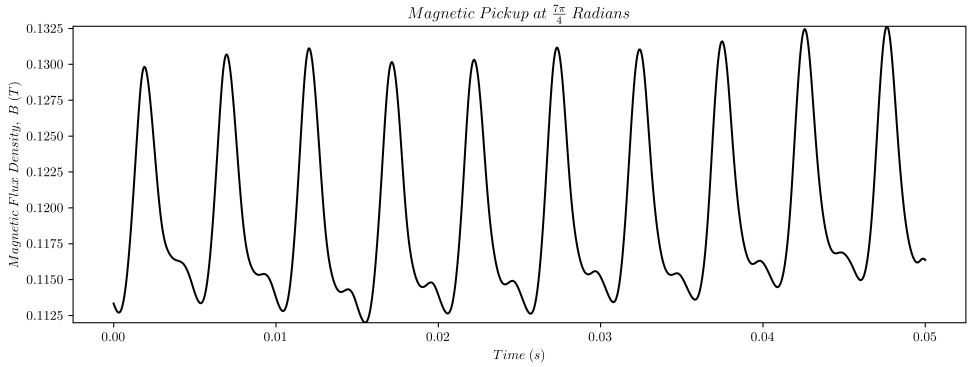


Figure 7.75: The magnetic flux density over time for the magnetic pickup signal of a plucked string of subjective force at the specified pickup position.

The initial conditions for the plucked string are different, given there is not a downward weight and bow weight applied downward onto the string, displacing it downward. Magnetic flux density over time for a subjectively plucked string are shown in figures, Fig. 7.73, Fig. 7.74, and Fig. 7.75. In contrast to the results shown in Sec. 7.6 and Sec. 7.7.4, the magnetic flux density over time does not exhibit a waveform indicative of displacement corresponding to Helmholtz motion. For all three figures, all appear to be sinusoidal and not emblematic of a sawtooth waveform. This makes sense given that the string was not excited by a bow which excites continuously. The length scale of magnetic flux density cannot be compared to those of Sec. 7.6 given the difference in time domain of the signals, 0.05 seconds versus 0.5 seconds. But for the plucked string, the pickup in the vertical position produces a signal with

expected voltage outputs and well-behaved (meaning that it is comparable to the other plots for different pickup positions) magnetic flux density over time when there is no considerable damping from the bow. The vertical transverse string displacement is not inhibited by a damping bow when it is instead plucked.

Chapter 8

Conclusion

8.1 Summary

This work focused on exploration of the behavior of a bowed string-magnetic pickup system, specifically examining maximum and average voltage outputs across different frequency distributions and their evolution over time. Through a combination of theoretical analysis and experimental investigation, the study analyzed frequency distributions over time and tracked changes in magnetic flux density. The primary objective of this work was to establish foundational insights for designing magnetic pickups for bowed instruments like the violin. A secondary objective of this work was to motivate a modified damping factor term or modified external force term associated with dampening of vertical bowed string motion based on experimental evidence.

Recall the description of the experiment provided in Sec. 1.3, where a monochord is excited by a controlled bow. A magnetic pickup can be rotated around this string with eight possible positions corresponding to the cardinal and inter-cardinal positions. One of the goals of the work (related to the primary objective) was to determine, out of the subset of magnetic pickup positions considered, what position for the magnetic pickup is most optimal. Note that the magnetic pickup locations can be specified by the cardinal and inter-

cardinal directions, corresponding to incremented counter-clockwise angles, $\frac{0\pi}{4}$ (along with the positive-y axis of the $y-z$ plane as viewed from the bridge endpoint of the monochord), $\frac{1\pi}{4}, \ldots, \frac{7\pi}{4}$.

An optimal magnetic pickup position is determined by criteria relevant to voltage outputs, frequency distributions, frequency distributions over time, and magnetic flux density over time. With this context in mind, the main results of this work can be summarized as follows.

1. When the magnetic pickup was at the bottom right diagonal position, $\frac{7\pi}{4}$, it produced the highest maximum and average voltages, had a favorable frequency distribution with respect to tonal quality, maintained consistent frequency amplitudes over time, and produced expected magnetic flux density levels.

2. When the magnetic pickup was in either vertical position, $\frac{2\pi}{4}$ or $\frac{6\pi}{4}$, the maximum and average voltage outputs were the lowest for all positions, the frequency distributions were chaotic and noisy, and the linear amplitudes for their frequencies were very low compared to other positions.

3. There is ample experimental evidence demonstrating significant damping of the vertical string oscillations by the combination of the presence of bow's bow hairs at the point of bow-string interface and the downward bow force applied. This strengthens the argument for updating governing bowed string equations to account for said dampening through either an additional damping factor as a function or constant of the bow hair's motion or an external force as a function of bow hair's motion.

4. For a magnetic pickup signal of 0.05 seconds in length, magnetic flux density over time exhibited a quasi-periodic sawtooth waveform for any signal when the magnetic pickup was in a horizontal or diagonal position. This sawtooth pattern is derivative of the displacement of Helmholtz motion from the horizontal transverse string oscillations of a bowed string. For signals of 0.5 seconds, there was local weak quasi-periodicity for the sawtooth pattern and global non-periodicity.

5. There is experimental evidence for continuous pitch glide for bowed strings.

6. Supposing a violin is used, when a string is excited by a bow, a magnetic pickup placed at an angle from the bottom produces sufficient signal amplitude unlike the vertically placed magnetic pickup. When placed at an angle from the bottom, the magnetic pickup has a spatial advantage over one placed horizontally at the string. This is because the most viable location for a pickup is between the bridge and the end of the fingerboard. Placing a pickup horizontally in this area would impede the bow.

There have been many research contributions presented in this work and can be summarized as the following. An overview of the theory surrounding the governing equations of bowed string motion was presented in Sec. 2. Under various simplifying assumptions, Faraday's Law of Induction was utilized and the non-uniform magnetic field was modeled in order to solve for magnetic flux density over time with the collected voltage signals from the magnetic pickup. Faraday's Law of Induction in this form was also related to the two transverse displacements of a bowed string. In addition to this, to theoretically account for the rotation of the magnetic pickup, a transformation matrix was derived to translate and rotate the magnetic field components to correlate the governing equations with how the experiment was to rotate the magnetic pickup, thus also the magnetic field. And finally, for Sec. 2, a brief qualitative description was provided for the bow-string interactions specifically related to the vertical motions of the string and bow. This part was dedicated to acknowledging the potential need for updated governing bowed string equations to account for the damping effects of the bow on the string. This potential need was contingent on what available evidence would be obtained from the experiment results.

The various parameters of the experiment detailed the design and construction of the monochord, the bow stroke mechanism, the magnetic pickup, the measurement position piece, and the fixtures to hold the optical switches. This was seen in Sec. 3. For those mentioned parts, the electronics, and the pertinent materials like the bow and string, parameters and measurements were given. These designs were made such that the experiment could, in

a simplified fashion, mimic playing a violin bow in an approximate position of typical violin playing with a magnetic pickup that would be placed in a fixed x-position along the string in accordance with the common distance between the bridge and the end of the fingerboard.

Details of the methods of how data was collected from the experiment were given and discussed. These were expounded upon in Sec. 4. There were three measurement types made by one magnetic pickup and two optical switches which were to capture the transverse string displacements and convert them to voltages. For magnetic flux density as a function of distance from the magnet pole face, a Gaussmeter was used to capture the data. The use of a Gaussmeter was also used to capture initial conditions for magnetic flux density over time. In addition, a step-by-step procedure for one repetition of the experiment was provided.

The various post-processing techniques used to interpret the collected data and produce results from the experiment were defined and discussed in Sec. 5. They describe first the derivation of the maximum and average voltage over magnetic pickup position for the magnetic pickup signals and the voltage outputs across all eight repetitions of an experiment iteration coming from each optical switch set of results. The section also details how frequency spectra were to be derived for all the signals obtained. The same is true for spectrograms for all the signals obtained. And for magnetic flux density, based on the assumptions to simplify Faraday's Law of Induction to better fit the method of capturing the string motion by the magnetic pickup. In addition, the section provided a description of how the oscilloscope was used to capture the signals and a description of how the data was converted to comma-separated values files which could be imported to Python for the post-processing techniques. And finally, a procedure describing how the experiment operates in its totality was given. Recall that the repetitions of the experiment, are all time consistent with one another, meaning that the same amount of time elapsed for the same distance of bow traveled for each repetition.

Results that strongly resemble results from the literature demonstrating the reliability

of the measurement tools and post-processing methods used were obtained and detailed in Sec. 6. The construction of the monochord shared similar design features to other authors [32, 28]. Results for magnetic flux density as functions of vertical distance above the magnet pole face and horizontal distance at a fixed distance above the magnet pole face demonstrated the same type of results found in the works of other authors [23]. In accordance with expected results from Fourier analysis in relation to tonal theory and the results of another author, accurate frequency spectra were obtained from both the magnetic pickup and both optical switches [28]. The distributions exhibited amplitude peaks at the fundamental frequency which the string was tuned to, specifically, 196 Hz. Accurate displays of horizontal bowed string displacement were also achieved. Aside from an anomalous short-time peak in voltage, the horizontal optical switch signals displayed waveforms that were sawtooth or triangular in nature. This correlated well with theory, other authors' results, and simulation [1, 4]. When using the voltage signals obtained by the optical switches, linear wave polarization was achieved in the $y - z$ plane for bowed string motion. Particularly, though, the polarization plots shown were derived with the voltage signals as opposed to with the actual string's transverse displacements. These plots were evidence demonstrating significant dampening of the vertical string oscillations, which further the argument for updating the governing bowed string equations. Though, the voltages are proportional to the displacements. It is possible with numerical methods to solve for displacement using the equation shown in Sec. 4.2, Eq. 4.2.1, which comes from Le Carrou et al. [18]. This was in accordance with theory behind parametric sinusoidal functions and more broadly that of Lissajous curves. For plucked string motion, some authors have displayed elliptical polarization of the string's transverse waves, but this was not replicated in the section [22]. Many attempts with various different plucking techniques were used, but hyperbolic polarization of the plucked string's transverse waves was demonstrated instead. And lastly, a short survey on expected results with respect to voltage outputs, frequency distributions, and magnetic flux densities was briefly given.

Results from the experimentation were obtained and the findings were discussed in Sec. 7. For the main experiment repetitions which featured 0.5 second long signals from the magnetic pickup at the eight rotational positions around the string, maximum and average voltage outputs revealed that the signal was strongest for when the pickup was at either horizontal position, $\frac{0\pi}{4}$ or $\frac{4\pi}{4}$, and at either bottom diagonal position, $\frac{5\pi}{4}$ or $\frac{7\pi}{4}$. This was true for both maximum and average voltage. They produced signals that exceeded expectations in voltage output, but this is partly due to the heavy downward bow force used to ensure frequency distributions comparable to those of a regularly played violin and due to the sensitivity of the magnetic pickup coming from the high number of coil revolutions. But, the bottom right diagonal position of the pickup produced the greatest outputs do to the large downward bow force and bow velocity moving the string's equilibrium, during horizontal oscillation, closer to the magnet pole face, making the signal much stronger. For both vertical positions, the magnetic pickup signal was significantly weaker, demonstrating the lack of energy and amplitude in vertical transverse string oscillations of a bowed string. The presence of downward bow force, which is unavoidable in bowed instruments, caused a bias in amplitude towards the bottom positions, though the signal of the magnetic pickup in the bottom vertical position was only greater than that of it in the top vertical position. This led to the implication that for purposes of amplification, viable magnetic pickup design for a violin would need to feature an angled orientation from below the string, such that it can be moved closer to the string with less consideration from string contact due to the lack of vertical displacement. This both avoids the lack of signal for amplification from the vertical position and the spatial limitations of having a horizontally placed magnetic pickup in or near the window of bowing for typical violin playing. These results also demonstrate that the bow provides significant dampening to the vertical transverse string displacement and the need for updating the governing bowed string equations to account for such dampening. And looking to the voltage outputs of the two optical switches, the results show very little variance across eight repetitions per whole experiment iteration, indicating the consistency

of the bow stroke mechanism.

Due to the oscilloscope's lack of resolution comparatively between signals lasting 0.05 seconds and 0.5 seconds (both signals had approximately the same amount of samples), frequency spectra of the main results, lasting 0.5 seconds, only reached up to the fifth harmonic, 980 Hz. The spectra for 0.05 seconds could account for up to the twelfth harmonic. This is to say that the frequency distributions, arguably, of the 0.5 second signals are not limited to the fifth harmonic. Of the results, spectra for pickup positions, $\frac{0\pi}{4}$, $\frac{1\pi}{4}$, $\frac{4\pi}{4}$, and $\frac{7\pi}{4}$ had the fundamental frequency, 196 Hz, as the most amplified frequency. Each had a strong presence of following harmonics as well. In some cases, there may have been instances of continuous pitch glide and temperature effects on the string, ultimately slightly varying the pitch of the string higher. In terms of tonal quality, the aforementioned pickup positions have spectra that would indicate good tonal quality. The pickup in the top vertical position had a spectrum which was dominated greatly by high amplitude noise. Comparing the frequency spectra of the optical switch signals to those of the pickup signals, the pickup signals clearly amplified higher harmonics present in the overall string displacement. This is a significant advantage musically, achieving a brighter and fuller sound. A small set of linear amplitude frequency spectra were also looked at. The results showed that for the fundamental frequency, its amplitude was significantly smaller when the magnetic pickup was in the bottom vertical position in comparison to when in the bottom right diagonal or right horizontal position. Again, this indicated a need to update the governing equations for bowed string motion to account for dampening of vertical string oscillations by the vertical bow hair motions.

Like for the frequency spectra, resolution was an issue for spectrograms. So a spectrogram for a 0.05 second signal was shown, revealing a fuller frequency distribution over time. The 0.5 signals, arguably, were not limited to the fifth harmonic for frequency makeup. Of the main experiment results, pickup positions, $\frac{0\pi}{4}$, $\frac{4\pi}{4}$, $\frac{5\pi}{4}$, and $\frac{7\pi}{4}$ had consistent frequency amplitude over time for their respective spectral envelopes. Musically, it is crucial that when a note is

played, it does not waver in tone or frequency amplitudes over time, unless this is an intended technique by a player, like *vibrato*, which is has a larger spectral envelope and is controllable. For the pickup in either vertical position, the frequency amplitudes are not consistent across time segments. The spectrograms for the horizontal optical switch signals show consistent frequency amplitude for present frequencies across time segments, while the vertical optical switch spectrograms shower less consistency. And for the frequency spectra with good results, their corresponding spectrograms typically exhibit similar amplitude results as well.

Analysis of magnetic flux density over time showed interesting results. The first and main result was that under simplifying assumptions of Faraday's Law of Induction and, thus, applying a basic modeling of a non-uniform magnetic field, the magnetic flux density over time for a 0.05 second-long magnetic pickup signal whose pickup position was in the bottom right diagonal or right horizontal position (non-exclusive list) exhibited a sawtooth waveform which most likely arose from the displacement of Helmholtz motion of the horizontal transverse string displacement of the bowed string. Connected to the main result concerns the results from the main experiment repetitions. For these 0.5 second long signals, magnetic flux density over time for signals of a magnetic pickup in either horizontal or diagonal positions exhibited sawtooth wave patterns locally. These waveforms exhibited local weak quasi-periodicity, while the plot in totality displayed global non-periodicity. The potential causes of those specific results likely are that the approximations made for Faraday's Law of Induction and the magnetic field are insufficient and that magnetic flux density is influenced by string displacement but not enough to be dominated by it. Depending on if the horizontal components of the pickup's direction pointed in the bowing direction or not, the sawtooth pattern would "travel" left or right, respectively. Another result obtained is that over time, magnetic flux density stayed relatively within the expected Tesla output range.

For the results from a bowed string of subjective downward bow force and bow velocity, the results for the pickup in the bottom vertical, bottom right diagonal, and right horizontal positions were very similar to those of the main experiment. With the author's two decade

experience as a violinist, a bow stroke of force to produce a medium loudness was made and the voltage outputs were about half of those of the experiment. In addition, for the right horizontal position, the pickup's magnetic flux density over time also exhibited a sawtooth waveform indicative of displacement from Helmholtz motion.

For the results from a plucked string of subjective excitation force, there were sufficiently high voltage outputs. The frequency spectra, however, featured less harmonic presence and low amplitude for lower harmonics. Another key difference was that the magnetic flux over time plots were sinusoidal and did not indicate any form of Helmholtz motion displacement or sawtooth wave patterns. But this was expected because the string was not continuously excited by a bow.

From analysis of voltage outputs, polarization types, and linear frequency amplitudes, it becomes more justifiable to explicitly account for the damping effect for a bowed string's vertical transverse string displacement in Eq. 2.1.14 which is observed in all of these result types. This could come potentially in the form of a modified damping factor or an external force for the vertical transverse bowed string equation. The problem lies in the interaction between the vertical oscillation of the bow hair of the bow and of the vertical oscillations of the string.

Magnetic pickups for bowed instruments are not common. To the knowledge of the author, in the last ninety years there have been very few patents for them and only a few luthiers who have made electric violins with this feature. Of these patents, many do not focus on magnetizing the strings. To the best of the author's knowledge and research into the topics, there has not been academic work on the behaviors of a bowed string-magnetic pickup system, theoretical or experimental. This work utilized key analysis techniques for acoustics and electromagnetism to provide results for the behaviors of this system. It provides key types of results, crucial to designing a magnetic pickup for a bowed instrument.

It was hypothesized that when the magnetic pickup was in either horizontal position, the maximum and average voltage outputs would be the greatest in comparison to the pickup in

other positions. However, this hypothesis was found to be incorrect, based on experimental evidence. Instead, maximum and average voltage outputs were greatest when the magnetic pickup was in the bottom right diagonal position. But it was determined this was due to the downward bow force moving the string's equilibrium closer to the magnet pole face, generating a more powerful signal. Though, the outputs from the horizontal positions were still optimal, not to exclude the results from the pickup in the bottom right diagonal position. Frequency distributions, spectrograms, and magnetic flux density over time for the horizontal positions produced good results. Though, after experimentation and analysis, with creating a design for a violin magnetic pickup, the bottom right diagonal position proves to be the best in all result types. Not only this, but from a design perspective, the magnetic pickup in this position avoids lack of signal for amplification like that of it in the vertical positions and it avoids the spatial limitations, imposed by the bow and location of bowing, of the horizontal positions. The magnetic pickup signals from this position, $\frac{7\pi}{4}$, provide excellent results, indicating it is viable musically and electrically for producing a sound faithful to what the player plays with unique tones unavailable to different types of amplification techniques and for producing a signal that can be amplified in general.

The magnetic pickup has certain advantages over other types of amplification methods. For a violin, a microphone is susceptible to background noise, stage noise, and even sounds from the player like speech. A piezoelectric pickup for a violin produces a sound that usually necessitates the use of an equalizer or pre-amplifier, which creates a greater financial investment by for the player. But a magnetic pickup avoids these disadvantages. Though both methods of amplification are good, consider what revolutionized the guitar. It was the magnetic pickup not only for its type of sound and for amplification purposes, but as people began to figure out, it was also that the influence of the body design of the guitar was greatly reduced from a tonal and loudness perspective. If one were to create a guitar with the neck, strings, middle sliver of the body, and a magnetic pickup, it will sound like a guitar. The advent of the magnetic pickup in the musical world of guitars made guitars more

affordable and more accessible to anyone, without sacrificing tonal quality or amplification. The same could be true for the violin. Many luthiers and companies take this approach for the violin but with merely different signal capturing techniques. And they do not enjoy the tonal benefits of the magnetic pickup. The development of a magnetic pickup for a violin could produce many commercial and musical benefits.

8.2 Suggestions for Improvement

For the experiment of this work, further improvements can be made. Most improvements concern precision for specific dimensions and data collection. The first improvement that could be made for future extensions of research is utilizing a higher quality oscilloscope. More information and accuracy can be gained with a better oscilloscope. This is because signals could have higher resolutions, or larger discretization of the data, allowing for more wave information to be preserved. Longer signals would also enjoy higher precision as a result.

Through the experimentation, particularly through consistent voltage outputs across all experiment repetitions for each measurement tool, the bow stroke mechanism shows itself to be reliably consistent. Though, as it was briefly discussed in Sec. 6.1, a modern version of Cronhjort's MUMS bowing machine can be made with the basis of the model being a belt-driven linear actuator typically found in a 3-D printer [5]. This would allow for even more precision in downward bow force and bow velocity. Another improvement that could be made would be to control the number of bow hairs and if the hairs interact with one another or not. This can be done in a way similar to the one seen in Ricca, where the bow would be replaced with a simpler design akin to a bow but allow for fastening of bow hairs as in Ricca's design [28].

Another area of improvement, particularly with future research in mind, is to create the monochord out of fewer pieces of more stable material like aluminum or acrylic plastic that

can be machined with higher precision. Being able to use a CNC mill and G-code would allow for greater precision when constructing the monochord. Ideally, fewer pieces could be used to prevent additional points of marginal errors in dimensions. Acrylic would be significantly more cost-effective than aluminum. With the use of a CNC mill, the bridge and nut positions can be better calibrated and the positioning of the measurement tool position pieces can be relative to the whole body and bridge and nut or relative to peg holes milled out in the monochord base.

Improvements can be made through taking a different approach would be to attempt to have radial symmetry for the distance between the magnetic pickup's pole face and the string with the influence of downward bow force on string equilibrium displacement. When the string is at rest, treating the bow as a third class lever and having a weight attached to the tip, it is possible to approximate the downward displacement of the string when considering this and the tension of the string tuned at a specific note. This influence was not considered in this work, but it did reveal the importance of downward bow force as a design factor for a violin magnetic pickup.

The experiment and work in general could benefit from applying more advanced modeling of the non-uniform magnetic field of the magnetic pickup in order to better calculate magnetic flux density over time. This would provide more insight in those result types and allow for more exploration in the already interesting results found using simpler methods of calculation.

8.3 Future Work

Through this work, there have been numerous allusions to potential future areas of research to explore. As it was mentioned in the introduction, study of a bowed string-magnetic pickup system is a new area of research. There are many sub areas of research that can be explored. The goal of Sec. 8.3 is to itemize the various potential areas of future work inspired by the

work conducted in this thesis.

One area of future research is conducting an experiment or modeling of various bow velocities and downward bow forces with a bow stroke machine for a bowed string-magnetic pickup system. For this experiment, simplicity and reduction was sought after. But, a parameter study, experimental or through simulation, on the bowed string-magnetic pickup system including bowing velocity and downward bow force would prove to be a worthwhile endeavor.

Again concerning the bow, a parameter study or simple modeling of bow inclination, the angle between the positive y-axis and the bow itself, in relation to an angled magnetic pickup is another potential area of future research [33]. The angle of bowing is critical to changing strings while playing, playing two strings at a time, and general musical expression. Given the magnet's magnetic field is directionally dependent and the oscillations of the string occur transversely in two planes relative to the direction of transverse excitation, bowing inclination is an important variable to consider.

Concerning wave polarization for plucked and bowed strings, this work was unable to reproduce elliptical polarization of a plucked string. Investigating potential material or structural influences from a monochord or maybe only the bridge and nut materials is a potential area of future research.

From the results of the main experiment, there are many areas of potential future work. Many of these come from the frequency analysis. One observation was that for some magnetic pickup signals generated by a bowed string, the associated frequency distribution had peaks in amplitudes at frequencies near harmonics, but only roughly 1% higher, indicating possible continuous pitch glide. Exploring the continuous nature of the bow force on the string and pitch glide at initial attacks on a string is an interesting topic to explore further. Given this concerns tonal quality for a magnetic pickup signal, there is application for this topic.

Another area of potential research is deriving the source of "twin peaks" in frequency spectra, where a harmonic is amplified, then a higher frequency near the harmonic is also

amplified. This occurred for certain magnetic pickup signals and even for some horizontal optical switch signals.

For spectrograms, there is future work to be done for longer time signals with a more precise oscilloscope. Music is partially time-dependent with time signatures, various tempos, and different length notes. Being able to design a magnetic pickup for a bowed instrument must include steady, consistent frequency distributions over time.

For magnetic flux density over time for the signals of the bowed string-magnetic pickup system, varying bow velocity and downward bow force can provide more insight into the magnetic flux density outputs. A potential area of future work is investigating multiple slip motion displacement, Helmholtz motion displacement, and non-period motion displacement appearing in magnetic flux density over time plots, derived from the signals of the bowed string-magnetic pickup system. Using other authors' models for magnetic pickups and further optimizing the simple approximations used in this work can provide more insight into the structure of magnetic flux density over time for a bowed string. Given this is one of the most interesting results of this work and experimentation, these related areas have potential to be a very fruitful research topics for further investigation.

There are more general areas of future research which extend what has already been done in this work. Based on observations made in the experimentation, different bowed string simulation can be modeled with more interest in the damping effects of the bow on the string. A fuller parameter study can be done for magnetic pickup rotational positions and even distances from the string for each position. Other extensions of this work have already been mentioned, like different bowing inclination, bowing velocity, downward bow force, and longer signals.

For the bowed string-magnetic pickup system, there is great potential for modeling various outputs through machine learning. This can be done in the frequency domain or even the time domain. There is certainly room for future work in predicting waveforms and frequency distributions based on bowing inclination, downward bow force, bowing velocity, and

magnetic pickup position.

Regarding additional theoretical work, further investigating the dampening effects of the bow onto the string as it vertically oscillates would be a potential route for future research. Much experimental evidence was put forward in this work showing the prominence of this form of dampening. Accurately defining it would further benefit the development of a magnetic pickup for a bowed instrument. It would better aid modeling and simulation for a bowed string-magnetic pickup system.

Bibliography

[1] Özge Akar and Kai Willner. Investigation of the helmholtz motion of a violin string: A finite element approach. *Journal of Vibration and Acoustics*, 142(5), Jun 2020.

[2] Stefan D. Bilbao. *Numerical Sound Synthesis: finite difference schemes and simulation in musical acoustics*. Wiley, 2009.

[3] G. F. Carrier. On the non-linear vibration problem of the elastic string. *Quarterly of Applied Mathematics*, 3(2):157–165, Jul 1945.

[4] Lothar Cremer, John S. Allen, and Lothar Cremer. *The Physics of the Violin*. MIT Press, 1984.

[5] Andreas Cronhjort. A computer-controlled bowing machine (mums). *STL-QPSR*, 33(2-3):061–066, 1992.

[6] Charlotte G. M. Desvages. *Physical Modelling of the Bowed String and Applications to Sound Synthesis*. Phd thesis, University of Edinburgh, Edinburgh, Scotland, United Kingdom, 2018.

[7] Robert Erickson. *Sound Structure in Music*. University of California Press, 1975.

[8] F. G. Friedlander. On the oscillations of a bowed string. *Mathematical Proceedings of the Cambridge Philosophical Society*, 49(3):516–530, Jul 1953.

[9] Colin Gough. The nonlinear free vibration of a damped elastic string. *The Journal of the Acoustical Society of America*, 75(6):1770–1776, Jun 1984.

[10] Colin Gough. *The Electric Guitar and Violin*, pages 393–417. Volume 1 of Rossing [29], 2010.

[11] Léo Guadagnin, Bertrand Lihoreau, Perrick Lotton, and Emmanual Brasseur. Analytical modeling and experimental characterization of a magnetic pickup for electric guitar. *Journal of the Audio Engineering Society*, 65(9):711–721, Sep 2017.

[12] Hermann L. F. Helmholtz. *On the Sensations of Tone*. Longman's, Green's, and Co., 1895.

[13] Jean-Théo Jiolat. *Vibro-Acoustic Study of the Clavichord*. Phd thesis, Sorbonne Université, Paris, France, 2021.

[14] Dmitri Kartofelev, Anatoli Stulov, and Vesa Välimäki. Pitch glide effect induced by a nonlinear string–barrier interaction. *AIP Conference Proceedings*, Oct 2015.

[15] Joseph B. Keller. Bowing of violin strings. *Communications on Pure and Applied Mathematics*, 6(4):483–495, Nov 1953.

[16] Gustav Robert Kirchhoff. *Mechanik*. B. G. Teubner, 1883.

[17] J. Kohut and M. V. Mathews. Study of motion of a bowed violin string. *The Journal of the Acoustical Society of America*, 49(2B):532–537, Feb 1971.

[18] J.-L. Le Carrou, D. Chadefaux, L. Seydoux, and B. Fabre. A low-cost high-precision measurement method of string motion. *Journal of Sound and Vibration*, 333(17):3881–3888, Aug 2014.

[19] Nelson Lee, Julius Orion Smith, Jonathan S. Abel, and David P. Berners. Pitch glide analysis and synthesis from recorded tones. In *Proc. of the* 12^{th} *Int. Conference on Digital Audio Effects*, pages DAFX–1–DAFX–8, Sep 2009.

[20] G.. Lemarquand and V.. Lemarquand. Calculation method of permanent-magnet pickups for electric guitars. *IEEE Transactions on Magnetics*, 43(9):3573–3578, Sep 2007.

[21] Hossein Mansour. *The bowed string and its playability: Theory, simulation and analysis*. Phd thesis, McGill University, Montréal, Québec, Canada, 2016.

[22] Mirko Mustonen, Dmitri Kartofelev, A Stulov, and Vesa Välimäki. Experimental verification of pickup nonlinearity. In *ISMA*, Jul 2014.

[23] Nicholas G. Norton and Thomas R. Moore. Modeling the magnetic pickup of an electric guitar. *American Journal of Physics*, 77(2):144–150, Feb 2009.

[24] Antonin Novak, Leo Guadagnin, Bertrand Lihoreau, Pierrick Lotton, Emmanuel Brasseur, and Laurent Simon. Measurements and modeling of the nonlinear behavior of a guitar pickup at low frequencies. *Applied Sciences*, 7(1):50, Jan 2017.

[25] Polievkt Perov, Walter Johnson, and Nataliia Perova-Mello. The physics of guitar string vibrations. *American Journal of Physics*, 84(1):38–43, Jan 2016.

[26] Chandrasekhara Venkata Raman. On the mechanical theory of the vibrations of bowed strings and of musical instruments of the violin family, with experimental verification of the results, part i. *Bulletin of the Indian Association for the Cultivation of Science*, 15:1–158, 1918.

[27] T. Ray, J. Kaljun, and B. Dolsak. Numerical model application to predict the sound quality of an instrument. *International Journal of Simulation Modelling*, 20(4):696–706, Dec 2021.

[28] Bernard Paul Ricca. *Measurements of the Impedance Presented by a bow to a Bowed String*. Phd thesis, The University of Michigan, Ann Arbor, MI, 1991.

[29] Thomas D. Rossing, editor. *The Science of String Instruments*. Springer, 2010.

[30] Riccardo Russo, Michele Ducceschi, and Stefan Bilbao. Efficient simulation of the bowed string in modal form. In *Proceedings of the* 25^{th} *International Conference on Digital Audio Effects*, Sep 2022.

[31] John C. Schelleng. The bowed string and the player. *The Journal of the Acoustical Society of America*, 53(1):26–41, Jan 1973.

[32] John C. Schelleng. The physics of the bowed string. *Scientific American*, 230(1):87–95, Jan 1974.

[33] Erwin Schoonderwaldt. *Mechanics and acoustics of violin bowing*. Phd thesis, KTH Royal Institute of Technology, Stockholm, Sweden, 2009.

[34] Julius O. Smith. *Physical Audio Signal Processing*. W3K Publishing, accessed 2023. online book, 2010 edition.

[35] Jin Jack Tan, Cyril Touzé, and Benjamin Cotté. Double polarisation in nonlinear vibrating piano strings. In *Proceedings of the Third Vienna Talk on Music Acoustics*, Sep 2015.

[36] Jim Woodhouse and Paul Galluzzo. The bowed string as we know it today. *Acta Acustica united with Acustica*, 90:579–589, Jul 2004.